Extended-soft-core Baryon-Baryon Model ESC08
II. Hyperon-Nucleon Interactions

M.M. Nagels

Institute of Mathematics, Astrophysics, and Particle Physics
University of Nijmegen, Nijmegen, The Netherlands

Th.A. Rijken

Institute of Mathematics, Astrophysics, and Particle Physics
University of Nijmegen, Nijmegen, The Netherlands and
Nishina Center for Accelerator-Based Science, Institute for Physical
and Chemical Research (RIKEN), Wako, Saitama, 351-0198, Japan

Y. Yamamoto

Nishina Center for Accelerator-Based Science, Institute for Physical
and Chemical Research (RIKEN), Wako, Saitama, 351-0198, Japan

(Dated: version of: September 25, 2016)

The YN results are presented from a new version of the Extended-soft-core (ESC) potential model for Baryon-baryon (BB) scattering. The potentials consist of local- and non-local-potentials due to (i) One-boson-exchanges (OBE), which are the members of nonets of pseudoscalar-, vector-, scalar-, and axial-vector mesons, (ii) Pomeron and Odderon exchanges, (iii) Two pseudoscalar exchange (PS-PS), and (iv) Meson-Pair-exchange (MPE). Both the OBE- and Pair-vertices are regulated by gaussian form factors producing potentials with a soft behavior near the origin. The assignment of the cut-off masses for the BBM-vertices is dependent on the $SU(3)$-classification of the exchanged mesons for OBE, and a similar scheme for MPE. In addition to these standard ingredients of the ESC-models also the possible short range repulsion due to the quark Pauli-principle in the BB-channels is included in the analysis, for the first time in a systematic way, in this paper.

The present version of the ESC-model, called ESC08, describes nucleon-nucleon (NN) and hyperon-nucleon (YN) as well as the S=-2 hyperon-hyperon/nucleon (YY/ΞN) in a unified way using broken $SU(3)$-symmetry. Major novel ingredients with respect to the former version ESC04 are the inclusion of (i) short-range gaussian Odderon-potentials corresponding to the odd number of gluon-exchanges, (ii) exceptional short range repulsion in specific YN and YY channels due to Pauli-forbidden six-quark cluster $(0s)^6$-configurations. Further new elements are (i) the extension of the $J^{PC} = 1^{++}$ axial-vector meson coupling, (ii) the inclusion of the $J^{PC} = 1^{+-}$ axial-vector mesons, and (iii) a completion of the $1/M$-corrections for the meson-pair-exchange (MPE) potentials. Like in the ESC04-model, the octet and singlet coupling constants and $F/(F + D)$-ratio's of the model are conform the predictions of the quark-antiquark pair-creation (QPC) model with dominance of the $^3P_0$-mechanism. This not only for the OBE-couplings but also for the MPE-couplings and $F/(F + D)$-ratio's.

Broken $SU(3)$-symmetry serves to connect the NN, the YN and the YY channels. The fitting of NN dominates the determination of the couplings and the cut-off masses. Only a few parameters are strongly influenced by the YN data, and by the constraints for the YY-interactions following from G-matrix analyses of hypernuclei and hyperonic matter. In particular, the meson-baryon coupling constants are calculated via $SU(3)$ using the coupling constants of the NN-analysis as input. In contrast to ESC04, we do not consider medium strong flavor-symmetry-breaking (FSB) of the coupling constants. The charge-symmetry-breaking (CSB) in the Λp and Λn channels, which is an $SU(2)$ isospin breaking, is included in the OBE-, TME-, and MPE-potentials.

For the ESC08-model we performed a simultaneous fit to the combined NN and YN scattering data, supplied with constraints on the YN and YY interaction originating from the G-matrix information on hypernuclei. In addition to the usual set of 35 YN-data and 3 $\Sigma^+ p$ cross-sections from a recent KEK-experiment E289, we added 11 elastic and inelastic Λp and 3 elastic $\Sigma^- p$ cross-sections at higher energy. We obtained within this simultaneous fit $\chi^2/NN_{data} = 1.087$ and $\chi^2/YN_{data} = 1.09$. In particular, we were able to fit the precise experimental datum $r_R = 0.468 \pm 0.010$ for the inelastic $\Sigma^- p$ capture ratio at rest rather well.

Besides the results for the fit to the scattering data, which defines the model largely, also the application to hypernuclear systems, using the G-matrix method, is rather important in establishing the ESC-model. Different versions of e.g. the ESC08-model give different results for hypernuclei. The reported G-matrix calculations are performed for YN (ΛN, ΣN, ΞN) pairs in nuclear matter and also for some hypernuclei. The obtained well depths (U_Λ, U_Σ, U_Ξ) reveal distinct features of the ESC-model.

The inclusion of a quark core Pauli-repulsion can make the Σ-nucleus interaction sufficiently repulsive, as seems to be required by the available experimental evidence. Furthermore, the ESC08-

model gives small spin-orbit splittings in Λ-hypernuclei, which is also indicated by experiment.

I. INTRODUCTION

This is the second in a series of papers [1–3] , henceforth referred to I, II, and III respectively, on the results of the Extended-soft-core (ESC) model for low and intermediate energy baryon-baryon interactions using the ESC08-model. The first results on the BB-channels and applications to hypernuclei were given in the review [4]. With the ESC04-models [5–7], it was shown that a very successful description of the presently available baryon-baryon scattering data could be achieved within the ESC-approach to the nuclear force problem. Also, such a description was obtained with meson-baryon coupling parameters which can be understood rather nicely within the context of the $^3P_0$- quark-pair creation mechanism [8, 9]. This mechanism has been shown to be dominant in the framework of lattice QCD [10]. The simultaneous and unified treatment of the NN and YN channels in ESC04, using broken $SU(3)$-flavor, has given already a rather successful potential model for the low and intermediate energy baryon-baryon scattering data. Furthermore, the basic ingredients of the model are physically motivated by the quark-model (QM) and QCD.

The G-matrix calculations showed that basic features of hypernuclear data are also reproduced rather well, improving several weak points of the soft-core OBE-models [11–13]. However, there remained the problem that the meson-exchange models seem to be unable to give a positive well depth U_Σ. A second problem posed the very small spin-orbit splittings in Λ-hypernuclei [14, 15]. In this paper we extend and refine the ESC-model in order to provide improvements and answers to these issues.

First, we list the new ingredients of the here presented version ESC08c, which are more or less in line with the ESC-approach as presented so far. In this category, the following additions to the ESC04-model are made for the present ESC08-model:

(i) For the axial-vector mesons with $J^{PC} = 1^{++}$, the A-mesons, next to the $\gamma_5\gamma_\mu$-coupling also the derivative $\gamma_5 k_\mu$-coupling is exploited.

(ii) The axial-vector mesons with $J^{PC} = 1^{+-}$, the B-mesons, are included as well. The latter have potentials of the same type as the pseudo-scalar mesons, but have an opposite sign. We notice that now the set of the exchanged quantum numbers for OBE-potentials is identical to that for MPE-potentials.

(iii) For the meson-exchange we have included the Brown-Downs-Iddings anti-symmetric spin-orbit potentials from pseudoscalar-, vector-, scalar-, and axial- meson exchange [16].

(iv) We have completed the $1/M$-corrections for meson-pair-exchange (MPE), in particular for the $J^{PC} = 1^{++}$- and $J^{PC} = 1^{+-}$-axial pairs. This also leads to new important contributions to the anti-symmetric-spin-orbit

interaction [17].

(v) For the diffractive contribution we have next to the Pomeron-exchange [18] added the Odderon-exchange [19]. Whereas in QCD the Pomeron can be associated with colorless even number (2,4, ...) of gluon-exchanges, the Odderon is associated with the colorless odd number (3,5, ...) of gluon-exchanges. At low energies the Pomeron has $J^{PC} = 0^{++}$, but the Odderon has $J^{PC} = 1^{--}$.

Secondly, we have opened the possibility to incorporate possible effects of a 'structural' or channel-dependent repulsion due to Pauli-blocking. This repulsion originates from a 'forbidden-state' in the $SU(6)_{fs}$ Quark-Cluster-Model (QCM) [20, 21]. This is the analog of a well known effect in $\alpha\alpha$-scattering discovered in the sixties [22]. This 'forbidden-state' is the [51]-irrep and this irrep occurs with a large weight in the two $J^P = 1/2^+$-baryon states in the $SU(3)_f$-irreps $\{10\}$ and $\{8_s\}$. These irreps are prominent in the $\Sigma^+ p(^3S_1)$- respectively the $\Sigma N(^1S_0)$-states. These are precisely the states where according to e.g. the G-matrix calculations the ESC-models possibly lack some repulsion. This repulsion seems to be indicated by experiment [23, 24]. The [51]-irrep also occurs in the other NN-, YN-, and YY-channels, but with roughly equal weights, see [20], apart from a few S=-2 channels, e.g. $\Xi N(I = 1, S = 0)$.

We account for the 'exceptional-repulsion' in a phenomenological way by enhancing the "pure" Pomeron-coupling. So the effective Pomeron-repulsion consists of the pure Pomeron-exchange contribution augmented with a fraction of Pauli-blocking repulsion, which varies for the different BB-channels. (The other typical quark-cluster effects like e.g. one-gluon-exchange (OGE) annex quark-interchange is in ESC-models taken care of by meson exchange.) In this work we try to determine the strength of this Pauli-blocking effect in BB-channels. The fit to NN determines the sum of both the pure Pomeron-repulsion and the Pauli-blocking repulsion. The fit to YN determines the fraction of Pauli-blocking in it.

The ESC08-model realizes a fusion between the soft-core meson-exchange potentials and QCM-aspects of the baryon-baryon interactions and can be called a 'hybrid' ESC-model. The soft-core meson-exchange model has been described in detail in previous papers, [5–7]. Therefore, we may refer here to those papers for a description of (a) the physical background, (b) the employed formalism, (c) the description of the potentials, either in details or in references to papers where further information may be obtained. In this paper we will derive (i) the new OBE-potentials employed here for the first time in the context of the ESC-model, (ii) the Odderon-potentials, and (iii) a derivation of the short-range phenomenology connected to the quark Pauli principle within the context

of the SU(3)$_f$-formalism as used in the Nijmegen potentials. Next to these items, we will also give the new $1/M$-corrections for the axial-meson-pair-exchange potentials, where we restrict ourselves to the spin-spin and tensor contributions. The YN symmetric and anti-symmetric spin-orbit potentials will be described in another paper.

In [5, 6] a detailed description of the basic features of the ESC-models has been given and motivated. Many of these were already present in the Nijmegen soft-core [12] and hard-core [25] OBE-models. We refer the reader to these references for the description and discussion of the items such as: (broken) SU(3)-flavor, charge-symmetry-breaking (CSB) in YN, meson-mixing in the pseudo-scalar-, vector-, scalar- meson SU(3)-nonets, the role of the quark-antiquark pair-creation $^3P_0$-model for BBM- and BBMP-couplings. Also, in e.g. [6] one finds a recapitulation of the goals of our continued investigation of the baryon-baryon systems.

In the soft-core Nijmegen OBE- and ESC-models the form factors are taken to be of the gaussian-type. In the (non-relativistic) QM's a gaussian behavior of the form factors for ground-state baryons is most natural. The two-particle branchpoints, corresponding to e.g. $\pi\pi, \pi\rho, K\rho$-etc., are in the ESC-models accounted for by the MPE-potentials. Gaussian residue functions are used in regge-pole models for two-particle reactions at high-energy and low momentum-transfers.

As pointed out in [5, 6] $SU(3)$-symmetry and the QPC-model give strong constraints on the coupling parameters. The $^3P_0$-model also offers the possibility to introduce a scheme for hypercharge breaking a la Gell-Mann-Okubo for the BBM-couplings. In order to keep some more flexibility in distinguishing the NN- and the $YN(S=-1)$-channels, such a medium-strong breaking was explored in the NSC97 [13] and ESC04 [6]. In the present study we do not apply such a breaking. The results show that a scheme of SU(3) symmetric couplings with only mass breaking can give an excellent description of all BB interactions.

The content of this paper is as follows. In section II we review very briefly the scattering formalism, the Lippmann-Schwinger equation for the T- and V-matrices. Similarly, in section III the NN and $S=-1$ YN-channels on the isospin and particle basis, and the use of the multi-channel Schrödinger equation is mentioned. The potentials in momentum and configuration space are defined by referring to the description given in [5]. Also SU(3)-breaking is reviewed briefly. In section IV on the OBE-potentials, the additions for ESC08 in comparison with the ESC04-model are described. Here, we give the new potentials in momentum and configuration space. In section V the SU(3) structure of the MPE-potentials is given and the additions in comparison with the ESC04-model are listed. The latter are the axial $J^{PC} = 1^{+-}$ ($\pi\omega$)-pair potentials, which is the content of Appexdix B. In section VI the short-range phenomenology is discussed. We derive the incorporation of the 'exceptional' Pauli-repulsion, which shows up 'exceptionally' large in the

SU(3)-irreps $\{10\}$ and $\{8_s\}$.

In section VII the simultaneous $NN \oplus YN \oplus YY$ fitting procedure is reviewed. In section VIII the results for the coupling constants and $F/(F+D)$-ratios for OBE and MPE are given. They are discussed and compared with the predictions of the QPC-model. Here, also the values of the BBM-couplings are displayed for pseudo-scalar, vector, scalar, and axial-vector mesons.

In section IX the YN-results for ESC08c from the combined $NN \oplus YN \oplus YY$-fit are discussed [26]. In section X we discuss the fit to the YN scattering data. In section X, the hypernuclear properties of ESC08 are studied through the G-matrix calculations for YN (ΛN, ΣN, ΞN) and their partial-wave contributions. Here, the implications of possible three-body effects for the nuclear saturation and baryon well-depths are discussed. Also, the $\Lambda\Lambda$ interactions in ESC08 are demonstrated to be consistent with the observed data of $^6_{\Lambda\Lambda}$He. In section XI we finish by a final discussion, draw some conclusions, and an outlook. In Appendix A we display the full SU(3) contents of the MPE-couplings, and in Appendix B for completeness the $J^{PC} = 1^{+-}$ axial-pair potentials are given. Finally, in Appendix C the antisymmetric spin-orbit potentials are derived explicitly for strange meson-exchange K and K*.

II. SCATTERING FORMALISM, THE LIPPMANN-SCHWINGER EQUATION, POTENTIALS

In this paper we treat the nucleon-nucleon (NN) and hyperon-nucleon (YN) reactions with strangeness $S = 0, -1$. Since in general there are both 'direct' and 'exchange' potentials, the ordering of the baryons in the incoming and outgoing states needs special attention. For keeping this ordering clear, we consider for definiteness the hyperon-nucleon reactions

$$Y(p_1, s_1) + N(p_2, s_2) \rightarrow Y'(p_1', s_1') + N'(p_2', s_2') . \quad (2.1)$$

Like in [12], whose conventions we will follow in this paper, we will also refer to Y and Y' as particles 1 and 3 and to N and N' as particles 2 and 4. The four momentum of particle i is $p_i = (E_i, \mathbf{p}_i)$ where $E_i = \sqrt{\mathbf{p}_i^2 + M_i^2}$ and M_i is the mass. The transition amplitude matrix M is related to the S-matrix via

$$\langle f|S|i \rangle = \langle f|i \rangle - i(2\pi)^4 \delta^4(P_f - P_i)\langle f|M|i \rangle , \quad (2.2)$$

where $P_i = p_1 + p_2$ and $P_f = p_1' + p_2'$ represent the total four momentum for the initial state $|i\rangle$ and the final state $|f\rangle$. The latter refer to the two-particle states, which we normalize in the following way

$$\langle \mathbf{p}_1', \mathbf{p}_2'|\mathbf{p}_1, \mathbf{p}_2 \rangle = (2\pi)^3 2E(\mathbf{p}_1)\delta^3(\mathbf{p}_1' - \mathbf{p}_1) \cdot$$
$$\times (2\pi)^3 2E(\mathbf{p}_2)\delta^3(\mathbf{p}_2' - \mathbf{p}_2) . \quad (2.3)$$

We follow section II of [12] in detail. The transformation to the non-relativistic normalization of the two-

particle states leads to states with

$$(\mathbf{p}_1', s_1'; \mathbf{p}_2', s_2' | \mathbf{p}_1, s_1; \mathbf{p}_2, s_2) = (2\pi)^6 \delta^3(\mathbf{p}_1' - \mathbf{p}_1) \cdot$$
$$\times \delta^3(\mathbf{p}_2' - \mathbf{p}_2) \, \delta_{s_1', s_1} \delta_{s_2', s_1} \, . \qquad (2.4)$$

For these states we define the T-matrix by

$$(f|T|i) = \{4M_{34}(E_3+E_4)\}^{-\frac{1}{2}} \langle f|M|i \rangle \{4M_{12}(E_1+E_2)\}^{-\frac{1}{2}} \, , \qquad (2.5)$$

which satisfies the Lippmann-Schwinger equation [12]

$$(3,4|T|1,2) = (3,4|V|1,2) + \frac{1}{(2\pi)^3} \sum_n \int d^3 k_n \, \cdot$$

$$\times (3,4|V|n_1,n_2) \frac{2M_{n_1,n_2}}{\mathbf{p}_n^2 - \mathbf{k}_n^2 + i\varepsilon} (n_1, n_2 | T | 1, 2) \, , \qquad (2.6)$$

and where analogously to Eq. (2.5) the potential V is defined as

$$(f|V|i) = \{4M_{34}(E_3+E_4)\}^{-\frac{1}{2}} \langle f|W|i \rangle \{4M_{12}(E_1+E_2)\}^{-\frac{1}{2}} \, . \qquad (2.7)$$

Above, we denoted the initial- and final-state CM-momenta by $\mathbf{p}_i$ and $\mathbf{p}_f$. Using rotational invariance and parity conservation we expand the T-matrix, which is a 4×4-matrix in Pauli-spinor space, into a complete set of Pauli-spinor invariants ([12, 27])

$$T = \sum_{i=1}^{8} T_i(\mathbf{p}_f^2, \mathbf{p}_i^2, \mathbf{p}_i \cdot \mathbf{p}_f) \, P_i \, . \qquad (2.8)$$

Introducing

$$\mathbf{q} = \frac{1}{2}(\mathbf{p}_f + \mathbf{p}_i), \qquad \mathbf{k} = \mathbf{p}_f - \mathbf{p}_i, \qquad \mathbf{n} = \mathbf{p}_i \times \mathbf{p}_f = \mathbf{q} \times \mathbf{k} \qquad (2.9)$$

with , of course, $\mathbf{n} = \mathbf{q} \times \mathbf{k}$, we choose for the operators P_i in spin-space

$$P_1 = 1 \, , \qquad (2.10a)$$
$$P_2 = \boldsymbol{\sigma}_1 \cdot \boldsymbol{\sigma}_2 \, , \qquad (2.10b)$$
$$P_3 = (\boldsymbol{\sigma}_1 \cdot \mathbf{k})(\boldsymbol{\sigma}_2 \cdot \mathbf{k}) - \frac{1}{3}(\boldsymbol{\sigma}_1 \cdot \boldsymbol{\sigma}_2)\mathbf{k}^2 \, , \qquad (2.10c)$$
$$P_4 = \frac{i}{2}(\boldsymbol{\sigma}_1 + \boldsymbol{\sigma}_2) \cdot \mathbf{n} \, , \qquad (2.10d)$$
$$P_5 = (\boldsymbol{\sigma}_1 \cdot \mathbf{n})(\boldsymbol{\sigma}_2 \cdot \mathbf{n}) \, , \qquad (2.10e)$$
$$P_6 = \frac{i}{2}(\boldsymbol{\sigma}_1 - \boldsymbol{\sigma}_2) \cdot \mathbf{n} \, , \qquad (2.10f)$$
$$P_7 = (\boldsymbol{\sigma}_1 \cdot \mathbf{q})(\boldsymbol{\sigma}_2 \cdot \mathbf{k}) + (\boldsymbol{\sigma}_1 \cdot \mathbf{k})(\boldsymbol{\sigma}_2 \cdot \mathbf{q}) \qquad (2.10g)$$
$$P_8 = (\boldsymbol{\sigma}_1 \cdot \mathbf{q})(\boldsymbol{\sigma}_2 \cdot \mathbf{k}) - (\boldsymbol{\sigma}_1 \cdot \mathbf{k})(\boldsymbol{\sigma}_2 \cdot \mathbf{q}) \, . \qquad (2.10h)$$

Here we follow [12, 27], except that we have chosen here P_3 to be a purely 'tensor-force' operator.

Similarly to (2.9) the potentials are expanded as

$$V = \sum_{i=1}^{6} V_i(\mathbf{k}^2, \mathbf{q}^2) P_i \, . \qquad (2.11)$$

The potentials in configuration space are described in Pauli-spinor space as follows

$$V(r) = V_C(r) + V_\sigma(r)\boldsymbol{\sigma}_1 \cdot \boldsymbol{\sigma}_2 + V_T(r) \, S_{12} + V_{SLS}(r) \cdot$$
$$\times \mathbf{L} \cdot \mathbf{S}_+ + V_{ALS}(r) \, \mathbf{L} \cdot \mathbf{S}_- + V_Q(r) \, Q_{12} \, , (2.12)$$

where $\mathbf{S}_\pm = (\boldsymbol{\sigma}_1 \pm \boldsymbol{\sigma}_2)/2$, and see e.g. [12] for a definition of the operators S_{12} and Q_{12}.

III. CHANNELS, POTENTIALS, AND $SU(3)$ SYMMETRY

A. Channels and Potentials

On the physical particle basis, there are three charge NN-channels:

$$q = +2, +1, 0 : \quad pp \to pp \, , \, pn \to pn \, , \, nn \to nn. \qquad (3.1)$$

Similarly, there are four charge YN-channels:

$$\begin{aligned} q = +2: & \quad \Sigma^+ p \to \Sigma^+ p, \\ q = +1: & \quad (\Lambda p, \Sigma^+ n, \Sigma^0 p) \to (\Lambda p, \Sigma^+ n, \Sigma^0 p), \\ q = \;\;0: & \quad (\Lambda n, \Sigma^0 n, \Sigma^- p) \to (\Lambda n, \Sigma^0 n, \Sigma^- p), \\ q = -1: & \quad \Sigma^- n \to \Sigma^- n. \end{aligned} \qquad (3.2)$$

Like in [12, 13], the potentials are calculated on the isospin basis. For $S = 0$ nucleon-nucleon systems there are two isospin-channels, namely $I = 1$ and $I = 0$. For $S = -1$ hyperon-nucleon systems there are also two isospin channels: (i) $I = \frac{1}{2}$: $(\Lambda N, \Sigma N \to \Lambda N, \Sigma N)$, and (ii) $I = \frac{3}{2}$: $\Sigma N \to \Sigma N$.

For the OBE-part of the potentials the treatment of $SU(3)$ for the BBM interaction Lagrangians and the coupling coefficients of the OBE-graphs has been given in detail in previous work of the Nijmegen group, e.g. [12] and [13], For the TME- and the MPE-parts the calculation of the coupling coefficients has been exposed in our paper on the ESC04-model [6]. There we described the method of an automatic computerized calculation of these coefficients by exploiting the 'cartesian-octet'-representation.

Also in this work we do not solve the Lippmann-Schwinger equation, but the multi-channel Schrödinger equation in configuration space, completely analogous to [12]. The multichannel Schrödinger equation for the configuration-space potential is derived from the Lippmann-Schwinger equation through the standard Fourier transform, and the equation for the radial wave function is found to be of the form [12]

$$u_{l,j}'' + (p_i^2 \delta_{i,j} - A_{i,j})u_{l,j} - B_{i,j}u_{l,j}' = 0, \qquad (3.3)$$

where $A_{i,j}$ contains the potential, nonlocal contributions, and the centrifugal barrier, while $B_{i,j}$ is only present when non-local contributions are included. The solution in the presence of open and closed channels is given, for

example, in Ref. [28]. The inclusion of the Coulomb interaction in the configuration-space equation is well known and included in the evaluation of the scattering matrix.

The momentum space and configuration space potentials for the ESC-models have been described in paper I [5] for baryon-baryon in general. Here, we will only give the new contributions to these potentials, both in momentum and configuration space.

B. SU(3)-Symmetry and -Breaking, Form Factors

The treatment of the mass differences among the baryons is handled in the same way as for ESC04, which is exactly that of other Nijmegen models [12, 13, 25]. Also, exchange potentials related to strange meson exchange K, K^* etc. , can be found in these references.

The breaking of SU(3)-symmetry occurs in several places. The physical masses of the baryons and mesons are used. Noticable is the SU(2) $\subset$ SU(3) breaking due to $\Lambda - \Sigma^0$-mixing [29]. This $\Lambda - \Sigma^0$-mixing leads also to a non-zero coupling of the Λ to the other $I = 1$ mesons: $\rho(760), a_0(980), a_1(1270)$, as well as to the $I = 1$ pairs. For the details of these OBE-couplings see e.g. [13], equations (2.15)-(2.17). Like in ESC04, the corresponding so-called CSB-potentials are included in the ESC08-model for OBE, TME, and MPE.

The medium-strong SU(3)-symmetry breaking of the BBM-coupling constants is not tried in ESC08. In the ESC04-model this was considered optional, and regulated by the $^3P_0$-model by a differentiation between the $s\bar{s}$-quark pair and the creation of a non-strange quark-antiquark pair. Of course, we could contemplate about such an option here, but we did not investigate this option.

The baryon mass differences in the intermediate states for TME- and MPE- potentials have been neglected for YN-scattering. This, although possible in principle, becomes rather laborious and is not expected to change the characteristics of the baryon-baryon potentials much.

Also in this work, like ESC04- [5–7] and in the NSC97-models [13], the form factors depend on the SU(3) assignment of the mesons, In principle, we introduce form factor masses, i.e. cut-off's, Λ_8 and Λ_1 for the {8} and {1} members of each meson nonet, respectively. In the application to YN and YY, we could allow for SU(3)-breaking, by using different cut-offs for the strange mesons K, K^*, and κ. However, in the ESC08-model we do not exploit this possible breaking, but assign for the strange $I = 1/2$ mesons the same cut-off as for the $I = 1$ mesons. Moreover, for the $I = 0$ mesons we assign the cut-offs as if there were no meson-mixing. For example we assign Λ_1 for the dominant singlet mesons η', ω, ϵ, and Λ_8 for η, ϕ, S^*, etc. This means a very slight form of SU(3)-symmetry breaking.

IV. OBE-POTENTIALS IN ESC08

The OBE-potentials in ESC08 are those contained already in ESC04 [5, 6], and some new additional contributions. The additions to the OBE-potentials w.r.t. the ESC04-models consist of the following elements: (i) extension of the baryon-baryon-meson vertex of the axial-vector mesons ($J^{PC} = 1^{++}$) by adding the derivative coupling, (ii) inclusion of the axial-vector mesons of the 2nd kind, having $J^{PC} = 1^{+-}$. In paper I [1] the potentials for non-strange meson exchange have been given. Here, we list the additions and the basic potentials for meson exchange with non-zero strangeness.

A. Additions to the OBE-Potentials in ESC08

The interaction Hamiltonian densities for the new couplings are

a) Axial-vector-meson exchange ($J^{PC} = 1^{++}, 1^{st}$ kind):

$$\mathcal{H}_A = g_A[\bar{\psi}\gamma_\mu\gamma_5\psi]\phi_A^\mu + \frac{if_A}{\mathcal{M}}[\bar{\psi}\gamma_5\psi]\ \partial_\mu\phi_A^\mu. \qquad (4.1)$$

In ESC04 the g_A-coupling was included, but not the derivative f_A-coupling.

b) Axial-vector-meson exchange ($J^{PC} = 1^{+-}, 2^{nd}$ kind):

$$\mathcal{H}_B = \frac{if_B}{m_B}[\bar{\psi}\sigma_{\mu\nu}\gamma_5\psi]\ \partial_\nu\phi_B^\mu, \qquad (4.2)$$

where m_B is the mass $b_1(1235)$. In ESC04 this coupling was not included. Like for the axial-vector mesons of the 1st-kind we include a SU(3)-nonet with members $b_1(1235), h_1(1170), h'_1(1380)$. In the quark-model they are $Q\bar{Q}(^1P_1)$-states.

The inclusion of the gaussian form factors is discussed in previous papers [12] and reviewed in paper I. For the approximations made in deriving the potentials from the relativistic Born-Approximation we refer also to paper I. Due to these approximations the dependence on $\mathbf{q}^2$ is linearized and we write

$$V_i(\mathbf{k}^2, \mathbf{q}^2) = V_{ia}(\mathbf{k}^2) + V_{ib}(\mathbf{k}^2)\ \left(\mathbf{q}^2 + \frac{1}{4}\mathbf{k}^2\right)\ , \qquad (4.3)$$

where $i = 1 - 8$. The combination $(\mathbf{q}^2 + \mathbf{k}^2/4)$ leads to a purely non-local potential. The additional OBE-potentials are obtained in the standard way, see [11, 12]. We write the potential functions V_i of (2.11) in the form

$$V_i(\mathbf{k}^2, \mathbf{q}^2) = \sum_X \Omega_i^{(X)}(\mathbf{k}^2) \cdot \Delta^{(X)}(\mathbf{k}^2, m^2, \Lambda^2)\ , \qquad (4.4)$$

where m denotes the mass of the meson, Λ the cut-off in the gaussian form factor, and $X = P, V, S, A, B$, and

D (P= pseudoscalar, V= vector, S= scalar, A= axial-vector, B= axial-vector, and D = Pomeron/Odderon). For meson-exchange the propagator $\Delta^{(X)}$-function is

$$\Delta^{(X)}(\mathbf{k}^2, m^2, \Lambda^2) = e^{-\mathbf{k}^2/\Lambda^2}/(\mathbf{k}^2 + m^2). \qquad (4.5)$$

For X=S,A we have included in the propagator a zero by the factor $(1 - \mathbf{k}^2/U^2)$, with U=750 MeV [5, 6]. In the case X=D the propagator is replaced by

$$\Delta^{(D)}(\mathbf{k}^2, m^2, \Lambda^2) = \frac{1}{\mathcal{M}^2} e^{-\mathbf{k}^2/4m_D^2}. \qquad (4.6)$$

Here, $\mathcal{M}$ is a universal scaling mass, taken to be the proton mass, which we also use in the derivative couplings above, as well as in the f_V- and f_A-coupling of the vector-mesons.

B. Meson-exchange with Non-zero Strangeness ($\Delta Y \neq 0$)

For the non-strange mesons the mass differences at the vertices are neglected, we take at the YYM- and the NNM-vertex the average hyperon and the average nucleon mass respectively. This implies that we do not include contributions to the Pauli-invariants P_7 and P_8. These exchanges lead to the so-called 'exchange-potentials'. For the invariants $O_1, \ldots, O_6$, the expressions analogous to those for the non-strange mesons given above apply. This with the amendments that (i) in momentum and configuration space there is a complete symmetric appearance of M_Y and M_N, (ii) in configuration space there appears the baryon-exchange operator $\mathcal{P} = -\mathcal{P}_x \, \mathcal{P}_\sigma$ operator, and (iii) for the antisymmetric spin-orbit potential $\mathcal{P} \to \mathcal{P}_x$. The details are given in Appendix C. Therefore, the $\Omega_i^{(X)}$ for these potentials can be obtained from those given in paper I Eqs. (4.14)-(4.18), by replacing both M_Y and M_N by $(M_Y M_N)^{1/2}$. Furthermore, in the case of the vector and axial-B mesons the Proca-formalism [30] is used, which gives for the vector mesons non-negligible contributions from the second part of the vector-meson propagator $(k_\mu k_\nu/m^2)$ of the K^* meson:

$$-V_i^{K^*} = V_i^{(V)} - \frac{(M_3 - M_1)(M_4 - M_2)}{m^2} V_i^{(S)}, \qquad (4.7)$$

where in $V_i^{(S)}$ the vector-meson-couplings have to be used, and M_Y and M_N must be replaced by $(M_Y M_N)^{1/2}$. In Eq. (4.7) $M_1 = M_4 = M_Y$ and $M_2 = M_3 = M_N$. For the axial-A mesons we use the B-field formalism, see paper I Appendix A, and there is no second-term in the propagator.

For the mesons with non-zero strangeness, K, K^*, κ, K_A and K_B, the mass differences at the vertices are not neglected, we take into account at the YNM-vertices the differences between the average hyperon and the average nucleon mass. This implies that we do include contributions to the Pauli-invariants P_8. There do not occur contributions to P_7. Furthermore, mass differences in the YN-propagation are included via a meson mass corrections in the strange-meson propagators.

(a) Pseudoscalar K-meson exchange:

$$\Omega_{2a}^{(P)} = -f_{13}^P f_{24}^P \left(\frac{\mathbf{k}^2}{3m_{\pi^+}^2} \right) \quad , \quad \Omega_{3a}^{(P)} = -f_{13}^P f_{24}^P \left(\frac{1}{m_{\pi^+}^2} \right), \qquad (4.8a)$$

$$\Omega_{2b}^{(P)} = +f_{13}^P f_{24}^P \left(\frac{\mathbf{k}^2}{6m_{\pi^+}^2} \right) \quad , \quad \Omega_{3b}^{(P)} = +f_{13}^P f_{24}^P \left(\frac{1}{2m_{\pi^+}^2 M_Y M_N} \right). \qquad (4.8b)$$

(b) Vector-meson K^*-exchange:

$$
\Omega_{1a}^{(V)} = \left\{ g_{13}^V g_{24}^V \left(1 - \frac{\mathbf{k}^2}{2M_Y M_N}\right) - (g_{13}^V f_{24}^V + f_{13}^V g_{24}^V) \frac{\mathbf{k}^2}{4\mathcal{M}\sqrt{M_Y M_N}} \right.
$$
$$
\left. + f_{13}^V f_{24}^V \frac{\mathbf{k}^4}{16\mathcal{M}^2 M_Y M_N} \right\} , \quad \Omega_{1b}^{(V)} = g_{13}^V g_{24}^V \left(\frac{3}{2M_Y M_N}\right),
$$

$$
\Omega_{2a}^{(V)} = -\frac{2}{3}\mathbf{k}^2 \, \Omega_{3a}^{(V)} , \quad \Omega_{2b}^{(V)} = -\frac{2}{3}\mathbf{k}^2 \, \Omega_{3b}^{(V)}
$$

$$
\Omega_{3a}^{(V)} = \left\{ (g_{13}^V g_{24}^V + (g_{13}^V f_{24}^V + g_{24}^V f_{13}^V) \frac{\sqrt{M_Y M_N}}{\mathcal{M}}) - f_{13}^V f_{24}^V \frac{\mathbf{k}^2}{8\mathcal{M}^2} \right\} /(4M_Y M_N)
$$

$$
\Omega_{3b}^{(V)} = -\left(g_{13}^V + f_{13}^V \frac{M_Y}{\mathcal{M}}\right)\left(g_{24}^V + f_{24}^V \frac{M_N}{\mathcal{M}}\right)/(8M_Y^2 M_N^2),
$$

$$
\Omega_{4}^{(V)} = -\left\{ 12 g_{13}^V g_{24}^V + 8(g_{13}^V f_{24}^V + f_{13}^V g_{24}^V)\frac{\sqrt{M_Y M_N}}{\mathcal{M}} - f_{13}^V f_{24}^V \frac{3\mathbf{k}^2}{\mathcal{M}^2} \right\} /(8M_Y M_N)
$$

$$
\Omega_{5}^{(V)} = -\left\{ g_{13}^V g_{24}^V + 4(g_{13}^V f_{24}^V + f_{13}^V g_{24}^V)\frac{\sqrt{M_Y M_N}}{\mathcal{M}} + 8 f_{13}^V f_{24}^V \frac{M_Y M_N}{\mathcal{M}^2} \right\} /(16M_Y^2 M_N^2)
$$

$$
\Omega_{6}^{(V)} = -\left\{ (g_{13}^V f_{24}^V - f_{13}^V g_{24}^V)\frac{1}{\sqrt{\mathcal{M}^2 M_Y M_N}} \right\}. \tag{4.9}
$$

(c) Scalar-meson κ-exchange:

$$
\Omega_{1a}^{(S)} = -g_{13}^S g_{24}^S \left(1 + \frac{\mathbf{k}^2}{4M_Y M_N}\right) , \quad \Omega_{1b}^{(S)} = +g_{13}^S g_{24}^S \frac{\mathbf{k}^2}{2M_Y M_N},
$$

$$
\Omega_{4}^{(S)} = -g_{13}^S g_{24}^S \frac{1}{2M_Y M_N}, \quad \Omega_{5}^{(S)} = g_{13}^S g_{24}^S \frac{1}{16M_Y^2 M_N^2}, \quad \Omega_{6}^{(S)} = 0. \tag{4.10}
$$

(d) Axial-vector K_{1A}-exchange $J^{PC} = 1^{++}$:

$$
\Omega_{2}^{(A)} = -g_{13}^A g_{24}^A \left[1 - \frac{2\mathbf{k}^2}{3M_Y M_N}\right] + \left[\left(g_{13}^A f_{24}^A + f_{13}^A g_{24}^A\right)\frac{\sqrt{M_Y M_N}}{\mathcal{M}} - f_{13}^A f_{24}^A \frac{\mathbf{k}^2}{2\mathcal{M}^2}\right] \frac{\mathbf{k}^2}{6M_Y M_N}
$$

$$
\Omega_{2b}^{(A)} = -g_{13}^A g_{24}^A \left(\frac{3}{2M_Y M_N}\right)
$$

$$
\Omega_{3}^{(A)} = -g_{13}^A g_{24}^A \left[\frac{1}{4M_Y M_N}\right] + \left[\left(g_{13}^A f_{24}^A + f_{13}^A g_{24}^A\right)\frac{\sqrt{M_Y M_N}}{\mathcal{M}} - f_{13}^A f_{24}^A \frac{\mathbf{k}^2}{2\mathcal{M}^2}\right] \frac{1}{2M_Y M_N}
$$

$$
\Omega_{4}^{(A)} = -g_{13}^A g_{24}^A \left[\frac{1}{2M_Y M_N}\right] , \quad \Omega_{5}^{(A)'} = -g_{13}^A g_{24}^A \left[\frac{2}{M_Y M_N}\right] , \quad \Omega_{6}^{(A)} = 0. \tag{4.11}
$$

Here, we used the B-field description with $\alpha_r = 1$, see paper I, Appendix A. The detailed treatment of the potential proportional to P_5', i.e. with $\Omega_5^{(A)'}$, is given in paper I, Appendix B.

(e) Axial-vector K_{1B}-exchange $J^{PC} = 1^{+-}$:

$$
\Omega_{2a}^{(B)} = +f_{13}^B f_{24}^B \frac{4M_N M_Y}{m_B^2} \left(1 - \frac{\mathbf{k}^2}{4M_Y M_N}\right)\left(\frac{\mathbf{k}^2}{12M_Y M_N}\right), \quad \Omega_{2b}^{(B)} = +f_{13}^B f_{24}^B \frac{4M_N M_Y}{m_B^2} \left(\frac{\mathbf{k}^2}{8M_Y^2 M_N^2}\right)
$$

$$
\Omega_{3a}^{(B)} = +f_{13}^B f_{24}^B \frac{4M_N M_Y}{m_B^2} \left(1 - \frac{\mathbf{k}^2}{4M_Y M_N}\right)\left(\frac{1}{4M_Y M_N}\right), \quad \Omega_{3b}^{(B)} = +f_{13}^B f_{24}^B \frac{4M_N M_Y}{m_B^2} \left(\frac{3}{8M_Y^2 M_N^2}\right), \tag{4.12}
$$

As in Ref. [12] in the derivation of the expressions for $\Omega_i^{(X)}$, given above, M_Y and M_N denote the mean hyperon and nucleon mass, respectively $M_Y = (M_1 + M_3)/2$ and $M_N = (M_2 + M_4)/2$, and m denotes the mass of the exchanged meson. Moreover, the approximation $1/M_N^2 + 1/M_Y^2 \approx 2/(M_N M_Y)$, is used, which is rather good since the mass differences between the baryons are not large.

C.   One-Boson-Exchange Interactions in Configuration Space I

In configuration space the BB-interactions are described by potentials of the general form

$$
V = \left\{ V_C(r) + V_\sigma(r)\boldsymbol{\sigma}_1 \cdot \boldsymbol{\sigma}_2 + V_T(r)S_{12} + V_{SO}(r)\mathbf{L}\cdot\mathbf{S} + V_Q(r)Q_{12} \right.
$$
$$
\left. + V_{ASO}(r)\frac{1}{2}(\boldsymbol{\sigma}_1 - \boldsymbol{\sigma}_2)\cdot\mathbf{L} - \frac{1}{2M_Y M_N}\left(\boldsymbol{\nabla}^2 V^{n.l.}(r) + V^{n.l.}(r)\boldsymbol{\nabla}^2\right) \right\} \cdot \mathcal{P}, \tag{4.13a}
$$

$$
V^{n.l.} = \left\{ \varphi_C(r) + \varphi_\sigma(r)\boldsymbol{\sigma}_1 \cdot \boldsymbol{\sigma}_2 + \varphi_T(r)S_{12} \right\}, \tag{4.13b}
$$

where

$$
S_{12} = 3(\boldsymbol{\sigma}_1 \cdot \hat{r})(\boldsymbol{\sigma}_2 \cdot \hat{r}) - (\boldsymbol{\sigma}_1 \cdot \boldsymbol{\sigma}_2), \tag{4.14a}
$$
$$
Q_{12} = \frac{1}{2}\left[(\boldsymbol{\sigma}_1 \cdot \mathbf{L})(\boldsymbol{\sigma}_2 \cdot \mathbf{L}) + (\boldsymbol{\sigma}_2 \cdot \mathbf{L})(\boldsymbol{\sigma}_1 \cdot \mathbf{L}) \right]. \tag{4.14b}
$$

For the basic functions for the Fourier transforms with gaussian form factors, we refer to Refs. [11, 12]. For the details of the Fourier transform for the potentials with P'_5, which occur in the case of the axial-vector mesons with $J^{PC} = 1^{++}$, we refer to paper I, Appendix B.

(a) Pseudoscalar-meson K-exchange:

$$
V_{PS}(r) = \frac{m}{4\pi}\left[f_{13}^P f_{24}^P \left(\frac{m^2}{m_{\pi^+}^2}\right)\left(\frac{1}{3}(\boldsymbol{\sigma}_1\cdot\boldsymbol{\sigma}_2)\,\phi_C^1 + S_{12}\phi_T^0\right) \right]\mathcal{P}, \tag{4.15a}
$$

$$
V_{PS}^{n.l.}(r) = -\frac{m}{4\pi}\left[f_{13}^P f_{24}^P \left(\frac{m^2}{2m_{\pi^+}^2}\right)\left(\frac{1}{3}(\boldsymbol{\sigma}_1\cdot\boldsymbol{\sigma}_2)\,\phi_C^1 + S_{12}\phi_T^0\right) \right]\mathcal{P}. \tag{4.15b}
$$

(b) Vector-meson K^*-exchange:

$$
V_V(r) = \frac{m}{4\pi}\left[\left\{ g_{13}^V g_{24}^V \left[\phi_C^0 + \frac{m^2}{2M_Y M_N}\phi_C^1\right] \right. \right.
$$
$$
+ (g_{13}^V f_{24}^V + f_{13}^V g_{24}^V)\frac{m^2}{4\mathcal{M}\sqrt{M_Y M_N}}\,\phi_C^1 + f_{13}^V f_{24}^V \frac{m^4}{16\mathcal{M}^2 M_Y M_N}\phi_C^2 \Bigg\}
$$
$$
+ \frac{m^2}{6M_Y M_N}\left\{\left[g_{13}^V g_{24}^V + (g_{13}^V f_{13}^V + g_{24}^V f_{13}^V)\frac{\sqrt{M_Y M_N}}{\mathcal{M}} + f_{13}^V f_{24}^V \frac{M_Y M_N}{\mathcal{M}^2}\right]\phi_C^1 + f_{13}^V f_{24}^V \frac{m^2}{8\mathcal{M}^2}\phi_C^2\right\}(\boldsymbol{\sigma}_1\cdot\boldsymbol{\sigma}_2)
$$
$$
- \frac{m^2}{4M_Y M_N}\left\{\left[g_{13}^V g_{24}^V + (g_{13}^V f_{24}^V + g_{24}^V f_{13}^V)\frac{\sqrt{M_Y M_N}}{\mathcal{M}}\right)\phi_T^0 + f_{13}^V f_{24}^V \frac{m^2}{8\mathcal{M}^2}\phi_T^1\right\}S_{12}
$$
$$
- \frac{m^2}{M_Y M_N}\left\{\left[\frac{3}{2}g_{13}^V g_{24}^V + (g_{13}^V f_{24}^V + f_{13}^V g_{24}^V)\frac{\sqrt{M_Y M_N}}{\mathcal{M}}\right]\phi_{SO}^0 + \frac{3}{8}f_{13}^V f_{24}^V \frac{m^2}{\mathcal{M}^2}\phi_{SO}^1\right\}\mathbf{L}\cdot\mathbf{S}
$$
$$
+ \frac{m^4}{16M_Y^2 M_N^2}\left\{\left[g_{13}^V g_{24}^V + 4(g_{13}^V f_{24}^V + f_{13}^V g_{24}^V)\frac{\sqrt{M_Y M_N}}{\mathcal{M}} + 8f_{13}^V f_{24}^V \frac{M_Y M_N}{\mathcal{M}^2}\right]\right\}\cdot
$$
$$
\left. \times \frac{3}{(mr)^2}\phi_T^0 Q_{12} + \frac{m^2}{M_Y M_N}\left\{(g_{13}^V f_{24}^V - f_{13}^V g_{24}^V)\frac{\sqrt{M_Y M_N}}{\mathcal{M}}\,\phi_{SO}^0\right\}\cdot\frac{1}{2}(\boldsymbol{\sigma}_1-\boldsymbol{\sigma}_2)\cdot\mathbf{L}\,\mathcal{P}_\sigma \right]\mathcal{P}, \tag{4.16a}
$$

$$
V_V^{n.l.}(r) = \frac{m}{4\pi}\left[\frac{3}{2}g_{13}^V g_{24}^V \phi_C^0 \right.
$$
$$
+ \frac{m^2}{6M_Y M_N}\left\{\left[\left(g_{13}^V + f_{13}^V \frac{\sqrt{M_Y M_N}}{\mathcal{M}}\right)\left(g_{24}^V + f_{24}^V \frac{\sqrt{M_Y M_N}}{\mathcal{M}}\right)\right]\phi_C^1\right\}(\boldsymbol{\sigma}_1\cdot\boldsymbol{\sigma}_2)
$$
$$
\left. - \frac{m^2}{4M_Y M_N}\left\{\left[\left(g_{13}^V + f_{13}^V \frac{\sqrt{M_Y M_N}}{\mathcal{M}}\right)\left(g_{24}^V + f_{24}^V \frac{\sqrt{M_Y M_N}}{\mathcal{M}}\right)\right]\phi_T^0\right\}S_{12} \right]. \tag{4.16b}
$$

(c) Scalar-meson κ-exchange:

$$
V_S(r) = -\frac{m}{4\pi}\left[g_{13}^S g_{24}^S \left\{\left[\phi_C^0 - \frac{m^2}{4M_Y M_N}\phi_C^1\right] + \frac{m^2}{2M_Y M_N}\phi_{SO}^0\,\mathbf{L}\cdot\mathbf{S} + \frac{m^4}{16M_Y^2 M_N^2}\frac{3}{(mr)^2}\phi_T^0 Q_{12}\right\} \right]\mathcal{P}, \tag{4.17a}
$$

$$
V_S^{n.l.}(r) = \frac{m}{4\pi}\left[\frac{1}{2}g_{13}^S g_{24}^S \phi_C^0 \right]\mathcal{P}. \tag{4.17b}
$$

(d) Axial-vector K_{1A}-meson exchange $J^{PC} = 1^{++}$:

$$V_A(r) = -\frac{m}{4\pi}\left[\left\{g_{13}^A g_{24}^A\left(\phi_C^0 + \frac{2m^2}{3M_Y M_N}\phi_C^1\right) + \frac{m^2}{6M_Y M_N}\left(g_{13}^A f_{24}^A + f_{13}^A g_{24}^A\right)\frac{\sqrt{M_Y M_N}}{\mathcal{M}}\phi_C^1\right.\right.$$

$$\left. + f_{13}^A f_{24}^A\frac{m^4}{12M_Y M_N \mathcal{M}^2}\phi_C^2\right\}(\boldsymbol{\sigma}_1 \cdot \boldsymbol{\sigma}_2)$$

$$- \frac{m^2}{4M_Y M_N}\left\{\left[g_{13}^A g_{24}^A - 2\left(g_{13}^A f_{24}^A + f_{13}^A g_{24}^A\right)\frac{\sqrt{M_Y M_N}}{\mathcal{M}}\right]\phi_T^0 - f_{13}^A f_{24}^A\frac{m^2}{2\mathcal{M}^2}\phi_T^1\right\}S_{12}$$

$$\left. + \frac{m^2}{2M_Y M_N}g_{13}^A g_{24}^A \phi_{SO}^0\ \mathbf{L}\cdot\mathbf{S}\right]\ \mathcal{P}, \tag{4.18a}$$

$$V_A^{n.l.}(r) = -\frac{m}{4\pi}\left[\frac{3}{2}g_{13}^A g_{24}^A \phi_C^0(\boldsymbol{\sigma}_1 \cdot \boldsymbol{\sigma}_2)\right]\ \mathcal{P}. \tag{4.18b}$$

(e) Axial-vector K_{1B}-meson exchange $J^{PC} = 1^{+-}$:

$$V_B(r) = -\frac{m}{4\pi}\frac{4M_N M_Y}{m^2}\left[f_{13}^B f_{24}^B\left\{\frac{m^2}{12M_Y M_N}\left(\phi_C^1 + \frac{m^2}{4M_Y M_N}\phi_C^2\right)\boldsymbol{\sigma}_1 \cdot \boldsymbol{\sigma}_2\right.\right.$$

$$\left.\left. + \frac{m^2}{4M_Y M_N}\left(\phi_T^0 + \frac{m^2}{4M_Y M_N}\phi_T^1\right)S_{12}\right\}\right]\ \mathcal{P}, \tag{4.19}$$

$$V_B^{n.l.}(r) = -\frac{m}{4\pi}\frac{3M_N M_Y}{2m^2}\left[f_{13}^B f_{24}^B\left(\frac{1}{3}(\boldsymbol{\sigma}_1 \cdot \boldsymbol{\sigma}_2)\ \phi_C^1 + S_{12}\phi_T^0\right)\right]\ \mathcal{P}. \tag{4.20}$$

(f) Diffractive-exchange: Since in the ESC08-model the diffractive Pomeron and Odderon exchanges are SU(3) singlets there are no contribution to $S \neq 0$-exchange potentials.

Above, in Eq.'s (4.15-4.20) the exchange operator is defined as

$$\mathcal{P} = -\mathcal{P}_x \mathcal{P}_\sigma, \tag{4.21}$$

where $\mathcal{P}_x$ and $\mathcal{P}_\sigma$ are the space- and spin-exchange operators respectively. The extra $(-\mathcal{P}_\sigma)$-operator in (4.16) for the antisymmetric spin-orbit potential is explained in Appendix C. We note that $-\mathcal{P}_\sigma \mathcal{P} = \mathcal{P}_x$, which is well defined for the coupled singlet-triplet systems.

D. One-Boson-Exchange Interactions in Configuration Space II

Here we give the extra potentials due to the zero's in the scalar and axial-A vector form factors:

a) Scalar-mesons:

$$\Delta V_S(r)\quad -\frac{m}{4\pi}\frac{m^2}{U^2}\left[g_{13}^S g_{24}^S\left\{\left[\phi_C^1 - \frac{m^2}{4M_Y M_N}\phi_C^2\right]\right.\right.$$

$$\left.\left. + \frac{m^2}{2M_Y M_N}\phi_{SO}^1\ \mathbf{L}\cdot\mathbf{S} + \frac{m^4}{16M_Y^2 M_N^2}\phi_T^1\ Q_{12}\right\}\right]\ \mathcal{P}. \tag{4.22}$$

b) Axial-mesons: The extra contribution to the potentials coming from the zero in the axial-vector meson form factor are obtained from the expression (4.11) by making substitutions as follows

$$\Delta V_A^{(1)}(r) = V_A^{(1)}\left(\phi_C^0 \to \phi_C^1, \phi_T^0 \to \phi_T^1, \phi_{SO}^0 \to \phi_{SO}^1\right)\cdot\frac{m^2}{U^2}. \tag{4.23}$$

Note that we do not include the similar $\Delta V_A^{(2)}(r)$ since they involve $\mathbf{k}^4$-terms in momentum-space. Then,

$$V_A^{(1)}(r) = -\frac{g_{13}^A g_{24}^A}{4\pi}\ m\left[\phi_C^0\ (\boldsymbol{\sigma}_1 \cdot \boldsymbol{\sigma}_2) - \frac{1}{12M_Y M_N}\left(\nabla^2\phi_C^0 + \phi_C^0\nabla^2\right)(\boldsymbol{\sigma}_1 \cdot \boldsymbol{\sigma}_2)\right.$$

$$+ \frac{3m^2}{4M_Y M_N}\ \phi_T^0\ S_{12} + \frac{m^2}{2M_Y M_N}\ \phi_{SO}^0\ \mathbf{L}\cdot\mathbf{S}$$

$$\left. + \frac{m^2}{4M_Y M_N}\frac{M_N^2 - M_Y^2}{M_Y M_N}\ \phi_{SO}^{(0)}\cdot\frac{1}{2}(\boldsymbol{\sigma}_1 - \boldsymbol{\sigma}_2)\cdot\mathbf{L}\right]\ \mathcal{P}. \tag{4.24}$$

E. PS-PS-exchange Interactions in Configuration Space

In Fig.'s 2 and 3 of paper I, the included two-meson exchange graphs are shown schematically. Explicit expressions for $K^{irr}(BW)$ and $K^{irr}(TMO)$ were derived [31], where also the terminology BW and TMO is explained. The TPS-potentials for nucleon-nucleon have been given in detail in [32]. The generalization to baryon-baryon is similar to that for the OBE-potentials. So, we substitute $M \to \sqrt{M_Y M_N}$, and include all PS-PS possibilities with coupling constants as in the OBE-potentials. As compared to nucleon-nucleon in [32] we have here in addition the potentials with double K-exchange. The masses are the physical pseudo-scalar meson masses. For the intermediate two-baryon states we take into account the effects of the different thresholds. We have not included uncorrelated PS-vector, PS-scalar, or PS-diffractive exchange. This because the range of these potentials is similar to that of the vector-,scalar-,and axial-vector-potentials. Moreover, for potentially large potentials, in particularly those with scalar mesons involved, there will be very strong cancellations between the planar- and crossed-box contributions.

F. MPE-exchange Interactions

In Fig. 4 of paper I the pair graphs are shown. In this work we include only the one-pair graphs. The argument for neglecting the two-pair graph is to avoid some 'double-counting'. Viewing the pair-vertex as containing heavy-meson exchange means that the contributions from $\rho(750)$ and $\epsilon = f_0(760)$ to the two-pair graphs is already accounted for by our treatment of the broad ρ and ϵ OBE-potential. The MPE-potentials for nucleon-nucleon have been given in Ref. [32]. The generalization to baryon-baryon is similar to that for the TPS-potentials. For the intermediate two-baryon states we neglect the effects of the different two-baryon thresholds. The inclusion of these, although in principle possible, would complicate the computation of the potentials considerably and the influence is not expected to be significant. The generalization of the pair-couplings to baryon-baryon is described in Ref. [6], section III. Also here in YN, we have in addition to [32] included the pair-potentials with KK-, KK*-, and Kκ-exchange. The convention for the MPE coupling constants is the same as in Ref. [32].

G. Meson-Pair Potentials, Axial-Pairs (2nd-kind, $J^{PC} = 1^{+-}$)

Recently we have completed the $1/M, 1/M^2$-corrections to the adiabatic approximation for the pair-potentials. The main reason is the need for a careful evaluation of the anti-symmetric spin-orbit terms

for ΛN, in particular for pair-interactions involving strangeness-exchange like $\pi - K, \pi - K^*$ etc. From this evaluation new contributions emerged, in particular for the axial pair-interactions $J^{PC} = 1^{++}, 1^{+-}$, leading to a substantial improvement w.r.t. experimental spin-orbit splittings [15]. In our fitting procedure for the YN-data the spin-orbit plays no role, therefore we will report on the details of the new spin-orbit terms in a separate paper [33]. However, also new $1/M$-corrections for the spin-spin and tensor potentials were obtained for the axial-pair interaction of the 2nd kind, i.e. $J^{PC} = 1^{+-}$. These are relevant for the fits presented in this paper, and will be given in this section. Below we give the full one-pair exchange potential as used at present, because it has not been published before. In the ESC04-models only the leading, i.e. the $(1/M)^0$-terms, were used. For the derivation of the soft-core pair-interactions we refer the reader to [32]. Below we report on this derivation for the axial-pair terms of the 2nd kind. The used pair-interaction Hamiltonian for e.g. the $(\pi\omega)$-pair is

$$\mathcal{H}_B = g_{(\pi\omega)}\bar\psi\gamma_5\sigma_{\mu\nu}\boldsymbol\tau\psi \cdot \partial^\nu \left(\boldsymbol\pi\, \phi_\omega^\mu\right)/(m_\pi\mathcal{M}) , \quad (4.25)$$

which gives the BBm_1m_2-vertex

$$\bar u(\mathbf{p}')\Gamma_B^{(2)} u(\mathbf{p}) = i\frac{g_{(\pi\omega)_1}}{m_\pi\mathcal{M}} \left[\left(\pm\omega_1 \pm \omega_2\right)\boldsymbol\sigma\cdot\boldsymbol\omega + \boldsymbol\sigma\cdot\mathbf{k}\,\omega^0\right] . \quad (4.26)$$

The full SU(3)-structure is given in [6], section IIIA. It is assumed that this pair-coupling is dominated by the SU(3)-octet symmetric coupling, and is given by the $SU(3)$-octet symmetric couplings Hamiltonian in terms of SU(2)-isospin invariants and SU(3) isoscalar-factors:

$$\begin{aligned}
\mathcal{H}_{B_8VP} = \frac{g_{B_8VP}}{\sqrt6} &\left\{ \frac{1}{2}\left[\left(\mathbf{B}_1^\mu\cdot\boldsymbol\rho_\mu\right)\eta_8 + \left(\mathbf{B}_1^\mu\cdot\boldsymbol\pi_\mu\right)\phi_8\right]\right. \\
&+\frac{\sqrt3}{4}\left[\mathbf{B}_1\cdot(K^{*\dagger}\boldsymbol\tau K) + h.c.\right] \\
&+\frac{\sqrt3}{4}\left[(K_1^\dagger\boldsymbol\tau K^*)\cdot\boldsymbol\pi + (K_1^\dagger\boldsymbol\tau K)\cdot\boldsymbol\rho + h.c.\right] \\
&-\frac{1}{4}\left[(K_1^\dagger\cdot K^*)\eta_8 + (K_1^\dagger\cdot K)\phi_8 + h.c.\right] \\
&\left.+\frac{1}{2}H^0\left[\boldsymbol\rho\cdot\boldsymbol\pi - \frac{1}{2}\left(K^{*\dagger}\cdot K + K^\dagger\cdot K^*\right) - \phi_8\eta_8\right]\right\}
\end{aligned}$$
$$(4.27)$$

Here, $\mathbf{B}_1 \sim \left[\bar\psi\gamma_5\boldsymbol\tau\sigma_{\mu\nu}\psi\right]$ etc. See for a definition of the octet-fields η_8, ϕ_8 in terms of the physical mesons [6]. From the pair-interaction Hamiltonian (4.27) one can easily read off the different meson-pairs that occur from the $J^{PC} = 1^{+-}$-vertex. In Appendix B we give the explicit potentials generated by the pair-interaction (4.27).

V.   SHORT-RANGE PHENOMENOLOGY

It is well known that the most extensive study of the baryon-baryon interactions using meson-exchange has difficulties to achieve sufficiently repulsive short-range interactions in two channels. Namely, (i) the $\Sigma^+ p(I = 3/2,{}^3S_1)$- and (ii) the $\Sigma N(I = 1/2,{}^1S_0)$-channel. The short-range repulsion in baryon-baryon comes in principle from two sources: (a) meson- and multi-gluon-exchange, and (b) the occurrence of forbidden states by the Pauli-principle, henceforth referred to as Pauli-repulsion or Quark-core. As for (a) in the ESC-model [5, 6] the short-range repulsion comes from vector-meson exchange and Pomeron/Odderon-exchange (i.e. multi-gluon). The possibility of mechanism (b) has been explored in the Quark-Cluster model. See the reviews [20, 21].

Analyzing the Pauli-repulsion in terms of the $SU_f(3)$-irreps we find that the "forbidden" $L = 0$ BB-states, which are classified in $SU_{fs}(6)$ by the [51]-irrep, indeed occur dominantly in the $SU_f(3)$-irreps $\{10\}$ and $\{8_s\}$. These $SU(3)$-irreps dominate the $\Sigma^+ p(I = 3/2,{}^3S_1)$- and the $\Sigma N(I = 1/2,{}^1S_0)$-states respectively. These facts open the possibility to incorporate the exceptionally strong Pauli-repulsion for these states by enhancing the Pomeron coupling in the ESC-approach to baryon-baryon. For the other BB-states the [51]-irrep is present also, but roughly with an equal weight as the [33]-irrep. Only in a few S=-2 channels,e.g. $\Xi N(I = 1, S = 0)$ there is a stronger presence of the irrep [51]. Therefore a slightly moderated $SU_f(3)$-singlet Pomeron-exchange can effectively take care of this Quark-core phenomenologically, together with multi-gluon-exchange effects.

A.   Relation $SU_f(3)$-irreps and $SU_{fs}(6)$-irreps Classification YN-states

In Table V A the $SU_f(3)$-contents of the NN and YN states are shown. In Table V A we show the the weights of the $SU(6)_{sf}$-irreps. These are taken from [20] Table I, where the $SU(6)_{fs}$-classifications are given. Analyzing now the $(\Lambda N, \Sigma N)$-system for $(S = 0, I = 1/2)$ we find from these tables

$$\begin{pmatrix} V_{\Lambda N,\Lambda N} \\ V_{\Sigma N,\Sigma N} \end{pmatrix} = \begin{pmatrix} \frac{1}{2} & \frac{1}{2} \\ \frac{17}{18} & \frac{1}{18} \end{pmatrix} \begin{pmatrix} V_{[51]} \\ V_{[33]} \end{pmatrix}$$
$$= \begin{pmatrix} \frac{9}{10} & \frac{1}{10} \\ \frac{1}{10} & \frac{9}{10} \end{pmatrix} \begin{pmatrix} V_{\{27\}} \\ V_{\{8_s\}} \end{pmatrix} . \quad (5.1)$$

1. From (5.1) we obtain by simple matrix operations the relation between the $SU(6)_{fs}$-irreps and the $SU(3)_f$-irreps, which read

$$\begin{pmatrix} V_{\{27\}} \\ V_{\{8_s\}} \end{pmatrix} = \begin{pmatrix} \frac{4}{9} & \frac{5}{9} \\ 1 & 0 \end{pmatrix} \begin{pmatrix} V_{[51]} \\ V_{[33]} \end{pmatrix} . \quad (5.2)$$

TABLE I: $SU(3)_f$-contents of the various potentials on the isospin basis.

Space-spin antisymmetric states ${}^1S_0,\ {}^3P,\ {}^1D_2,...$			
$NN \to NN$	$I = 1$	$V_{NN}(I = 1) = V_{27}$	
$\Lambda N \to \Lambda N$		$V_{\Lambda\Lambda}\left(I = \frac{1}{2}\right) = (9V_{27} + V_{8_s})/10$	
$\Lambda N \to \Sigma N$	$I = \frac{1}{2}$	$V_{\Lambda\Sigma}\left(I = \frac{1}{2}\right) = (-3V_{27} + 3V_{8_s})/10$	
$\Sigma N \to \Sigma N$		$V_{\Sigma\Sigma}\left(I = \frac{1}{2}\right) = (V_{27} + 9V_{8_s})/10$	
$\Sigma N \to \Sigma N$	$I = \frac{3}{2}$	$V_{\Sigma\Sigma}\left(I = \frac{3}{2}\right) = V_{27}$	
Space-spin symmetric states ${}^3S_1,\ {}^1P_1,\ {}^3D,...$			
$NN \to NN$	$I = 0$	$V_{NN}(I = 0) = V_{10^\star}$	
$\Lambda N \to \Lambda N$		$V_{\Lambda\Lambda}\left(I = \frac{1}{2}\right) = (V_{10^\star} + V_{8_a})/2$	
$\Lambda N \to \Sigma N$	$I = \frac{1}{2}$	$V_{\Lambda\Sigma}\left(I = \frac{1}{2}\right) = (V_{10^\star} - V_{8_a})/2$	
$\Sigma N \to \Sigma N$		$V_{\Sigma\Sigma}\left(I = \frac{1}{2}\right) = (V_{10^\star} + V_{8_a})/2$	
$\Sigma N \to \Sigma N$	$I = \frac{3}{2}$	$V_{\Sigma\Sigma}\left(I = \frac{3}{2}\right) = V_{10}$	

TABLE II: $SU(6)_{fs}$-contents of the various potentials on the spin,isospin basis.

	(S, I)	$V = aV_{[51]} + bV_{[33]}$
$NN \to NN$	$(0, 1)$	$V_{NN} = \frac{4}{9}V_{[51]} + \frac{5}{9}V_{[33]}$
$NN \to NN$	$(1, 0)$	$V_{NN} = \frac{4}{9}V_{[51]} + \frac{5}{9}V_{[33]}$
$\Lambda N \to \Lambda N$	$(0, 1/2)$	$V_{\Lambda\Lambda} = \frac{1}{2}V_{[51]} + \frac{1}{2}V_{[33]}$
$\Lambda N \to \Lambda N$	$(1, 1/2)$	$V_{\Lambda\Lambda} = \frac{1}{2}V_{[51]} + \frac{1}{2}V_{[33]}$
$\Sigma N \to \Sigma N$	$(0, 1/2)$	$V_{\Sigma\Sigma} = \frac{17}{18}V_{[51]} + \frac{1}{18}V_{[33]}$
$\Sigma N \to \Sigma N$	$(1, 1/2)$	$V_{\Sigma\Sigma} = \frac{1}{2}V_{[51]} + \frac{1}{2}V_{[33]}$
$\Sigma N \to \Sigma N$	$(0, 3/2)$	$V_{\Sigma\Sigma} = \frac{4}{9}V_{[51]} + \frac{5}{9}V_{[33]}$
$\Sigma N \to \Sigma N$	$(1, 3/2)$	$V_{\Sigma\Sigma} = \frac{8}{9}V_{[51]} + \frac{1}{9}V_{[33]}$

2. Also, we can read off from the tables the following relations

$$V_{NN}(I = 1, S = 0) = \frac{4}{9}V_{[51]} + \frac{5}{9}V_{[33]} = V_{\{27\}}, \quad (5.3a)$$

$$V_{NN}(I = 0, S = 1) = \frac{4}{9}V_{[51]} + \frac{5}{9}V_{[33]} = V_{\{10^*\}}, \quad (5.3b)$$

$$V_{\Lambda N}\left(I = \frac{1}{2}, S = 1\right) = \frac{1}{2}V_{[51]} + \frac{1}{2}V_{[33]}$$
$$= \frac{1}{2}V_{\{10^*\}} + \frac{1}{2}V_{\{8_a\}} . \quad (5.3c)$$

From these equations we can solve the $SU(3)_f$-irreps $\{27\}, \{10^*\}$, and $\{8_a\}$ in terms of the $SU(6)_{fs}$-irreps. Listing the results we now have

$$V_{\{27\}} = \frac{4}{9}V_{[51]} + \frac{5}{9}V_{[33]} , \quad (5.4a)$$

$$V_{\{10^*\}} = \frac{4}{9}V_{[51]} + \frac{5}{9}V_{[33]} , \quad (5.4b)$$

$$V_{\{10\}} = \frac{8}{9}V_{[51]} + \frac{1}{9}V_{[33]} , \quad (5.4c)$$

$$V_{\{8_a\}} = \frac{5}{9}V_{[51]} + \frac{4}{9}V_{[33]} , \quad (5.4d)$$

$$V_{\{8_s\}} = V_{[51]} . \quad (5.4e)$$

We see from these results that the [51]-irrep has a large weight in the $\{10\}$- and $\{8_s\}$-irrep, which gives an argument for the presence of a strong Pauli-repulsion in these $SU(3)_f$-irreps.

According to the study of the wide range of meson-exchange models in the last decade using the ESC-approach, as a working hypothesis, we assume that the apparent lack of an exceptionally strong repulsion in the ESC-model for the states in the $SU(3)_f$-irreps $\{10\}$ and $\{8_s\}$ cannot be cured by meson-exchange. The inclusion of this possible "forbidden state" effect can be done phenomenologically in the ESC-approach by making an effective Pomeron potential as the sum of 'pure' Pomeron exchange and of a Pomeron-like representation of the Pauli-repulsion. As a consequence the effective Pomeron potential gets quite stronger in the $SU(3)_f$-irreps $\{10\}$ and $\{8_s\}$. This way we incorporate the Pauli repulsion effect in the ESC-approach in this paper.

B. Parametrization Quark-core effects

1. Linear method: we split the repulsive short-range Pomeron-like NN potential as follows:

$$V_{PNN} = (1 - a_{PB})V_{PNN} + a_{PB}V_{PNN}$$
$$\equiv V_{NN}(POM) + V_{NN}(PB) \quad (5.5)$$

where $V_{NN}(POM)$ represents the genuine Pomeron and $V_{NN}(PB)$ the structural effects of the Quark-core forbidden [51]-configuration, i.e. a Pauli-blocking (PB) effect. So a_{PB} denotes the Quark-core fraction of the total

TABLE III: Effective Pomeron+PB contribution on the spin,isospin basis.

	(S, I)	V_{PBB}/V_{PNN}	ESC08c
$NN \to NN$	$(0, 1)$	1	1.000
$NN \to NN$	$(1, 0)$	1	1.000
$\Lambda N \to \Lambda N$	$(0, 1/2)$	$1 + \frac{1}{8}a_{PB}$	1.037
$\Lambda N \to \Lambda N$	$(1, 1/2)$	$1 + \frac{1}{8}a_{PB}$	1.037
$\Sigma N \to \Sigma N$	$(0, 1/2)$	$1 + \frac{9}{8}a_{PB}$	1.334
$\Sigma N \to \Sigma N$	$(1, 1/2)$	$1 + \frac{1}{8}a_{PB}$	1.037
$\Sigma N \to \Sigma N$	$(0, 3/2)$	1	1.000
$\Sigma N \to \Sigma N$	$(1, 3/2)$	$1 + a_{PB}$	1.297

Pomeron-like potential. A similar relation holds for all BB channels.

$$V_{PBB} = (1 - a_{PB})V_{PBB} + a_{PB}V_{PBB}$$
$$\equiv V_{BB}(POM) + V_{BB}(PB) \quad (5.6)$$

Since the Pomeron is a unitary-singlet its contribution is the same for all BB-channels (apart from some small baryon mass breaking effects). The PB-effect for the BB-channels is assumed to be proportional to the relative weight of the forbidden [51]-configuration compared to its weight in NN

$$V_{BB}(PB) = (w_{BB}[51]/w_{NN}[51]) \cdot V_{NN}(PB) \quad (5.7)$$

Then we have

$$V_{PBB} = (1 - a_{PB})V_{PNN} + a_{PB}\left(\frac{w_{BB}[51]}{w_{NN}[51]}\right) \cdot V_{PNN} \quad (5.8)$$

For example, in the SU(3)-irrep $\{10\}$, e.g. the $\Sigma^+ p(^3S_1, T = 3/2)$-channel, one has $w_{BB}[51] = 8/9 = 2w_{NN}[51]$ and therefore $V_{10}(PB) = 2V_{NN}(PB)$. Consequently, the total short-range repulsive potential, i.e. the 'effective Pomeron', becomes $V_{10} = (1 - a_{PB})V_{PNN} + 2a_{PB}V_{PNN} = (1 + a_{PB})V_{PNN}$. In Table V B we give the factors for the various S=0 and S=-1 BB channels as well as the results in the ESC08c model.

In principle one might choose a different mass for the Quark-core repulsive potential. However, this extra parameter does not lead to better fits to NN and/or YN. Therefore we keep for the Pauli-blocking the same mass as the Pomeron mass. The value of the PB factor a_{PB} is searched in the fit to the YN-data. The S=-2 PB effects are then also entirely determined. In the case of the models ESC08a' and ESC08b' only the channels

where $w_{BB}[51]$ is conspicuously large are treated approximately this way, but with equal weights. These channels are: $\Sigma^+ p(^3S_1, T = 3/2), \Sigma N(^1S_0, T = 1/2)$, and $\Xi N(^1S_0, T = 1)$. A subtle treatment of *all* BB channels according to this linear scheme is characteristic for the ESC08c-model. The parameter a_{PB} turns out to be about 30%. This means that the Quark-core repulsion is roughly 43% of the genuine Pomeron repulsion. Around r=0 the Quark-core repulsion comes out at 102 MeV, whereas the pure Pomeron repulsion is 240 MeV.

2. Non-linear method: we introduce next to the fraction parameter a_{PB} a nonlinear function $f(w_{BB}[51])$ in (5.6) by writing

$$V_{BB} = (1 - a_{PB})V_{PNN} + a_{PB}f(w_{BB}[51])V_{PNN} \quad (5.9)$$

with the requirement that $f(w_{NN}[51]) = 1$. Such a scheme is more flexible than the linear method. For example, by taking a steeper function than the linear function for arguments larger than $w_{NN}[51]$ one could reduce the PB-effects for small $w_{BB}[51]$ values like in ΛN or ΞN) and at the same time one could preserve a strong PB-effect in the $\{10\}$-irrep having $f(w_{10}[51])$ around 2. Therefore starting from the ESC08c solutions alternative YN/YY solutions can be obtained easily. As an example one could take the function $f(w_{BB}[51]) = \tan(\varphi_{BB})$ with $\varphi_{NN} = 45^o$. Taking for $\arctan(\varphi_{10}) = 2$ one recovers the same $V_{10}(PB)$ as in the linear scheme above. Exploiting the weights $w_{BB}[51]$ by parametrizing φ_{BB} in the following way

$$\varphi_{BB} = \left(\frac{w_{BB}[51] - w_{NN}[51]}{w_{10}[51] - w_{NN}[51]} \right) \cdot (\varphi_{10} - \varphi_{NN}) + \varphi_{NN}. \quad (5.10)$$

one gets the same PB-repulsion for $\Sigma^+ p(^3S_1, T = 3/2)$ as in the linear method, but smaller PB-repulsions in the ΛN and ΞN channels.

However, given the present experimental $\Sigma^+ p$ X-sections and the constraint for the $\Sigma^+ P(^1S_0)$ from SU(3)-symmetry, the non-linear prescription does not lead to different results than the linear one. Hence, in this work we use only the linear scheme.

VI. ESC08: FITTING $NN \oplus YN \oplus YY$-DATA

In this section we describe mainly the recent changes in the fitting process. For details on the standard NN⊕YN-fitting we refer to [13].

(i) As usual we fit to the 1993 Nijmegen representation of the χ^2-hypersurface of the NN scattering data below $T_{lab} = 350$ MeV [34, 35]. The NN low-energy parameters are fitted along with the scattering data. In order to accomodate the differences between the $^1S_0$-waves for pp, np, and nn in the model, we introduce some charge independence breaking by taking different electric ρ-couplings $g_{pp\rho} \neq g_{np\rho} \neq g_{nn\rho}$, where $g_{nn\rho}$ is considered to be the $SU(3)$-octet coupling. With this phenomenological device we fit the difference between the $^1S_0(pp)$ and $^1S_0(np)$ phases, and the different NN scattering lengths and effective ranges very well. We have found $g_{pp\rho} = 0.6330$, $g_{np\rho} = 0.5841$, which are not far from $g_{nn\rho} = 0.6343$ (cfr.Table V).

(ii) Simultaneously we fit to 52 YN scattering data. These data consist of the usual set of 35 low-energy YN-data, as used in [12, 13] and [6] plus 3 total $\Sigma^+ p$ X-sections from the recent KEK-experiment E289 [36] and some Λp elastic and inelastic data Ref. [37] and $\Sigma^- p$ elastic data at higher energies Ref. [38]. For the total $\Sigma^+ p$ and $\Sigma^- p$ elastic X-sections we have performed the same redefinition as eq. (6.3) of [13].

(iii) A novel feature in the simultaneous fitting procedure is the inclusion of constraints from information derived from hypernuclei and hypernuclear matter. For the ΛN-interaction this means not only a) the usual absence of bound states but also b) the requirement of a sizable spin-splitting leading to $U_{\sigma\sigma} > 1$ (cfr. section VII A). c) Because of the experimental absence of Σ-hypernuclei we require the total single particle Σ-potential in nuclear matter U_Σ to be overall repulsive. In the S=-2 channels there are two clear experimental indications: d) from the analysis of the Nagara event [39] of the double-Λ hypernucleus $^6_{\Lambda\Lambda}$He it appears that the forces in the $\Lambda\Lambda(^1S_0)$-channel are weakly attractive, indicated by a scattering length $a_{\Lambda\Lambda}(^1S_0) > -1$ fm [40]. This evidence has been incorporated in the fit in the form of 'pseudo-data' for the $(^1S_0)\Lambda\Lambda$ scattering length $a_{\Lambda\Lambda} = -0.8 \pm (0.2 - 0.4)$. the error depending on the desired impact in the fitting process. e) Experimentally the Ξ-nucleus interaction seems to be attractive from analyses of events with twin-Λ hypernuclei in emulsion data, where the initial Ξ^- energies were determined after $\Xi^- p - \Lambda\Lambda$ conversion in nuclei. The Ξ-nucleus interaction can be described well with a Wood-Saxon potential with a depth of ≈ 14 MeV [41]. As a consequence we require the total single particle Ξ-potential in nuclear matter U_Ξ to be overall attractive. We calculate U_Ξ with the G-matrix formalism (cfr. section X). It appears that in the ESC08 model the $\Xi N(^3S_1, T = 1)$ channel is quite sensitive to variation of the coupling constants, whereas the other s- and p-wave contributions have rather shallow dependencies. The total sum of the contributions of the other $T = 0$ and $T = 1$ s- and p-waves to U_Ξ is $\approx +4$ MeV. In order to ensure a clearly total attractive U_Ξ we add 'pseudo-data' for the $\Xi N(^3S_1, T = 1)$ contribution $U_\Xi(^3S_1, T = 1) = -12 \pm (2-4)$, the error depending on the desired impact in the fitting process. In practice this particular partial wave channel plays a very important role in the simultaneous fitting of the total BB-description. The fit has resulted in an excellent simultaneous $NN \oplus YN \oplus YY$-fit. We obtained for the NN-data $\chi^2/Ndata = 1.087$ with also very good results for the NN low energy parameters: the deuteron binding energy and the pp, np and nn scattering lengths and effective ranges. For the YN-data $\chi^2/YN_{data} = 1.09$. The ESC08 fits were achieved with only physical meson-coupling parameters, which are partial-wave independent. The quality

of the NN-fit is at par with models of Reid-like potentials like the Nijm93, Nijm I, and II, which are effective NN-potentials with some meson parameters adjusted per partial wave [42, 43]. Since the ESC08-model is an extension of the ESC04-model, it is not surprising that in the simultaneous NN-, YN and YY fit the OBE-couplings could be kept in line with the 'naive' predictions of the QPC-model [5, 9]. Just as in ESC04 most of the $F/(F + D)$-ratios are fixed by QPC, both for the OBE and MPE couplings. Once more we stress the fact that the in the simultaneous fit of the NN-, YN- and YY-data, a *single set of parameters* was used. Of course, the accurate and very numerous NN-data put strong constraints on the parameters. However, the YN-data, plus the constraints for the YN- and YY- channels, are also quite relevant for the set of parameters finally obtained. In particular, certain fitted $F/(F + D)$-ratios, are obviously influenced by the YN-data. The requirement of an overall attractive U_Ξ results in the model always in the occurrence of a bound state in $\Xi N(^3S_1, T = 1)$-channel with a binding energy of ≈ 1.3 MeV.

A.   Coupling Parameters and $NN \oplus YN \oplus YY$ Fit

The treatment of the broad mesons ρ and ϵ is as usual in the Nijmegen models. For the ρ-meson the same parameters are used in the OBE-models [11, 12]. For the $\epsilon = f_0(760)$ assuming $m_\epsilon = 760$ MeV and $\Gamma_\epsilon = 640$ MeV we use the Bryan-Gersten parametrization [44]. For the choosen mass and width they are: $m_1 = 496.39796$ MeV, $m_2 = 1365.59411$ MeV, and $\beta_1 = 0.21781, \beta_2 = 0.78219$. For the 'diffractive' 0^{++}-exchanges we restrict ourselves to the SU(3)-singlet part, henceforth referred to as 'Pomeron'. The possible J=0 part of the tensor-meson exchange [11, 12] is not considered. The 'mass' parameter of the Pomeron is fitted to be $m_P = 223.12$ MeV. The 'diffractive' 1^{--}-exchange 'Odderon' is also an SU(3)-singlet with a fitted mass $m_O = 270.48$ MeV.

Summarizing the fitted parameters in ESC08c we have:

1. Meson-couplings: $f_{NN\pi}, f_{NN\eta'}, g_{NN\rho}, g_{NN\omega}$, $f_{NN\rho}, f_{NN\omega}, g_{NNa_0}, g_{NN\epsilon}$, $g_{NNa_1}, f_{NNa_1}, g_{NNf'_1}, f_{NNf'_1}, f_{NNb_1}, f_{NNh'_1}$

2. Pair couplings: $g_{NN(\pi\pi)_1}, f_{NN(\pi\pi)_1}, g_{NN(\pi\rho)_1}$, $g_{NN\pi\omega}, g_{NN\pi\eta}, g_{NN\pi\epsilon}$

3. Diffractive-couplings/masses: $g_{NNP}, g_{NNO}, f_{NNO}, a_{PB}, m_P, m_O$

4. $F/(F + D)$-ratio's: α_V^m, α_A

5. Cut-off masses: $\Lambda_8^P = \Lambda_1^P, \Lambda_8^V, \Lambda_1^V, \Lambda_8^S, \Lambda_1^S$, $\Lambda_8^A = \Lambda_1^A$

These are in total 34 physical parameters, of which are (i) 14 meson-couplings, (ii) 2 $F/(F + D)$-ratio's, (iii) 4 'diffractive' couplings and 2 mass parameters, (iv) 6 meson-pair couplings, and (v) 6 cut-off mass parameters.

As compared to the ESC04-model, we have added in ESC08 the following fitting parameters: (i) the derivative axial-couplings $f_{NNa_1}, f_{NNf'_1}$, (ii) the 1^{+-} axial-couplings $f_{NNb_1}, f_{NNh'_1}$, (iii) the Odderon-couplings g_{NNO}, f_{NNO}, and mass m_O (iv) the Pomeron Pauli-blocking parameter a_{PB}, i.e. 8 new physical parameters. All new parameters have been explained above. They introduce new dynamical refinements/effects into the model, which have resulted in a quality of the combined NN+YN+YY fit for the NN-phases equal to those of a purely NN-fit. Some other parameters have been set, like e.g. many $F/(F + D)$-ratio's, see below, and a few cut-off parameters.

The pair coupling $g_{NN(\pi\pi)_0}$ is set to be zero, which is motivated in the Nijmegen soft-core models in view of the fact that in πN it is constrained by chiral-symmetry. In the fitting process we look for solutions which have meson-couplings which are reasonably close to the 'naive' predictions of the QPC-model. This is also the case for the $F/(F + D)$-ratio's, both for meson- and for pair-couplings. During the fitting we experienced a rather shallow dependence on the $F/(F + D)$-ratio α^P for the pseudoscalar octet. In fact we could obtain a very good YN and NN fit in a values range 0.33-0.40. Therefore we have fixed it on the value $\alpha_P = 0.365$ obtained from the Cabibbo theory of semileptonic decay of baryons [49]. Furthermore, the meson-pair couplings turn out to come out rather close to predictions based on the 'heavy-meson-saturation'-model. So, the fit-parameters are (i) physical parameters, i.e. they can be checked in other reactions, and (ii) many are 'constraint' by the QPC-model.

In this work like in the ESC04-models [5, 6], the form factors depend on the SU(3) assignment of the mesons, In principle, we introduce form factor masses Λ_8 and Λ_1 for the {8} and {1} members of each meson nonet, respectively. Moreover, for the $I = 0$-mesons we assign the {1} cut-off to the dominant singlet meson and the {8} cut-off to the dominant octet meson, as if there were no meson-mixing. For example we assign Λ_1 to η', ω, ϵ, and Λ_8 to η, ϕ, S^*, etc. Notice that the strange octet-mesons K etc. are given the same {8} form factors as their non-strange companions. For the cut-off masses Λ we used as free search parameters $\Lambda_8^P = \Lambda_1^P$ for the pseudoscalar mesons, Λ_8^V and Λ_1^V for the vector mesons and Λ_8^S and Λ_1^S for the scalar mesons. Furthermore, we finally used $\Lambda_8^A = \Lambda_1^A$ for the axial-mesons with $J^{PC} = 1^{++}$. For the axial-mesons with $J^{PC} = 1^{+-}$ (B-mesons) the cut-off masses have been set equal to those of the pseudoscalar mesons $\Lambda_8^B = \Lambda_8^P$ and $\Lambda_1^B = \Lambda_1^P$. Some of the previous {8} and {1} form factors have been chosen to be equal as a consequence of the impossibility to distinguish them in the fitting process.

Similar to ESC04 we introduce a zero in the form factors of mesons, which are P-wave bound states in a $q\bar{q}$-picture. These are the scalar mesons ($^3P_0$) and the axial-vector ($^3P_1$) mesons. Like in ESC04, we use a fixed

TABLE IV: Meson couplings and parameters employed in the ESC08c-potentials. Coupling constants are at $\mathbf{k}^2 = 0$. An asterisk denotes that the coupling constant is constrained via SU(3). The masses and Λ's are given in MeV. Note that the B-meson couplings are scaled with m_{B_1}. The mesons with strangeness are the (i) pseudoscalar $K(495.8)$, (ii) vector $K^*(892.6)$, (iii) scalar $\kappa(841)$, (iv) axial $K_{1A}(1273)$ and $K_{1B}(1400)$, with masses as indicated in the parentheses. The $K_{1A}(1273)$ and the $K_{1B}(1400)$ have a mixing of 45° and therefore we used the average mass 1336 MeV, which is an excellent approximation.

meson	mass	$g/\sqrt{4\pi}$	$f/\sqrt{4\pi}$	Λ
π	138.04		0.2687	1029.42
η	547.45		0.1314^*	,,
η'	957.75		0.2519	,,
ρ	768.10	0.6343	3.8307	688.40
ϕ	1019.41	-1.2915^*	3.1377^*	,,
ω	781.95	3.3692	-0.7683	771.32
a_1	1270.00	-0.8168	2.5849	1076.56
f_1	1420.00	0.6826^*	1.3884^*	,,
f_1'	1285.00	-0.7687	-0.5448	,,
b_1	1235.00		-1.7670	1029.42
h_1	1380.00		-0.2684^*	,,
h_1'	1170.00		-0.6768	,,
a_0	962.00	0.6351		893.53
f_0	993.00	-1.5129^*		,,
ε	760.00	4.0454		1136.10
Pomeron	223.12	3.3267		
Odderon	270.48	4.3575	-4.1556	

zero by taking $U = 750$ MeV in (4.22) and (4.24).

VII. COUPLING CONSTANTS, $F/(F + D)$ RATIOS, AND MIXING ANGLES

Like in ESC04, we constrained the OBE-couplings by the 'naive' predictions of the QPC-model [8]. We kept during the searches all OBE-couplings in the neighborhood of these predictions, but less tight than in ESC04. The same holds for the searched $\alpha = F/(F + D)$-ratios, i.e. for the BBM-couplings and the BB-Pair-couplings. In fact only two meson-coupling $F/(F + D)$-ratio's were allowed to vary during the searches: α_V^m for the vector mesons, and α_A for the axial-vector mesons. As mentioned above α_P was kept at the fixed value $\alpha_P = 0.365$. Furthermore we kept $\alpha_V^E = 1$ and $\alpha_S = 1$ at their QPC values. The input and fitted values are displayed in Table V.
The mixing angles for the various meson nonets are discussed in paper I. The used values can be found in Table V. For completeness we reproduce in Table IV the fitted ESC08c NN meson couplings and cut-off masses from paper I. Here we discuss only aspects specific for the YN-channels. In Table V the ESC08 $SU(3)$ singlet and octet couplings $g/\sqrt{4\pi}$ are listed, the $F/(F + D)$-ratios and the used mixing angles.
In Table VI we list the couplings of the physical mesons to the nucleons $(Y = 1)$, and to the hyperons with $Y = 0$ or $Y = -1$. These were calculated using unbroken SU(3)-symmetry. Next to the values in the table we have incorporated, like in the ESC04 model [6], Charge Symmetry Breaking (CSB) between Λp and Λn with nonzero Λ-couplings of the I=1 mesons and I=1 pairs due to $\Lambda - \Sigma^0$ mixing.

In Table VII we present the fitted Pair-couplings for the MPE-potentials. We recall that only One-pair graphs are included, in order to avoid double counting, see paper I. The $F/(F + D)$-ratios are all fixed, assuming heavy-boson dominance of the pair-vertices. The ratios are taken from the QPC-model for $q\bar{q}$-systems with the same quantum numbers as the dominating boson. Only the ratio in the system with the pseudoscalar quantum numbers deviates slightly from QPC, since it has been set equal to the value of $\alpha_P = 0.365$. The BB-Pair couplings are calculated, assuming unbroken $SU(3)$-symmetry, from the NN-Pair coupling and the $F/(F + D)$-ratio using $SU(3)$.
Unlike in [32], we did not fix pair couplings using a theoretical model, based on heavy-meson saturation and chiral-symmetry. So, in addition to the 14 coupling parameters used in [32] we now have 6 pair-coupling fit parameters. In Table VII the fitted pair-couplings are given, and in Appendix A the SU(3)-structure of the pair-couplings. As noted in paper I the $(\pi\pi)$-coupling gets a non-zero contribution from the $\{8_s\}$ pairs, giving $g_{(\pi\pi)_0} = -1.18/2 = -0.59$, which is opposite to that of [32]. Also the $f_{(\pi\pi)_1}$-pair coupling has an opposite sign as compared to [32]. In a model

TABLE V: ESC08c SU(3) coupling constants, $F/(F+D)$-ratio's, mixing angles etc. The values with $\star$) have are theoretical input or determined by the fitting and the constraint from the YN-analysis.

mesons		{1}	{8}	$F/(F+D)$	angles
ps-scalar	f	0.2750	0.2687	$\alpha_P = 0.365^{*)}$	$\theta_P = -13.00^{0\ *)}$
vector	g	3.4369	0.6343	$\alpha_V^e = 1.0^{*)}$	$\theta_V = 38.70^{0\ *)}$
	f	-2.5614	3.8307	$\alpha_V^m = 0.4744$	
axial(A)	g	-1.0171	-0.8168	$\alpha_A = 0.3296$	$\theta_A = +50.00^{0\ *)}$
	f	-1.4137	2.5849	$\alpha_A^p = 0.3296^{*)}$	
axial(B)	f	-0.3988	-1.7665	$\alpha_B = 0.40^{*)}$	$\theta_B = 35.26^{0\ *)}$
scalar	g	4.1766	0.6351	$\alpha_S = 1.00^{*)}$	$\theta_S = 35.26^{0\ *)}$
diffractive	g_P	3.3267			$a_{PB} = 0.2970$
	g_O	4.3575			
	f_O	-4.1556			

TABLE VI: Coupling constants for model ESC08c, divided by $\sqrt{4\pi}$. M refers to the meson. The coupling constants are listed in the order pseudoscalar, vector (g and f), axial vector A (g and f), scalar, axial vector B, and diffractive.

	M	NNM	$\Sigma\Sigma M$	$\Sigma\Lambda M$	$\Xi\Xi M$	M	ΛNM	$\Lambda\Xi M$	ΣNM	$\Sigma\Xi M$
f	π	0.2687	0.1962	0.1970	-0.0726	K	-0.2684	0.0714	0.0726	-0.2687
g	ρ	0.6343	1.2686	0.0000	0.6343	K^*	-1.0986	1.0986	-0.6343	-0.6343
f		3.8307	3.6200	2.3333	-0.2107		-4.3017	1.9684	0.2107	-3.8307
g	a_1	-0.8168	-0.5384	-0.6323	0.2784	K_{1A}	0.7824	-0.1501	-0.2784	0.8168
f		2.5849	1.7039	2.0011	-0.8810		-2.4761	0.4751	0.8810	-2.5849
g	a_0	0.6351	1.2702	0.0000	0.6351	κ	-1.1001	1.0001	-0.6351	-0.6351
f	b_1	-1.7665	-1.4132	-1.2239	0.3533	K_{1B}	1.8358	-0.6119	-0.3533	1.7665
	M	NNM	$\Lambda\Lambda M$	$\Sigma\Sigma M$	$\Xi\Xi M$	M	NNM	$\Lambda\Lambda M$	$\Sigma\Sigma M$	$\Xi\Xi M$
f	η	0.1314	-0.1301	0.2539	-0.1997	η'	0.2519	0.3123	0.2236	0.3283
g	ω	3.3691	2.6823	2.6823	1.9954	ϕ	-1.2915	-2.1489	-2.1489	-3.0063
f		-0.7683	-3.4579	-0.5401	-4.6886		3.1377	-0.2195	3.4225	-1.7557
g	f_1'	-0.7687	-0.1694	-1.1381	-0.0544	f_1	0.6826	1.1855	0.3727	1.2820
f		-0.5448	-2.4416	-0.6242	-2.8056		1.3884	-0.2033	2.3692	-0.5086
g	ε	4.0454	3.4104	3.4104	2.7753	f_0	-1.5129	-2.4111	-2.4111	-3.3093
f	h_1'	-0.6788	0.3810	-1.0321	0.7342	h_1	-0.2695	1.2295	-0.7692	1.7292
g	P	3.3267	3.3267	3.3267	3.3267					
g	O	4.3575	4.3575	4.3575	4.3575					
f		-4.1556	-4.1556	-4.1556	-4.1556					

with a more complex and realistic meson-dynamics [45] this coupling is predicted as found in the present ESC-fit. The $(\pi\rho)_1$-coupling agrees nicely with A_1-saturation, see [32]. The pair-couplings are used in a phenomelogical way in the ESC-approach. They are in general not yet quantitatively understood, and certainly deserve more study in the future.

The ESC-model described here, is fully consistent with $SU(3)$-symmetry using a straightforward extension of the NN-model to YN and YY. For example $g_{(\pi\rho)_1} = g_{A_8VP}$, and besides $(\pi\rho)$-pairs one sees also that $KK^*(I = 1)$- and $KK^*(I = 0)$-pairs contribute to the $N\bar{N}$ potentials. All $F/(F+D)$-ratio's are taken fixed with heavy-meson

TABLE VII: Pair-meson coupling constants employed in the ESC08c MPE-potentials. Coupling constants are at $\mathbf{k}^2 = 0$. The F/(F+D)-ratio are QPC-predictions, except that $\alpha_{(\pi\omega)} = \alpha_P$, which is very close to QPC.

J^{PC}	$SU(3)$-irrep	$(\alpha\beta)$	$g/4\pi$	$F/(F+D)$
0^{++}	$\{1\}$	$g(\pi\pi)_0$	—	—
0^{++}	,,	$g(\sigma\sigma)$	—	—
0^{++}	$\{8\}_s$	$g(\pi\eta)$	-1.1816	1.000
1^{--}	$\{8\}_a$	$g(\pi\pi)_1$	0.2324	1.000
		$f(\pi\pi)_1$	-1.6979	0.400
1^{++}	,,	$g(\pi\rho)_1$	5.0652	0.400
1^{++}	,,	$g(\pi\sigma)$	-0.2985	0.400
1^{++}	,,	$g(\pi P)$	—	—
1^{+-}	$\{8\}_s$	$g(\pi\omega)$	-0.0557	0.365

saturation in mind. The approximation we have made in this paper is to neglect the baryon mass differences, i.e. we put $m_\Lambda = m_\Sigma = m_N$. This because we have not yet worked out the formulas for the inclusion of these mass differences, which is straightforward in principle.

A. Parameters and Hyperon-nucleon Fit

All 'best' low-energy YN-data are included in the fitting, This is a selected set of 35 low-energy YN-data, the same set has been used in [12] and [13]. We added (i) 3 total Σ^+p X-sections from the KEK-experiment E289 [36], (ii) 7 elastic and 4 inelastic Λp X-sections from Berkeley [37], and (iii) 3 elastic Σ^-p X-sections [38]. In section VIII these are given together with the results. Next to these we added 'pseudo-data' for the Λp and Σ^+p scattering length's in order to ensure that the $\Lambda p(^1S_0)$ forces are sufficiently stronger than the $\Lambda p(^3S_1)$. In the construction of the ESC04-models, the experience with the NSC97 models was used in hypernuclear calculations. Technically 'favored' values of the s-wave scattering lengths for ΛN were imposed as pseudo-data during the fitting procedures, in order to get the right spin-splitting for the ΛN-interaction in hypernuclei. In nuclear matter this implies $U_{\sigma\sigma} > 1$. In this succeeding model ESC08, however, the ΛN behavior is slightly different leading to smaller values of $U_{\sigma\sigma}$. This time, we impose instead a larger difference between the s-wave scattering lengths with, of course, $|a_s| > |a_t|$ in order to fulfill the constraint $U_{\sigma\sigma} > 1$. Furthermore we added 'pseudo-data' for the $\Sigma^+p(^3S_1)$ scattering length with the goal to get enough repulsion in this wave in order to reach a total repulsive U_Σ. For the pseudo-data in the S=-2 channels we refer to section VI. In the final stages of the fitting process all pseudo-data were turned off. In fm:

$$\hat{a}_{\Lambda p}(^1S_0) = -2.60 \pm (0.10 - 0.20) \quad , \quad \hat{a}_{\Lambda p}(^3S_1) = -1.60 \pm (0.10 - 0.20) \quad ,$$
$$\hat{a}_{\Sigma^+p}(^3S_1) = +0.65 \pm (0.10 - 0.20) \quad , \tag{7.1}$$

Also, during the fitting process checks were done to prevent the occurrence of bound Λp states. Parameters, typically strongly influenced by the YN-data, are

1. $F/(F+D)$-parameters: α_V^m and to a less extent α_A, For the sensitivity of α_P see section VII.

2. Pauli-blocking fraction parameter a_{PB}.

The dependence of a_{PB} in the fit to YN and YY is rather shallow in a range $0.20 - 0.30$. An increase of 0.01 in a_{PB} raises the χ^2 approximately 1.2%. The final value has been determined by a minimal value of χ^2 of the set of the 52 YN data, while simultaneously providing a repulsive U_Σ. This implies that the S=-2 (and -3, -4) results of ESC08c are completely determined. Finally we want to mention that in the fitting process we have, if necessary, accounted for the vast difference in quality of the data. The abundance of the 4313 precise NN data is to be contrasted to the 52 less precise YN data. In the simultaneous fit we require for both the NN and for the YN that the quality of the partial fit is comparable, i.e. $\chi^2/NN_{data} \approx \chi^2/YN_{data}$. If necessary we add weight factors to the partial sums in the total χ^2. It turned out that in the last stages of the fitting process the weight factors are equal.

VIII.   ESC08-MODEL , *YN*-RESULTS

A.   Hyperon-nucleon (S=-1) X-sections, phases, etc.

The used *YN* scattering data from Refs. [46]-[52] in the combined *NN* and *YN* fit are shown in Table VIII. The *NN* interaction puts very strong constraints on most of the parameters, and so we are left with only a limited set of parameters which have some freedom to steer the YN channels as compared to the NN-channels. The fitted parameters are given in paper I, Table's III-VI and X.

The aim of the present study was to construct a realistic potential model for baryon-baryon systems with parameters that are optimal theoretically, but at the same time describes the baryon-baryon scattering data very satisfactory.

This model can then be used with a great deal of confidence in calculations of hypernuclei and in their predictions for the $S = -2, -3,$ and -4 sectors. Especially for the latter application, these models will be the first models for the $S = -2, -3, -4$ sectors to have their theoretical foundation in the *NN* and *YN* sectors.
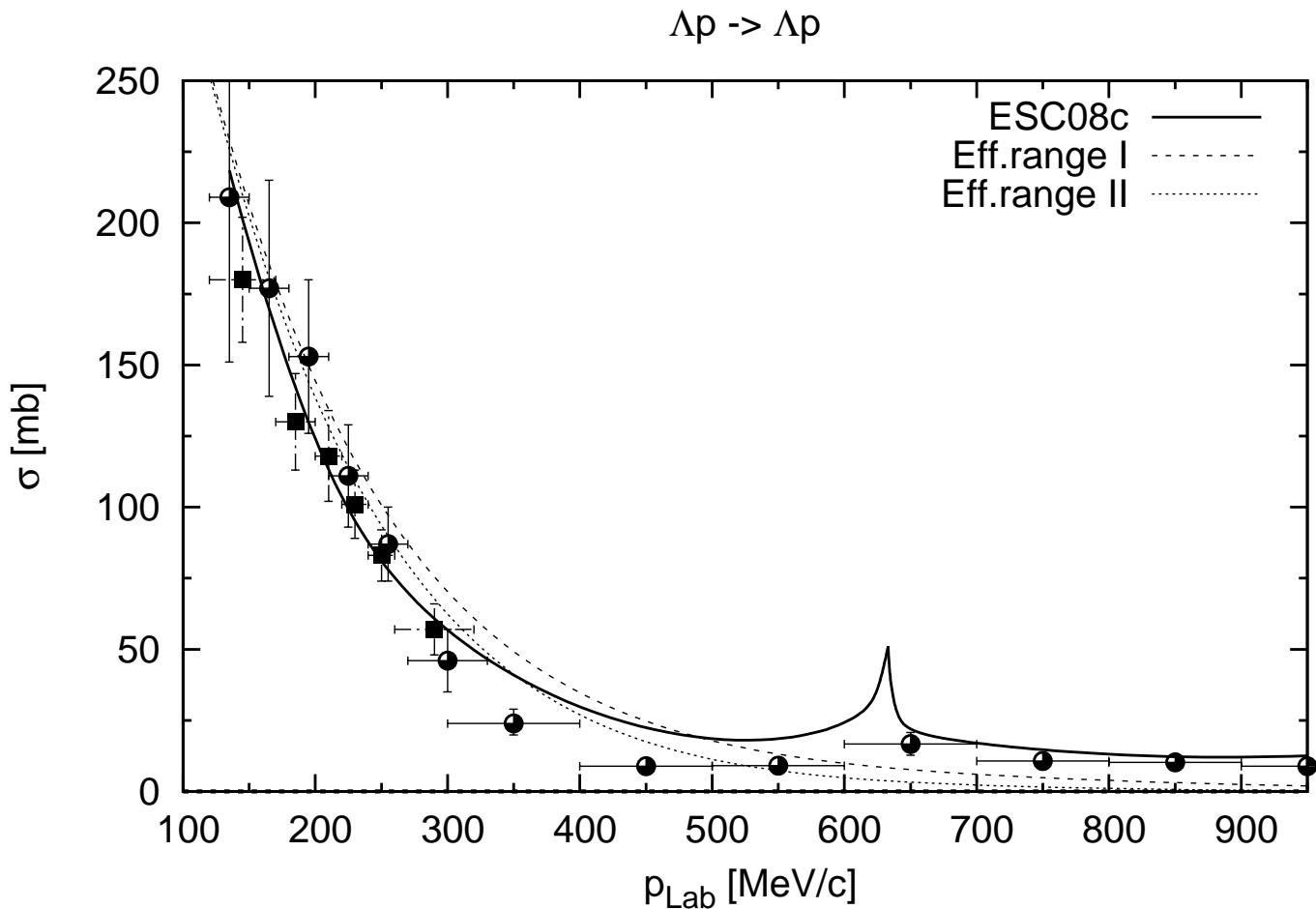
FIG. 1: Model fits total X-sections Λp. Rehovoth-Heidelberg-, Maryland-, and Berkeley-data

The χ^2 on the 52 *YN* scattering data for the ESC08c model is given in Table VIII. The ΛN total cross sections have been calculated with $L \leq 2$, and the ΣN total cross sections with $L \leq 1$. The capture ratio at rest, given in the last row of the table, for its definition see e.g. [13]. This capture ratio turns out to be rather constant in the momentum range from 100 to 170 MeV/c. Obviously, for very low momenta the cross sections are almost completely dominated by s waves, and so the capture ratio in flight converges to the capture ratio at rest. For more details on the evaluation of these observables, we refer to earlier Nijmegen work on this subject.

The $\Sigma^+ p$ nuclear-bar phase shifts as a function of energy are given in Table IX. Notice that the $^3S_1$-phase shows repulsion.

TABLE VIII: Comparison of the calculated ESC08c and experimental values for the 52 YN-data that were included in the fit. The superscipts RH and M denote, respectively, the Rehovoth-Heidelberg Ref. [46] and Maryland data Ref. [47]. Also included are (i) 3 $\Sigma^+ p$ X-sections at $p_{lab} = 400, 500, 650$ MeV from Ref. [36], (ii) Λp X-sections from Ref. [37]: 7 elastic between $350 \leq p_{lab} \leq 950$, and 4 inelastic with $p_{lab} = 667, 750, 850, 950$ MeV, and (iii) 3 elastic $\Sigma^- p$ X-sections at $p_{lab} = 450, 550, 650$ MeV from Ref. [38]. The laboratory momenta are in MeV/c, and the total cross sections in mb. The total $\chi^2 = 56.9$

$\Lambda p \to \Lambda p$		$\chi^2 = 3.2$	$\Lambda p \to \Lambda p$		$\chi^2 = 3.2$
p_Λ	σ_{exp}^{RH}	σ_{th}	p_Λ	σ_{exp}^{M}	σ_{th}
145	180±22	200.5	135	209.0±58	218.5
185	130±17	138.4	165	177.0±38	166.5
210	118±16	109.6	195	153.0±27	126.1
230	101±12	90.9	225	111.0±18	95.2
250	83± 9	75.3	255	87.0±13	71.9
290	57± 9	51.8	300	46.0±11	47.1
$\Lambda p \to \Lambda p$		$\chi^2 = 5.0$			
350	23.9±5.0	29.6	750	10.7±3.0	10.4
450	8.9±3.0	12.5	850	10.2±3.0	11.3
550	9.1±3.0	9.2	950	8.9±3.0	12.5
650	16.7±4.0	20.2			
$\Lambda p \to \Sigma^0 p$		$\chi^2 = 7.3$			
667	2.8 ±2.0	3.2	850	10.7±3.0	4.0
750	7.5±2.5	4.0	950	5.6±2.0	3.9
$\Sigma^+ p \to \Sigma^+ p$		$\chi^2 = 20.9$	$\Sigma^- p \to \Sigma^- p$		$\chi^2 = 5.0$
p_{Σ^+}	σ_{exp}	σ_{th}	p_{Σ^-}	σ_{exp}	σ_{th}
145	123.0±62	153.9	142.5	152±38	153.2
155	104.0±30	140.2	147.5	146±30	147.6
165	92.0±18	128.3	152.5	142±25	142.3
175	81.0±12	117.6	157.5	164±32	137.3
			162.5	138±19	132.5
			167.5	113±16	127.9
400	93.5±28.1	34.2	450.0	31.7±8.3	29.8
500	32.5±30.4	29.2	550.0	48.3±16.7	20.6
650	64.6±33.0	26.1	650.0	25.0±13.3	15.5
$\Sigma^- p \to \Sigma^0 n$		$\chi^2 = 5.7$	$\Sigma^- p \to \Lambda n$		$\chi^2 = 4.3$
p_{Σ^-}	σ_{exp}	σ_{th}	p_{Σ^-}	σ_{exp}	σ_{th}
110	396±91	193.8	110	174±47	236.4
120	159±43	170.3	120	178±39	203.4
130	157±34	151.4	130	140±28	177.1
140	125±25	135.9	140	164±25	155.7
150	111±19	123.0	150	147±19	138.1
160	115±16	112.2	160	124±14	123.4
$r_R^{exp} = 0.468 \pm 0.010$			$r_R^{th} = 0.452$		$\chi^2 = 2.4$

The ΛN nuclear-bar phase shifts as a function of energy are given in Table X. In Fig. 1 the Λp total X-sections are shown for ESC08c together with the data. At the ΣN-threshold the cross section shows a large cusp with a large D-wave nuclear-bar phaseshift $\delta(^3D_1) = 79.5^o$. This signals the fact that in the $\Sigma N(^3S_1, I = 1/2)$-state there is a strong attraction, with a deuteron-like virtual bound-state on the unphysical sheet. Also, in Fig. 1 we show the cross sections in the effective range approximation, dashed lines I and II. Line II is including the shape parameter in the effective range expansion. The two-term effective range expansion with the a and r parameters describes the s-wave
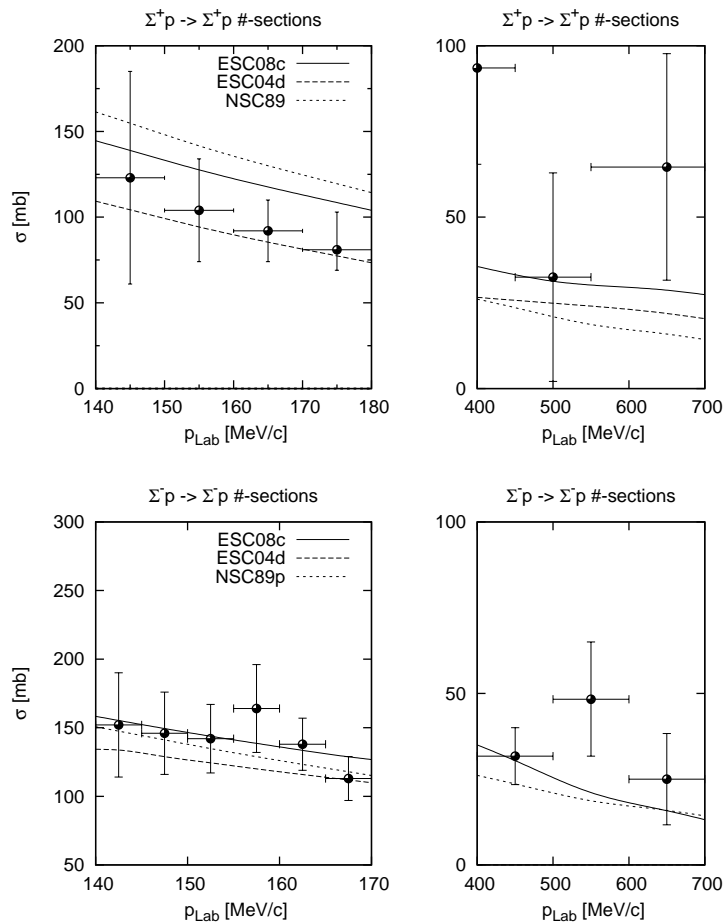
FIG. 2: Model fits total elastic X-sections $\Sigma^{\pm}p$. Rehovoth-Heidelberg-, KEK-data

phases well up to $p_\Lambda \approx 400$ MeV/c.

In Table XI the low-energy parameters for Λp and Λn are shown. The singlet and triplet parameters are displayed with the $\Lambda\Sigma^0$-mixing turned on for pseudoscalar-, vector-, scalar-, meson-pairs-, and ps-ps- exchanges. Notice that the effect for the scalar mesons of the $\Lambda\Sigma^0$-mixing is zero because $\alpha_s = 1.00$. It is clear from these tables that the total effect of the $\Lambda\Sigma^0$-mixing is about given by pseudoscalar and vector exchanges. The differences in the scattering lengths are

$$\Delta a_s = a_s(\Lambda p) - a_s(\Lambda n) = +0.139 fm, \tag{8.1a}$$

$$\Delta a_t = a_t(\Lambda p) - a_t(\Lambda n) = -0.022 fm. \tag{8.1b}$$

These differences are comparable to those for the soft-core OBE models [12, 13], and therefore predict a too small binding energy difference in the A=4 hypernuclei, which is $\Delta B_\Lambda(exp) = B_\Lambda(^4_\Lambda He) - B_\Lambda(^4_\Lambda H) = (0.29 \pm 0.06)$ MeV. This in contrast to the HC-model D, which has a much larger Δa_t [25]. It appeared that CSB via meson-mixing, like $\pi^0 - \eta, \rho^0 - \omega$ etc., is small and does not improve the CSB for ESC08, which is understandable in view of the large cancellations. However, as a consequence of the ESC-models there is a three-body force produced by the MPE-interactions, which are fixed by the BB-fit. Therefore, the CSB in the ΛNN-potential may improve the CSB predictions significantly.

In Table XII we list the Σ^+p scattering lengths and effective ranges. Here, (a_s, r_s) are these quantities for $\Sigma^+p(^1S_0)$
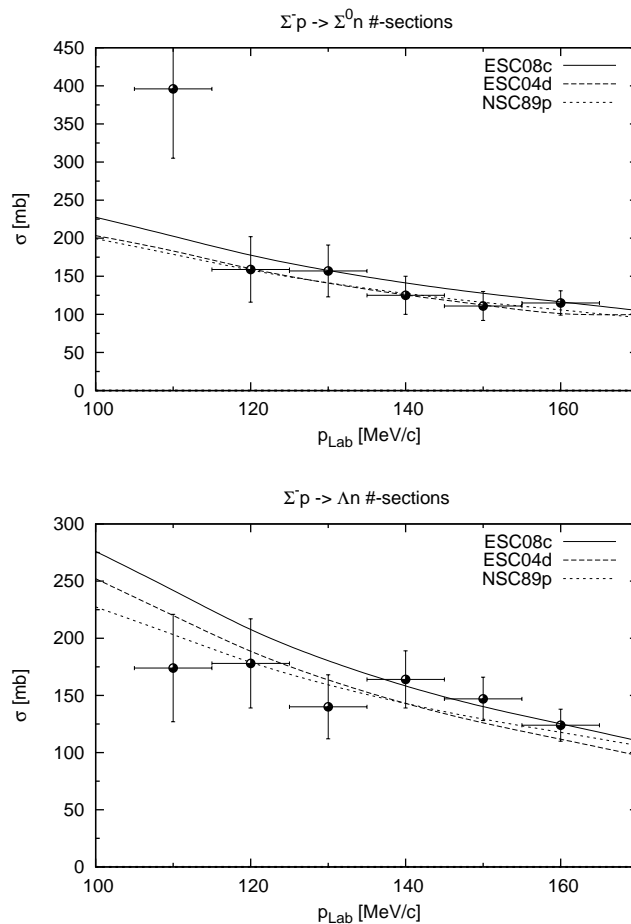
FIG. 3: Model fits total inelastic X-sections $\Sigma^- p \to \Sigma^0 n, \Lambda n$. Rehovoth-Heidelberg-data

and (a_t, r_t) for $\Sigma^+ p(^3S_1)$. Notice that the difference between ESC08a″ and ESC08c is small. This is because with SU(3) the $^1S_0$-wave is constrained by NN, because the $^1S_0$-states in NN and $\Sigma^+ p$ are both in the {27}-irrep, and so there is little room for variations in the $^3S_1$-wave because of the X-section fit. Therefore, much extra repulsion in the triplet wave is impossible.

In Fig. 2 and Fig. 3 the elastic and inelastic X-sections are shown respectively. In Fig. 4 we plot the total potentials for the S-wave channels $\Lambda N \to \Lambda N$, $\Lambda N \to \Sigma N$, and $\Sigma N \to \Sigma N$. Note the for the soft-core model typical structure of the $\Sigma^+ p(^3S_1)$-potential. Most contributions to the spin-spin potentials are proportional to $\mathbf{k}^2$, and hence have zero volume integral. This causes the attraction in the inner region.

Figures for the OBE-, TME-, and MPE-contributions are similar to those for the ESC04-model and have been displayed in Ref. [6] and we refer the interested reader to this reference. Likewise for the contributions of the various types of mesons to the OBE-potentials, and also for the contributions of the different kind of pair-potentials to MPE.

B. Potentials in SU(3)-irreps

In Fig. 5 the potentials $V_{\{\mu\}}$[GeV] in the SU(3) representations for BB-channels are shown. The solid/red curves include SU(3)-breaking and the dashed/green ones are the SU(3)-symmetric curves. In the latter average masses are

TABLE IX: ESC08c nuclear-bar $\Sigma^+ p$ phases in degrees.

p_{Σ^+}	100	200	300	400	500	600	700	800	900	1000
T_{lab}	4.2	16.7	37.3	65.5	100.8	142.8	190.7	244.0	302.1	364.5
$^1S_0$	36.09	41.68	35.76	27.52	18.83	10.26	2.00	−5.88	-13.39	−20.51
$^3S_1$	-5.35	−11.65	−17.78	−23.78	-29.37	−34.30	−38.50	−42.02	−45.05	−47.76
ϵ_1	-0.37	−1.80	-3.30	−4.40	−5.02	−5.24	−5.19	−4.96	−4.66	−4.32
$^3P_0$	0.99	5.17	9.19	10.54	9.30	6.40	2.67	−1.38	−5.42	−9.28
$^1P_1$	0.42	2.23	4.53	6.41	7.29	7.00	5.66	3.50	0.73	−2.46
$^3P_1$	−0.58	−2.95	−5.96	−9.15	−12.51	−16.02	−19.60	−23.17	−26.64	−29.97
$^3P_2$	0.10	0.92	2.65	4.83	6.91	8.58	9.78	10.47	10.62	10.23
ϵ_2	−0.03	−0.37	−1.06	−1.81	−2.44	−2.84	−3.02	−3.01	−2.85	−2.63
$^3D_1$	0.02	0.30	0.85	1.35	1.43	0.84	−0.51	−2.530	−5.08	−8.01
$^1D_2$	0.02	0.31	0.98	2.03	3.46	5.16	6.88	8.36	9.399	9.81
$^3D_2$	−0.03	−0.45	−1.30	−2.34	−3.48	−4.78	−6.29	−8.02	−9.93	−12.00
$^3D_3$	0.00	0.05	0.25	0.61	1.03	1.32	1.41	1.29	1.03	0.67

TABLE X: ESC08c nuclear-bar Λp phases in degrees.

p_Λ	100	200	300	400	500	600	633.0
T_{lab}	4.5	17.8	39.6	69.5	106.9	151.1	167.3
$^1S_0$	25.20	30.74	27.11	20.47	12.97	5.55	3.47
$^3S_1$	19.13	25.47	23.95	19.36	13.88	9.01	7.67
ϵ_1	0.04	0.17	0.26	0.30	0.62	3.97	13.55
$^3P_0$	0.05	0.29	0.45	−0.06	−1.48	−3.57	−4.26
$^1P_1$	−0.09	−0.68	−2.13	−4.58	−7.83	−11.53	−12.76
$^3P_1$	0.02	−0.00	−0.33	−1.19	−2.53	−3.89	−3.98
$^3P_2$	0.11	0.75	1.92	3.22	4.27	4.96	5.10
ϵ_2	0.00	−0.00	−0.04	−0.16	−0.34	−0.58	−0.69
$^3D_1$	0.00	0.08	0.57	2.25	7.00	26.43	79.51
$^1D_2$	0.00	0.06	0.38	1.17	2.50	4.23	4.85
$^3D_2$	0.00	0.08	0.43	1.21	2.45	3.97	4.52
$^3D_3$	0.00	0.04	0.23	0.66	1.28	1.92	2.11

used for the SU(3)-nonets. The curves resemble strongly (qualitatively) those obtained in lattice QCD, except for the {1}-irrep [53]. In the ESC-model the behavior in the typical for potentials with a strong spin-spin part, because the spin-spin potentials from pseudoscalar- and vector-exchange have zero volume integral forcing them to change sign for $r \sim 0.5$ fm.

The similarity between the meson-exchange and QCD-lattice potentials shows that with the ESC realization of the program starting from the nuclear force, using $\text{SU}_f(3)$-symmetry and the QM, a realistic generalization to the BB-force is achieved.

IX. ANALYSES WITH G-MATRIX INTERACTIONS

The G-matrix theory gives a good starting point for studies of hyperonic many-body systems on the basis of free-space YN interaction models [54–56]. Here, the correlations induced by hyperonic coupling interactions such as ΛN-ΣN ones are renormalized into single-channel G-matrices. These G-matrix interactions are considered as effective interactions used in models of hypernuclei. Thus, the hypernuclear phenomena and the underlying YN interaction

TABLE XI: Comparison Λp and Λn scattering lengths and effective ranges in fm for different Nijmegen models.

	Λp		Λn	
Model	a_s	a_t	a_s	a_t
ESC08c	-2.46	-1.74	-2.60	-1.72
NSC97e	-2.10	-1.86	-2.24	-1.83
NSC97f	-2.51	-1.75	-2.68	-1.67
NSC89	-2.73	-1.48	-2.86	-1.24
HC-D	-2.06	-1.77	-2.03	-1.84
Model	r_s	r_t	r_s	r_t
ESC08c	3.18	3.47	3.22	3.43
NSC97e	3.19	3.19	3.24	3.14
NSC97f	3.03	3.32	3.07	3.34
NSC89	2.87	3.04	2.91	3.33
HC-D	3.78	3.18	3.66	3.32

TABLE XII: $\Sigma^+ p$ scattering lengths and effective ranges in fm.

Model	a_s	a_t	r_s	r_t
ESC08c	-4.45	+0.60	3.21	-2.79
ESC08a$''$	-3.85	+0.62	3.40	-2.13
ESC04d	-3.43	+0.217	3.98	-28.94

models are linked through the YN G-matrix interactions, and the hypernuclear information gives a feedback to the interaction models. Here, the properties of ΛN and ΣN sectors of ESC08c in nuclear medium are studied on the basis of the G-matrix theory.

In Refs.[57, 58], the three-body interaction is added on ESC08c, being composed of the multi-pomeron exchange repulsive potential (MPP) and the phenomenological three-baryon attraction (TBA). The effective two-body potential derived from MPP is given as

$$V_{MPP}(r;\rho) = g_P^{(3)}(g_P)^3 \frac{\rho}{\mathcal{M}} \cdot \frac{1}{4\pi} \frac{4}{\sqrt{\pi}} \left(\frac{m_P}{\sqrt{2}} \right)^3 \exp\left(-\frac{1}{2} m_P^2 r^2 \right) , \qquad (9.1)$$

where the pomeron mass m_P and the pair pomeron coupling g_P are fitted to the NN-data etc. In a similar way, one can obtain an effective two-body potential with a quartic pomeron coupling $g_P^{(4)}$. TBA also is given by a density-dependent two-body potential

$$V_{TBA}(r;\rho) = V_{TBA}^0 \exp(-(r/2.0)^2) \rho \exp(-\eta\rho) (1 + P_r)/2 , \qquad (9.2)$$

P_r being a space-exchange operator. The values of $g_P^{(3)}$, $g_P^{(4)}$, V_{TBA}^0 and η are adjusted to reproduce the angular distribution of $^{16}O + ^{16}O$ elastic scattering at $E/A = 70$ MeV with use of the G-matrix folding potential, and values of the saturation density and the energy per nucleon there in nuclear matter. Among three sets given in Refs.[57, 58], we adopt here the set MPa ($g_P^{(3)} = 2.34$, $g_P^{(4)} = 30.0$), which gives rise to the stiff EoS of neutron matter to reproduce a maximum mass $2M_\odot$ of a neutron star.

MPP works universally in all baryon-baryon channels according to its definition. Assuming here that TBA works also in ΛN channels, the parameters are adjusted to reproduce well energy spectra of Λ hypernuclei. As shown later, we take $V_{TBA}^0 = -26.0$ MeV and $\eta = 5.0$ fm^3 in ΛN channels. Hereafter, the interaction ESC08c+MPP+TBA is denoted as ESC08c$^+$.

We start from the channel-coupled G-matrix equation for the baryon pair $B_1 B_2$ in nuclear matter [54], where $B_1 B_2 = \Lambda N$ and ΣN:

$$G_{cc_0} = v_{cc_0} + \sum_{c'} v_{cc'} \frac{Q_{y'}}{\omega - \epsilon_{B_1'} - \epsilon_{B_2'} + \Delta_{yy'}} G_{c'c_0} , \qquad (9.3)$$

where c denotes a YN relative state (y, T, L, S, J) with $y = (B_1, B_2)$. S and T are spin and isospin quantum numbers, respectively. Orbital and total angular momenta are denoted by L and J, respectively, with $\mathbf{J} = \mathbf{L} + \mathbf{S}$. Then,
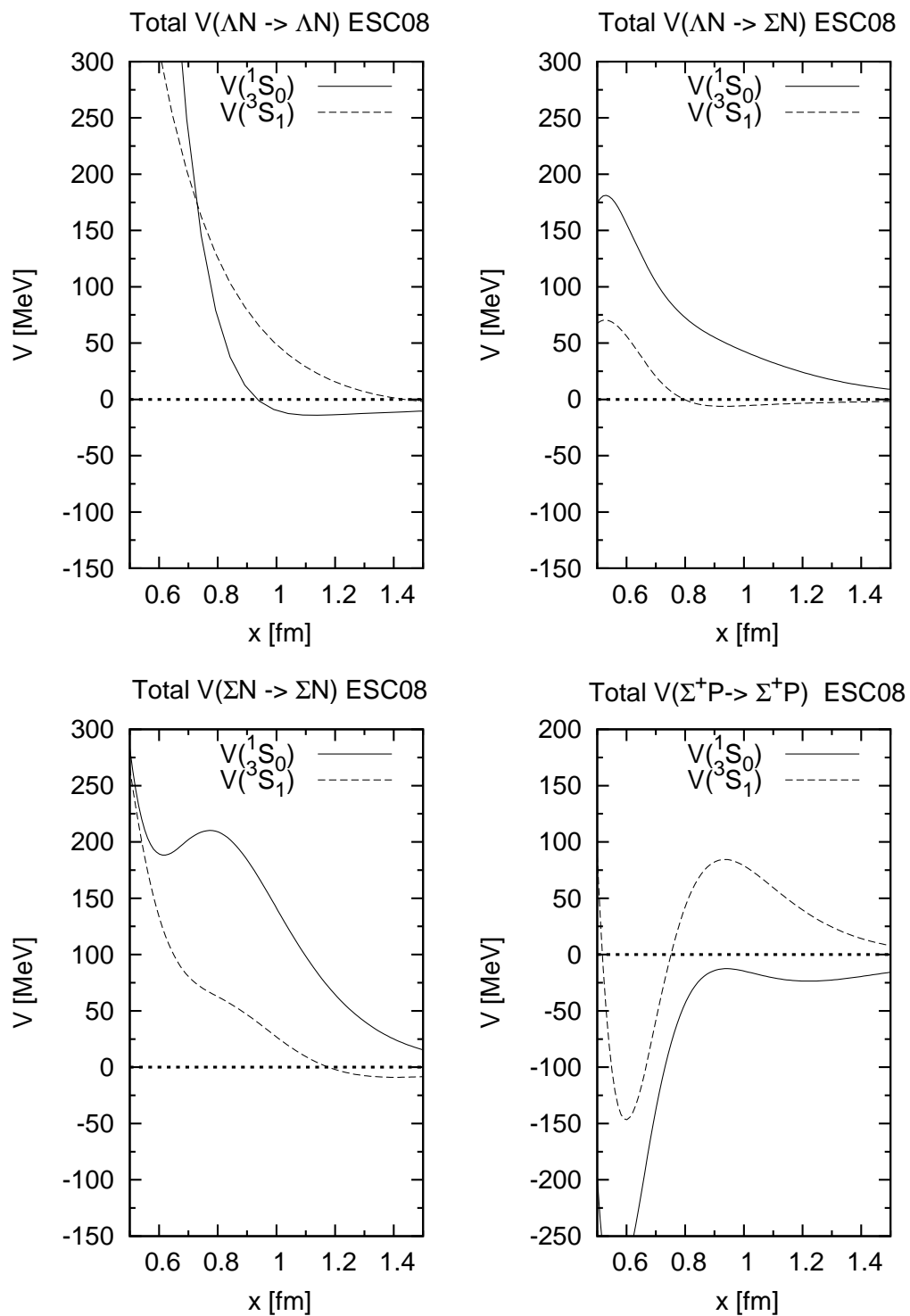
FIG. 4: Total potentials in the partial waves $^1S_0$ and $^3S_1$, for $I = 1/2$- and $I = 3/2$-states.
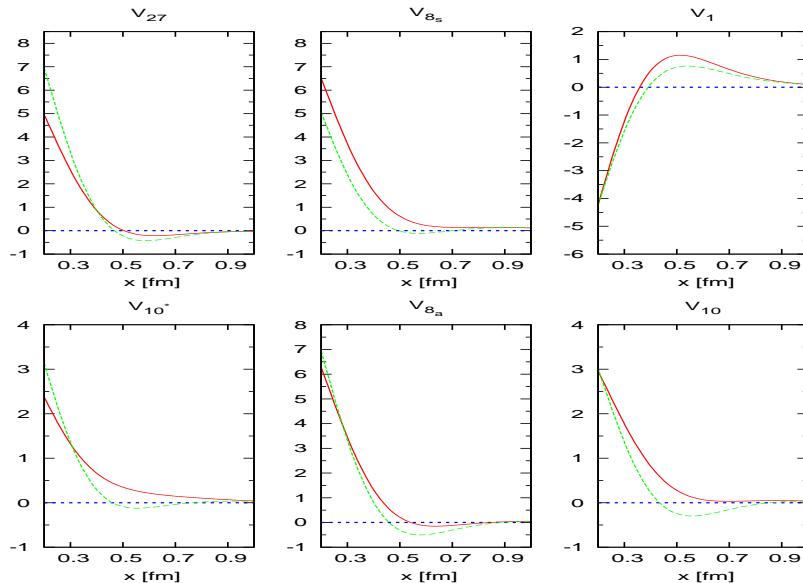
FIG. 5: Exact flavor SU(3)-symmetry: $m_\pi = m_K = m_\eta = 450$ MeV

a two-particle state is represented as $^{2S+1}L_J$. In Eq. (9.3), ω gives the starting energy in the starting channel c_0. $\Delta_{yy'} = M_{B_1} + M_{B_2} - M_{B_1'} - M_{B_2'}$ denotes the mass difference between two baryon channels. The Pauli operator Q_y acts on intermediate nucleon states in a channel $y = (B_1, B_2) = (\Lambda N, \Sigma N)$. We adopt here the continuous (CON) choice for intermediate single particle potentials in the G-matrix equation. The G-matrix equation (9.3) is represented in the coordinate space, whose solutions give G-matrix elements. The hyperon single particle (s.p.) energy ϵ_Y in nuclear matter is given by

$$\epsilon_Y(k_Y) = \frac{\hbar^2 k_Y^2}{2M_Y} + U_Y(k_Y) \, , \tag{9.4}$$

where k_Y is the hyperon momentum. The potential energy U_Y is obtained self-consistently in terms of the G-matrix as

$$U_Y(k_Y) = \sum_{|\mathbf{k}_N|} \langle \mathbf{k}_Y \mathbf{k}_N \mid G_{YN}(\omega = \epsilon_Y(k_Y) + \epsilon_N(k_N)) \mid \mathbf{k}_Y \mathbf{k}_N \rangle \tag{9.5}$$

A. ΛN G-matrix

TABLE XIII: Values of $U_\Lambda(\rho_0)$ and partial wave contributions in $^{2S+1}L_J$ states from the G-matrix calculations (in MeV). The value specified by D gives the sum of $^{2S+1}D_J$ contributions. Contributions from S-state spin-spin interactions are given by $U_{\sigma\sigma} = (U_\Lambda(^3S_1) - 3U_\Lambda(^1S_0))/12$.

	$^1S_0$	$^3S_1$	$^1P_1$	$^3P_0$	$^3P_1$	$^3P_2$	D	U_Λ	$U_{\sigma\sigma}$
ESC08c	−13.3	−25.4	2.6	0.0	1.1	−3.0	−1.6	−39.6	1.22
ESC08c$^+$	−13.3	−25.6	3.0	0.2	1.5	−2.1	−2.3	−38.6	1.19

Let us calculate Λ binding energies in nuclear matter. In Table XIII we show the potential energies $U_\Lambda(\rho_0)$ for a zero-momentum Λ and their partial-wave contributions in $^{2S+1}L_J$ states at normal density ρ_0 (k_F=1.35 fm^{-1}) in the CON choice, where a statistical factor $(2J + 1)$ is included in each contribution in $^{2S+1}L_J$ state. The value specified by D gives the sum of $^{2S+1}D_J$ contributions. Results for ESC08c and ESC08c$^+$ are found to be not so different from each other, because repulsive contributions of MPP are rather cancelled by attractive TBA contributions in normal and lower density regions. The contributions to U_Λ from S-state spin-spin components can be seen qualitatively in

values of $U_{\sigma\sigma} = (U_\Lambda(^3S_1) - 3U_\Lambda(^1S_0))/12$. These values of $U_{\sigma\sigma}$ also are given in Table XIII. In the same treatment, we obtain $U_{\sigma\sigma}$=1.54 and 0.92 MeV for NSC97f and NSC97e, respectively. Various analyses suggest that the reasonable value of $U_{\sigma\sigma}$ is between these values [56]. Then, one should note that the $U_{\sigma\sigma}$ values for ESC08c/c$^+$ are reasonable.

TABLE XIV: Parameters of YNG-ESC08c Continuous choice : $\mathcal{G}(k_F; r) = \sum_{i=1}^{3}(a_i + b_i k_F + c_i k_F^2)\exp-(r/\beta_i)^2$

	β_i	0.50	0.90	2.00
	a	−3437.	392.3	−1.631
^1E	b	7074.	−1079.	0.0
	c	−2687.	424.1	0.0
	a	−1944.	197.0	−1.210
^3E	b	4659.	−723.7	0.0
	c	−1958.	326.9	0.0
	a	2161.	83.98	−.7368
^1O	b	−458.0	40.14	0.0
	c	205.8	−.9091	0.0
	a	2362.	−253.9	−.9114
^3O	b	−2370.	200.0	0.0
	c	845.1	−43.53	0.0

TABLE XV: $\Delta\mathcal{G}(k_F; r) = (a + bk_F + ck_F^2)\exp-(r/0.9)^2$

	^1E	^3E	^1O	^3O
a	24.45	22.66	19.99	18.76
b	−62.13	−59.41	−56.72	−55.00
c	32.80	31.38	50.53	52.64

For applications to various hypernuclear problems, it is convenient to construct k_F-dependent effective local potentials $\mathcal{G}(k_F; r)$ which simulate the G-matrices in coordinate space. Here we parameterize them in a three-range Gaussian form

$$\mathcal{G}(k_F, r) = \sum_{i=1}^{3}(a_i + b_i k_F + c_i k_F^2)\exp\left(-r^2/\beta_i^2\right).\tag{9.6}$$

The parameters (a_i, b_i, c_i) are determined so as to simulate the calculated G-matrix for each $^{2S+1}L_J$ state. The procedures to fit the parameters are given in Ref. [56]. The obtained parameters for ESC08c are shown in Table XIV. For ESC08c$^+$, contributions from MPP+TBA are represented by modifying the second-range parts of $\mathcal{G}(k_F, r)$ for ESC08c by $\Delta\mathcal{G}(k_F, r) = (a + bk_F + ck_F^2)\exp-(r/0.9)^2$. The parameters for $\Delta\mathcal{G}(k_F, r)$ are given in Table XV. Then, the G-matrix interaction for ESC08c$^+$ is given by $\mathcal{G}(k_F, r) + \Delta\mathcal{G}(k_F, r)$.

Here, it is worthwhile to comment about a qualitative feature of $\Delta\mathcal{G}(k_F, r)$. The MPP contributions increase rapidly with matter density: In high (low) density region, they are very large (small), and cancelled substantially by TBA at normal-density region. Then, net contributions of MPP+TBA given by $\Delta\mathcal{G}(k_F, r)$ are attractive for smaller values of k_F than 1.35 fm^{-1}.

The solved G-matrices include not only ΛN-ΛN diagonal parts but also ΛN-ΣN coupling parts, and it is possible to extract such coupling parts to treat ΛN-ΣN mixing problems. The ΛN-ΣN coupling interaction is determined so that its matrix elements in k space simulate the corresponding G-matrix elements and its radial form tend to that of the bare interaction in the outermost region. In Table XVI (Table XVII), the parameters of the central

(tensor) parts of ΛN-ΣN and ΣN-ΣN interactions in S states are given in a three-range Gaussian (r^2-Gaussian) form. Here, the k_F dependences are represented in the same form as the above diagonal parts. These coupling interactions can be used for ΛN-ΣN mixing problems together with the ΛN-ΛN diagonal interactions in the Table XIV.

The SLS interactions $\mathcal{G}_{SLS}(r)$ are derived from G-matrices $\mathcal{G}_{LL'}^{JS}(r)$ with $S = 1$ by the linear transformation. The ALS G-matrix interaction $\mathcal{G}_{ALS}$ between $^3P_1$ and $^1P_1$ states is given so that its matrix elements in k space simulate the corresponding G matrix elements $\langle ^3P_1 \mid G \mid ^1 P_1 \rangle$. Because $\langle ^3P_1 \mid G \mid ^1 P_1 \rangle$ and $\langle ^1P_1 \mid G \mid ^3 P_1 \rangle$ are different from each other, we derive $\mathcal{G}_{ALS}$ from their averaged values. The SLS and ALS G-

TABLE XVI: Central coupling parts of G-matrix interactions for ESC08c, represented in a Gaussian form $\sum_{i=1}^{3}(a_i+b_ik_F+c_ik_F^2)\exp(-(r/\beta_i)^2)$.

		β_i	0.50	0.90	2.00
ΛN-ΣN $^1S_0$	a		4884.	-742.7	8.537
	b		$-7614.$	1235.	0.0
	c		2948.	-469.4	0.0
ΣN-ΣN $^1S_0$	a		-337.0	170.3	8.806
	b		839.1	-71.28	0.0
	c		-339.0	63.77	0.0
ΛN-ΣN $^3S_1$	a		$-1977.$	266.7	-2.755
	b		3451.	-543.5	0.0
	c		$-1508.$	246.5	0.0
ΣN-ΣN $^3S_1$	a		902.7	-149.6	-4.167
	b		258.3	-35.61	0.0
	c		-207.7	43.12	0.0

TABLE XVII: Tensor coupling parts of G-matrix interactions for ESC08c, represented in a r^2-Gaussian form $\sum_{i=1}^{3}(a_i+b_ik_F+c_ik_F^2)r^2\exp(-(r/\beta_i)^2)$.

		β_i	0.50	0.90	2.00
ΛN-ΣN $^3S_1$	a		$-39810.$	472.4	$-.7455$
	b		62150.	-903.1	0.0
	c		$-23830.$	343.6	0.0
ΛN-ΛN $^3S_1$	a		-598.3	-816.6	$-.0220$
	b		758.8	$-1615.$	0.0
	c		230.6	740.3	0.0

matrix interactions obtained as a function of k_F are represented in three-range Gaussian forms, the parameters of which are given for ESC08c in Table XVIII.

In order to compare clearly the SLS and ALS components, it is convenient to derive the strengths of the Λ l-s potentials in hypernuclei. In the same way as in Refs. [6, 13], the expression can be derived with the Scheerbaum approximation [59] as $U_\Lambda^{ls}(r) = K_\Lambda \frac{1}{r}\frac{d\rho}{dr}\mathbf{l}\cdot\mathbf{s}$. The values of K_Λ can be calculated with use of $\mathcal{G}_{SLS}(r)$ and $\mathcal{G}_{ALS}(r)$: The obtained value at $k_F = 1.0$ fm^{-1} is 6.8 MeV fm^5. This value is smaller (larger) than those for NSC97e/f (ESC08a/b) [56].

B. Λ hypernuclei by G-matrix folding potentials

The ΛN G-matrix interaction given by Table XIV is expressed as $\mathcal{G}_{(\pm)}^S(r)$, S and $(\pm)$ denoting spin and party quantum numbers, respectively. A Λ-nucleus potential in a finite system is derived from this ΛN interaction by the expression

$$U_\Lambda(\mathbf{r},\mathbf{r}') = U_{dr} + U_{ex} ,$$
$$U_{dr} = \delta(\mathbf{r} - \mathbf{r}')\int d\mathbf{r}'' \rho(\mathbf{r}'') V_{dr}(|\mathbf{r} - \mathbf{r}''|; k_F)$$
$$U_{ex} = \rho(\mathbf{r},\mathbf{r}')V_{ex}(|\mathbf{r} - \mathbf{r}'|; k_F) , \qquad (9.7)$$

TABLE XVIII: Parameters of SLS and ALS G-matrix interactions represented by three-range Gaussian forms $\mathcal{G}(r;k_F) = \sum_i(a_i + b_ik_F + c_ik_F^2)\exp{-(r/\beta_i)^2}$ in the cases of ESC08c.

		β_i	0.40	0.80	1.20
SLS	a		$-12590.$	366.2	-1.870
	b		24300.	-830.5	0.0
	c		$-10070.$	334.0	0.0
ALS	a		1818.	1.630	.7936
	b		$-1573.$	38.12	0.0
	c		591.5	-16.15	0.0

$$\begin{pmatrix} V_{dr} \\ V_{ex} \end{pmatrix} = \frac{1}{4}\sum_{S=0,1}(2S+1)[\mathcal{G}_{(\pm)}^S \pm \mathcal{G}_{(\mp)}^S] . \quad (9.8)$$

Here, densities $\rho(r)$ and mixed densities $\rho(r,r')$ are obtained from spherical Skyrme-HF wave functions.

An important problem is how to treat k_F values included in G-matrix interactions. We use here the following Averaged-Density Approximation (ADA), where an averaged value $\langle\rho\rangle$ is calculated by $\langle\phi_\Lambda(r)|\rho(r)|\phi_\Lambda(r)\rangle$ for each Λ state $\phi_\Lambda(r)$, and $\langle k_F\rangle$ is obtained by $(1.5\pi^2\langle\rho\rangle)^{1/3}$.

Let us calculate the energy spectra of Λ hypernuclei systematically ($^{13}_\Lambda$C, $^{16}_\Lambda$O, $^{28}_\Lambda$Si, $^{51}_\Lambda$V, $^{89}_\Lambda$Y, $^{139}_\Lambda$La, $^{208}_\Lambda$Pb). In Fig. 6, the calculated values are compared with the experimental values marked by open circles, the horizontal axis being given as $A^{-2/3}$, where solid and dashed curves are for ESC08c$^+$ and ESC08c, respectively. Here, the experimental data are shifted by 0.5 MeV from the values given in Ref.[60], which has been recently proposed according to the improved calibration [64]. The G-matrix interaction for ESC08c is found to reproduce rather well experimental values of B_Λ. In ESC08c$^+$ values of $V_{TBA}^0 = -26.0$ MeV and $\eta = 5.0$ fm^3 are chosen so that the value of $B_\Lambda(^{89}_\Lambda$Y$)$ is reproduced well and the global fitting of B_Λ values is improved in comparison with that for ESC08c. In such a procedure, the choice of V_{TBA}^0 and η depends on the adopted two-body interaction. In [58], the earlier version of ESC08c was used, giving $U_\Lambda(\rho_0) = -39.4$ MeV deeper than the value -38.6 MeV in the present work, where they took $V_{TBA}^0 - 32.8$ MeV and $\eta = 3.5$ fm^3 both in the NN and ΛN channels.

The difference between ESC08c$^+$ and ESC08c is due to the extra terms $\Delta\mathcal{G}(k_F,r)$ originated from MPP+TBA. Especially, MPP plays an essential role to reproduce the nuclear saturation property and the stiffness of the EoS of neutron-star matter [57, 58]. Then, it is very important that ESC08c$^+$ gives better fitting than ESC08c: The density-dependent attraction $\Delta\mathcal{G}(k_F,r)$ in low-density region works to reproduce better the energy spectra of heavy systems and B_Λ values of light systems. In high-density region, this extra term is dominated by MPP and leads to the stiff EoS of the hyperon-mixed neutron-star matter [58]. The present result suggests that such an effect of MPP+TBA can be tested in terrestrial data of
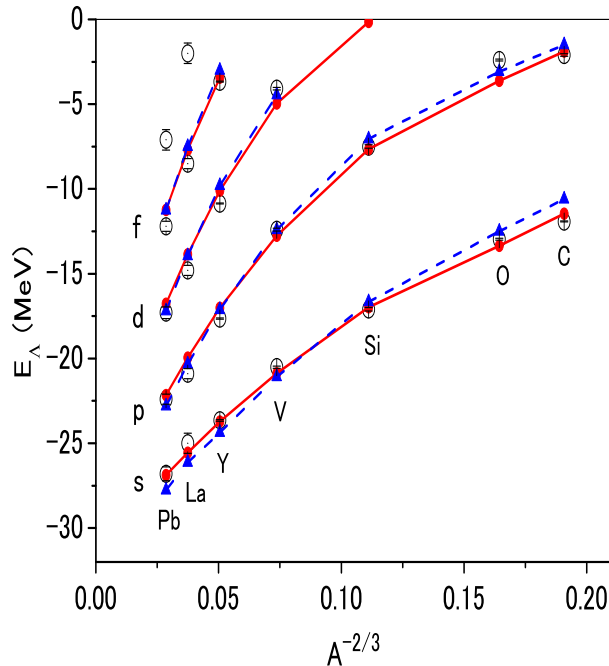
FIG. 6: Energy spectra of $^{13}_{\Lambda}$C, $^{28}_{\Lambda}$Si, $^{51}_{\Lambda}$V, $^{89}_{\Lambda}$Y, $^{139}_{\Lambda}$La and $^{208}_{\Lambda}$Pb are given as a function of $A^{-2/3}$, A being mass numbers of core nuclei. Solid (dashed) lines show calculated values by the G-matrix folding model derived from ESC08c$^+$ (ESC08c). Open circles denote the experimental values taken from Ref. [60].

B_{Λ} values.

Finally, we comment that the Λ s.p. energies in finite systems are not related simply to the $U_{\Lambda}(\rho_0)$ values given in Table XIV. The $U_{\Lambda}(\rho_0)$ values of -39.6 MeV (-38.6 MeV) for ESC08c (ESC08c$^+$) are very attractive compared to the value of -30 MeV, which is the depth U_{WS} of the Λ Woods-Saxon (WS) potential suitable to the data of Λ hypernuclei. However, it is misleading to compare the $U_{\Lambda}(\rho_0)$ value directly to the U_{WS} one. The Λ-nucleus folding potential depends not only on the strengths of ΛN G-matrices but also on their k_F dependences. Then, it is only of qualitative meaning to consider the depth U_{WS} of the phenomenological Woods-Saxon potential of Λ as the Λ potential depth in nuclear matter.

C. ΣN G-matrix

We study here Σ binding energies in nuclear matter by solving the ΣN starting channel G-matrix equation. In Table XIX we show the potential energies $U_{\Sigma}(\rho_0)$ for a zero-momentum Σ and their partial-wave contributions in $(^{2S+1}L_J, T)$ states for ESC08c. It should be noted here that the strongly repulsive contributions in $^3S_1$ $T = 3/2$ and $^1S_0$ $T = 1/2$ states are due to the Pauli-forbidden effects in these states, being taken into

TABLE XIX: Values of $U_{\Sigma}(\rho_0)$ at normal density and partial wave contributions in $(^{2S+1}L_J, T)$ states for ESC08c/c$^+$ (in MeV).

model	T	$^1S_0$	$^3S_1$	$^1P_1$	$^3P_0$	$^3P_1$	$^3P_2$	D	U_{Σ}
ESC08c	1/2	10.6	-22.1	2.0	2.1	-5.1	-1.5	-0.6	
	3/2	-12.6	30.2	-3.4	-2.1	5.2	-3.2	-0.2	$+0.8$
ESC08c$^+$	1/2	11.0	-18.9	2.1	2.2	-4.9	0.2 6	-0.6	
	3/2	-11.2	33.2	-3.0	-2.0	5.5	-2.6	-0.1	$+11.0$

account by strengthening the pomeron coupling in the ESC08 modeling.

The universal repulsion MPP has to work also in ΣN channels. Then, the problem is how to choose the phenomenological TBA part on the basis of experimental information. The positive values of $U_{\Sigma}(\rho_0)$ can be compared roughly with the repulsive component of the Σ nuclear potential obtained from analyzing strong-interaction shifts and widths in Σ^- atoms[65]. The size of repulsion is model dependent, giving rise to the estimation of 30 ± 20 MeV. Another experimental information for the repulsive Σ-nucleus potentials are given by the observed (π^-, K^-) spectra [24, 61, 62]. In Ref.[61], they performed the DWIA analysis for the data of ^{28}Si(π^-, K^-) reaction, where some ΣN interaction models were studied. The experimental spectrum was

reproduced nicely by the Σ-nucleus potential obtained from G-matrices for the Nijmegen model F [66] with the local density approximation, where the value of $U_\Sigma(\rho_0)$ was 24 MeV.

Considering that the experimentally suggested values of $U_\Sigma(\rho_0)$ are far more repulsive than the calculated values in Table XIX, we take $V^0_{TBA} = 0.0$ MeV: ESC08c$^+$ in ΣN channels is given by ESC08c+MPP without TBA. Table XIX includes also the result for ESC08c$^+$.
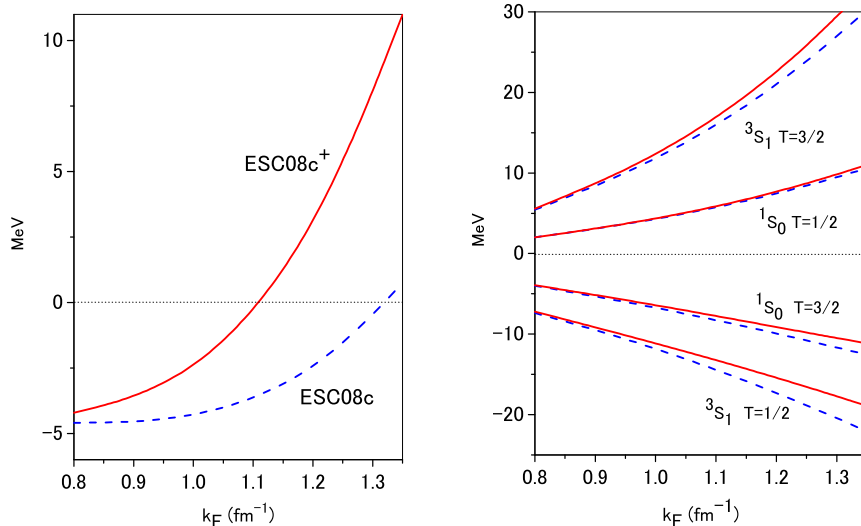

FIG. 7: In the left (right) panel, the values of U_Σ (partial-wave contributions) are drawn as a function of k_F by dashed and solid curves for ESC08c and ESC08c$^+$, respectively.

In the left (right) panel of Fig. 7, U_Σ values (their S-state contributions) are drawn as a function of k_F for ESC08c and ESC08c$^+$ by dashed and solid curves, respectively. It is demonstrated that the repulsive U_Σ values are due to $T = 3/2$ $^3S_1$ and $T = 1/2$ $^1S_0$ contributions, and the repulsions are enhanced by the MPP contributions. It is a future problem to calculate (π^-, K^-) spectra with use of G-matrix interactions for ESC08c/c$^+$.

X. DISCUSSION, CONCLUSIONS AND OUTLOOK

We have again shown in this paper that the ESC-approach to the nuclear force problem is able to make a connection between on the one hand the at present available baryon-baryon data and on the other hand the underlying quark structure of the baryons and mesons. Namely, a very successful description of both the NN- and YN-scattering data is obtained with meson-baryon coupling parameters which are almost all explained by the QPC-model. This at the same time in obediance of the strong constraint of no bound states in the $S = -1$-systems. Therefore, the ESC08c model of this paper is an important further step in the determination of the baryon-baryon interactions for low energy scattering and the description of hypernuclei in the context of broken SU(3)-symmetry. The values for many parameters, which in previous work were considered to be free to a large extend, are now limited strongly, and tried to be made consistent with the present theoretical view on low energy hadron physics. This is in particularly the case for the $F/(F + D)$-ratios of the MPE-interactions. These ratio's for the vector- and scalar-mesons are rather close to the QPC-model predictions.

In analyzing the effect of the Pauli-blocking repulsion the conclusion is that from the standpoint of the BB scattering-data fitting such a repulsion is not strong. This conclusion is in line with arguments from strong-coupling QCD (SCQCD). Namely, it has been argued in [67] that quark-exchange effects are small. The G-matrix results show that basic features of hyper-nuclear data are reproduced nicely by ESC08c, improving the weak points of the soft-core OBE-models NSC89 [12], NSC97 [13], and ESC04-models [5–7]. The ESC08-

models are superior for hypernuclear data and many aspects of the effective (two-body) interactions in hypernuclei can be obtained using the ESC08-model. For example, this is the case for the well depth U_Σ.

Experience has shown that a good fit to the scattering data not necessarily means success in the G-matrix results. To explain this one can think of two reasons: (i) the G-matrix results are sensitive to the two-body interactions below 1 fm, whereas the present YN-scattering data are not, (ii) other than two-body forces play an important role. However, since the $NN+YN$-fit is so much superior for ESC08 than for OBE-models, we are inclined to look for solutions to the remaining problems outside the two-body forces. A natural possibility is the presence of three-body forces (TBF) in hypernuclei which can be viewed as generating effective two-body forces, which could solve the well-depth issues. In the case of the $\Delta B_{\Lambda\Lambda}$ also TBF could be operating. This calls for an evaluation of the TBF's NNN, ΛNN, ΣNN, $\Lambda\Lambda N$, etc. for the soft-core ESC-model, consistent with its two-body forces.

The ΛN p-waves seem to be better, which is the result of the truly simultaneous $NN+YN$-fitting. This is also reflected in the better K_Λ-value, making the well-known small spin-orbit splitting smaller.

In the course of the development of the ESC-model for baryon-baryon, up to and including ESC06 [68] it was tried to solve all problems for NN and YN, both for scattering and hypernuclear well-depth's, by keeping the potentials restricted to meson-exchange. For that purpose, in ESC06 a 'super-extended' ESC-approach was studied by including the second generation of the mesons, i.e. the heavy pseudo-scalar, vector, and scalar meson nonets. In the Quark-Model they would correspond to the first radially excited $q\bar{q}$-states, with masses in the range $1 GeV/c^2 < M < 1.7 GeV/c^2$. With this extension it is possible to produce extra repulsion in the $\Sigma^+ p({}^3S_1)$, but correlated with this was an exremely strong attraction in the $\Sigma^+ p({}^1P_1)$ partial-wave. Although the ESC06-approach is not ruled out by the data, we think that the solutions presented with ESC08 are much more superior. In the future, such a 'super-extended' ESC08-model may be explored. For example, the axial-vector and heavy pseudoscalar ($\pi(1300)$) meson sectors can be studied more closely. furthermore, for the scalar mesons the inclusion of a finite width for the broad κ-meson can be investigated.

APPENDIX A: MPE INTERACTIONS AND $SU(3)$

Below, $\sigma, \mathbf{a}_0, \mathbf{A}_1, \ldots$ are short-hands for respectively the baryon SU(3)-singlet and -octet densities $\bar{\psi}\psi$, $\bar{\psi}\boldsymbol{\lambda}\psi$, $\bar{\psi}\gamma_5\gamma_\mu\boldsymbol{\lambda}\psi, \ldots$. Here, λ_i, $i = 0, 1, ..., 8$ are the Gell-Mann $SU(3)$-matrices.

For the pseudoscalar-, vector-, scalar-, and axial-vector mesons The $SU(3)$ octet and singlet states appearing in the meson-pairs, denoted by the subscript 8 respectively

1, are in terms of the physical ones defined as follows:

(i) <u>Pseudo-scalar-mesons</u>:

$$\eta_1 = \cos\theta_P \eta' - \sin\theta_P \eta$$
$$\eta_8 = \sin\theta_P \eta' + \cos\theta_P \eta$$

Here, η' and η are the physical pseudo-scalar mesons $\eta(957)$ respectively $\eta(548)$.

(ii) <u>Vector-mesons</u>:

$$\phi_1 = \cos\theta_V \omega - \sin\theta_V \phi$$
$$\phi_8 = \sin\theta_V \omega + \cos\theta_V \phi$$

Here, ϕ and ω are the physical vector mesons $\phi(1019)$ respectively $\omega(783)$.

Then, one has the following $SU(3)$-invariant pair-interaction Hamiltonians:

1. $J^{PC} = 0^{+-}$: $SU(3)$-singlet couplings $S_\beta^\alpha = \delta_\beta^\alpha \sigma/\sqrt{3}$,

$$\mathcal{H}_{S_1 PP} = \frac{g_{S_1 PP}}{\sqrt{3}} \left\{ \boldsymbol{\pi} \cdot \boldsymbol{\pi} + 2K^\dagger K + \eta_8 \eta_8 \right\} \cdot \sigma$$

2. $J^{PC} = 0^{++}$: $SU(3)$-octet symmetric couplings I, $S_\beta^\alpha = (S_8)_\beta^\alpha \Rightarrow (1/4)Tr\{S[P,P]_+\}$,

$$\mathcal{H}_{S_8 PP} = \frac{g_{S_8 PP}}{\sqrt{6}} \left\{ (\mathbf{a}_0 \cdot \boldsymbol{\pi})\eta_8 + \frac{\sqrt{3}}{2}\mathbf{a}_0 \cdot (K^\dagger \boldsymbol{\tau} K) \right.$$
$$+ \frac{\sqrt{3}}{2}\left\{ (K_0^\dagger \boldsymbol{\tau} K) \cdot \boldsymbol{\pi} + h.c. \right\}$$
$$- \frac{1}{2}\left\{ (K_0^\dagger K)\eta_8 + h.c. \right\}$$
$$\left. + \frac{1}{2}f_0 \left(\boldsymbol{\pi} \cdot \boldsymbol{\pi} - K^\dagger K - \eta_8 \eta_8 \right) \right\}$$

3. $J^{PC} = 1^{+-}$: $SU(3)$-octet symmetric couplings II, $S_\beta^\alpha = (B_8)_\beta^\alpha \Rightarrow (1/4)Tr\{B^\mu[V_\mu,P]_+\}$,

$$\mathcal{H}_{B_8 VP} = \frac{g_{B_8 VP}}{\sqrt{6}} \left\{ \frac{1}{2}\left[(\mathbf{B}_1^\mu \cdot \boldsymbol{\rho}_\mu)\eta_8 + (\mathbf{B}_1^\mu \cdot \boldsymbol{\pi}_\mu)\phi_8 \right] \right.$$
$$+ + \frac{\sqrt{3}}{4}\left[\mathbf{B}_1 \cdot (K^{*\dagger}\boldsymbol{\tau} K) + h.c. \right]$$
$$+ \frac{\sqrt{3}}{4}\left[(K_1^\dagger \boldsymbol{\tau} K^*) \cdot \boldsymbol{\pi} + (K_1^\dagger \boldsymbol{\tau} K) \cdot \boldsymbol{\rho} + h.c. \right]$$
$$- \frac{1}{4}\left[(K_1^\dagger \cdot K^*)\eta_8 + (K_1^\dagger \cdot K)\phi_8 + h.c. \right]$$
$$\left. + \frac{1}{2}H^0 \left[\boldsymbol{\rho} \cdot \boldsymbol{\pi} - \frac{1}{2}\left(K^{*\dagger} \cdot K + K^\dagger \cdot K^* \right) - \phi_8 \eta_8 \right] \right\}$$

4. $J^{PC} = 1^{--}$: $SU(3)$-octet a-symmetric couplings I, $A_\beta^\alpha = (V_8)_\beta^\alpha \Rightarrow (-i/\sqrt{2})Tr\{V^\mu[P,\partial_\mu P]_-\}$,

$$\mathcal{H}_{V_8 PP} = g_{A_8 PP} \left\{ \frac{1}{2}\boldsymbol{\rho}_\mu \cdot \boldsymbol{\pi} \times \overset{\leftrightarrow}{\partial}{}^\mu \boldsymbol{\pi} + \frac{i}{2}\boldsymbol{\rho}_\mu \cdot (K^\dagger \boldsymbol{\tau} \overset{\leftrightarrow}{\partial}{}^\mu K) \right.$$
$$+ \frac{i}{2}\left(K_\mu^{*\dagger} \boldsymbol{\tau}(K\overset{\leftrightarrow}{\partial}{}^\mu \boldsymbol{\pi}) - h.c. \right) + i\frac{\sqrt{3}}{2}\left(K_\mu^{*\dagger} \cdot \right.$$
$$\left. (K \cdot \overset{\leftrightarrow}{\partial}{}^\mu \eta_8) - h.c. \right) + \frac{i}{2}\sqrt{3}\phi_\mu(K^\dagger \overset{\leftrightarrow}{\partial}{}^\mu K) \right\}$$

5. $J^{PC} = 1^{++}$ $SU(3)$-octet a-symmetric couplings II, $A^\alpha_\beta = (A_8)^\alpha_\beta \Rightarrow (-i/\sqrt{2})Tr\{A^\mu[P, V_\mu]_-\}$:

$$\mathcal{H}_{A_8VP} = g_{A_8VP}\left\{ \mathbf{A}_1 \cdot \boldsymbol{\pi} \times \boldsymbol{\rho} \right.$$
$$+\frac{i}{2}\mathbf{A}_1 \cdot \left[(K^\dagger \boldsymbol{\tau} K^*) - (K^{*\dagger}\boldsymbol{\tau} K)\right]$$
$$-\frac{i}{2}\left(\left[(K^\dagger \boldsymbol{\tau} K_A) \cdot \boldsymbol{\rho} + (K_A^\dagger \boldsymbol{\tau} K^*) \cdot \boldsymbol{\pi}\right] - h.c.\right)$$
$$-i\frac{\sqrt{3}}{2}\left(\left[(K^\dagger \cdot K_A)\phi_8 + (K_A^\dagger \cdot K^*)\eta_8\right] - h.c.\right)$$
$$\left. +\frac{i}{2}\sqrt{3}f_1\left[K^\dagger \cdot K^* - K^{*\dagger} \cdot K\right] \right\}$$

The relation with the pair-couplings used in this paper and paper I, see also [32], is $g_{S_1PP}/\sqrt{3} = g_{(\pi\pi)_0}/m_\pi$, $g_{A_8VP} = g_{(\pi\rho)_1}/m_\pi$ etc.

APPENDIX B: $J^{PC} = 1^{+-}$ AXIAL-PAIR POTENTIALS

In this appendix we document the $J^{PC} = 1^{+-}$-axial $(\pi\omega)$ 1-pair potentials, which have not been reported elsewhere yet. The involved meson-pairs can be read off from the SU(2) structure of the interaction Hamiltonian (4.27).

Below, we denote the type of potentials by writing $V^{(n)}_{\sigma+T}$, where $n = 0, 1$ refers to the $(1/M)$-order, and the subscript $\sigma + T$ indicates that only the spin-spin and tensor contributions are given here and not the spin-orbit potentials.

1. NN-Potentials $(S = 0, I = 1)$-exchange, $(\pi\omega_1)$ etc.

To be specific, consider $(\pi\omega)_1$-exchange for NN and elastic ΣN potentials. One obtains:

1. The leading, i.e. $(1/M)^0$-terms in momentum and configuration space are

$$\widetilde{V}^{(0)}_{\sigma+T}(\mathbf{q}, \mathbf{k}) = +g_{(\pi\omega)_1;NN}f_{NN\pi}G_{NN\omega}\left(\boldsymbol{\sigma}_1 \cdot \mathbf{k}\boldsymbol{\sigma}_2 \cdot \mathbf{k}_1 + \boldsymbol{\sigma}_1 \cdot \mathbf{k}_1\boldsymbol{\sigma}_2 \cdot \mathbf{k}\right) \times \frac{1}{\omega_1^2\omega_2^2} \cdot \frac{1}{m_\pi^2\mathcal{M}} , \tag{B1a}$$

$$V^{(0)}_{\sigma+T}(r) = -2g_{(\pi\omega;NN)}f_{NN\pi}G_{NN\omega}\left[F^{(0)}_{B,\sigma}(r)\boldsymbol{\sigma}_1 \cdot \boldsymbol{\sigma}_2 + F^{(0)}_{B,T}(r) S_{12}\right] \cdot \frac{1}{m_\pi^2\mathcal{M}} , \tag{B1b}$$

where

$$F^{(0)}_{B,\sigma}(r) = \frac{1}{3}\left(\frac{2}{r}F'G + F'G' + F''G\right) \quad , \quad F^{(0)}_{B,T}(r) = \frac{1}{3}\left(-\frac{1}{r}F'G + F'G' + F''G\right) . \tag{B2}$$

Above $\omega_1 = \sqrt{\mathbf{k}_1^2 + m_\pi^2}$ and $\omega_2 = \sqrt{\mathbf{k}_2^2 + m_\omega^2}$. For the Fourier transforms of the momentum pair-exchange potentials with gaussians form factors, we refer to the basic papers [32]. The superscript for the functions $F_{B,\sigma,T}$ refers to the denominators $1/(\omega_1^2\omega_2^2)$ in (B1). For these denominators, in the notation of [32], the functions F and G are

$$F(r) = I_2(r, m_\pi, \Lambda_\pi) \quad , \quad G(r) = I_2(r, m_\omega, \Lambda_\omega) . \tag{B3}$$

Similar formulas apply to e.g. ΣN-potentials, and also to $(K^*K)_1$-pair exchange.

2. The non-leading, i.e. $(1/M)$-terms, are

$$\widetilde{V}^{(1)}_{\sigma+T}(\mathbf{q}, \mathbf{k}) = -g_{(\pi\omega)_1;NN}f_{NN\pi}G_{NN\omega}\frac{1}{2M_N}\left(\boldsymbol{\sigma}_1 \cdot \mathbf{k}\boldsymbol{\sigma}_2 \cdot \mathbf{k}_2 + \boldsymbol{\sigma}_1 \cdot \mathbf{k}_2\boldsymbol{\sigma}_2 \cdot \mathbf{k}\right) \times \frac{1}{\omega_1\omega_2(\omega_1 + \omega_2)} \cdot \frac{1}{m_\pi^2\mathcal{M}} , \tag{B4a}$$

$$V^{(1)}_{\sigma+T}(r) = +2g_{(\pi\omega)_1;NN}f_{NN\pi}G_{NN\omega}\frac{m_\pi}{2M_N}\left[F^{(1)}_{B,\sigma}(r)\boldsymbol{\sigma}_1 \cdot \boldsymbol{\sigma}_2 + F^{(1)}_{B,T}(r) S_{12}\right] \cdot \frac{1}{m_\pi^3\mathcal{M}} , \tag{B4b}$$

where now superscript for the functions $F^{(1)}_{B,\sigma,T}$ refers to the denominators $1/[\omega_1\omega_2(\omega_1 + \omega_2)]$ in (B4). For this denominator the basic Fourier transform is [32]

$$F^{(1)}_B(r) = \frac{2}{\pi}\int_0^\infty d\lambda \, F(\Lambda, r) \, G(\lambda, r) , \tag{B5}$$

where the functions F and G are

$$F(r) = I_2(r, m_\pi(\lambda), \Lambda_\pi) \quad , \quad G(r) = I_2(r, m_\omega(\lambda), \Lambda_\omega) , \tag{B6}$$

with the understanding that under the λ-integral in (B5) there occur the combinations

$$F_{B,\sigma}^{(1)}(r) = \frac{1}{3}\left(\frac{2}{r}FG' + F'G' + F\,G''\right) \quad , \quad F_{B,T}^{(1)}(r) = \frac{1}{3}\left(-\frac{1}{r}FG' + F'G' + FG''\right) \; . \tag{B7}$$

3. The symmetric spin-orbit $(1/M)^2$-terms, are

$$\widetilde{V}_{SLS}^{(2)}(\mathbf{q},\mathbf{k}) = -g_{(\pi\omega)_1;NN}f_{NN\pi}G_{NN\omega}\frac{1}{M_N^2}\frac{i}{2}(\boldsymbol{\sigma}_1 + \boldsymbol{\sigma}_2)\cdot\mathbf{q}\times\mathbf{k}_2\times\frac{1}{\omega_2^2} \; , \tag{B8a}$$

$$V_{SLS}^{(2)}(r) = -g_{(\pi\omega)_1;NN}f_{NN\pi}G_{NN\omega}\frac{1}{m_\pi^2 M_N^2}\,I_0(m_\pi,r)\,\left(-\frac{1}{r}\frac{d}{dr}I_2(m_\omega,\Lambda_V,r)\right)\mathbf{L}\cdot\mathbf{S} \; , \tag{B8b}$$

where

$$I_0(\Lambda_P,r) = \frac{1}{4\pi}\frac{1}{2\sqrt{\pi}}\left(\frac{\Lambda_P}{m_\pi}\right)^3 \exp\left(-\frac{1}{4}\Lambda_P^2 r^2\right) \; . \tag{B9}$$

We note that important contributions to the anti-symmetric spin-orbit potentials are proportional to $(1/M_N - 1/M_Y) \sim 1/M^2$. Also, spin-orbit potentials from OBE are order $1/M^2$. Therefore, we included this SLS-potential in the ESC08-model.

2. YN-potentials, (S=0,I=0)-Exchange, $(\pi\rho)_0$ etc.

The above given potentials also occur in YN- and YY-channels, of course. In this subsection we give as an illustration only the $1/M$-contribution for the spin-spin and tensor. Again, to be specific, now we consider $(\pi\rho)_0$-exchange for ΛN potentials. We obtain:

$$\widetilde{V}_{\sigma+T}^{(1)}(\mathbf{q},\mathbf{k}) = -2g_{\Lambda\Lambda;(\pi\rho)_0}f_{NN\pi}G_{NN\rho}\frac{1}{2M_N}\left[\boldsymbol{\sigma}_1\cdot\mathbf{k}\boldsymbol{\sigma}_2\cdot\mathbf{k}_2\right]\times\frac{1}{\omega_1\omega_2(\omega_1+\omega_2)}$$
$$-2g_{NN;(\pi\rho)_0}f_{\Lambda\Sigma\pi}G_{\Lambda\Sigma\rho}\frac{1}{M_\Lambda + M_\Sigma}\left[\boldsymbol{\sigma}_1\cdot\mathbf{k}_2\boldsymbol{\sigma}_2\cdot\mathbf{k}\right]\times\frac{1}{\omega_1\omega_2(\omega_1+\omega_2)} \; . \tag{B10}$$

In configuration space we get

$$V_{\sigma+T}^{(1)}(r) = +2g_{\Lambda\Lambda;(\pi\rho)_0}f_{NN\pi}G_{NN\rho}\frac{1}{2M_N}\left[G_{B,\sigma}^{(1)}(r)\boldsymbol{\sigma}_1\cdot\boldsymbol{\sigma}_2 + G_{B,T}^{(1)}(r)\,S_{12}\right]$$
$$+2g_{NN;(\pi\rho)_0}f_{\Lambda\Sigma\pi}G_{\Lambda\Sigma\rho}\frac{1}{M_\Lambda + M_\Sigma}\left[G_{B,\sigma}^{(1)}(r)\boldsymbol{\sigma}_1\cdot\boldsymbol{\sigma}_2 + G_{B,T}^{(1)}(r)\,S_{12}\right] \; , \tag{B11}$$

where

$$G_{B,\sigma}^{(1)}(r) = \frac{1}{3}\left(\frac{2}{r}F_\pi \otimes F_\omega' + F_\pi' \otimes F_\omega' + F_\pi \otimes F_\omega''\right) \; , \tag{B12a}$$

$$G_{B,T}^{(1)}(r) = \frac{1}{3}\left(-\frac{1}{r}F_\pi \otimes F_\omega' + F_\pi' \otimes F_\omega' + F \otimes_\pi F_\omega''\right) \; . \tag{B12b}$$

Here, again the superscript on the G-functions refers to the denominator in momentum space. For the denominators in (B10) the functions $F \otimes g$ are given by[32]

$$F_\alpha \otimes F_\beta(r) = \frac{2}{\pi}\int_0^\infty d\lambda\,F_\alpha(\lambda,r)F_\beta(\lambda,r) \; , \tag{B13}$$

where

$$F_\alpha(\lambda,r) = e^{-\lambda^2/\Lambda_\alpha^2}I_2(\sqrt{m_\alpha^2 + \lambda^2},r) \; . \tag{B14}$$

3. YN-potentials, $(S = \pm 1, I = 1/2)$-Exchange, $(\pi K^*)_{1/2}$ etc.

Again, to be specific, consider $(\pi K^*)_{1/2}$-exchange for ΛN potentials. One obtains:
The leading, i.e. $(1/M)^0$-potentials

$$\widetilde{V}^{(0)}_{\sigma+T}(\mathbf{q},\mathbf{k}) = +g_{(\pi K^*);\Lambda N}f_{NN\pi}G_{N\Lambda K^*}\left(\boldsymbol{\sigma}_1 \cdot \mathbf{k}\boldsymbol{\sigma}_2 \cdot \mathbf{k}_1 + \boldsymbol{\sigma}_1 \cdot \mathbf{k}_1\boldsymbol{\sigma}_2 \cdot \mathbf{k}\right) \times \frac{1}{\omega_1^2\omega_2^2}$$

$$+g_{(\pi K^*);\Lambda N}f_{\Lambda\Sigma\pi}G_{N\Sigma K^*}\left(\boldsymbol{\sigma}_1 \cdot \mathbf{k}\boldsymbol{\sigma}_2 \cdot \mathbf{k}_1 + \boldsymbol{\sigma}_1 \cdot \mathbf{k}_1\boldsymbol{\sigma}_2 \cdot \mathbf{k}\right) \times \frac{1}{\omega_1^2\omega_2^2}. \tag{B15}$$

The configuration space potentials are:

$$V^{(0)}_{\sigma+T}(r) = -2g_{(\pi K^*);\Lambda N}f_{NN\pi}G_{N\Lambda K^*}\left(F^{(0)}_{B,\sigma}(r)\boldsymbol{\sigma}_1 \cdot \boldsymbol{\sigma}_2 + F^{(0)}_{B,T}\ S_{12}\right) \cdot \mathcal{P}_f$$

$$-2g_{(\pi K^*);\Lambda N}f_{\Lambda\Sigma\pi}G_{N\Sigma K^*}\left(F^{(0)}_{B,\sigma}(r)\boldsymbol{\sigma}_1 \cdot \boldsymbol{\sigma}_2 + F^{(0)}_{B,T}(r)\ S_{12}\right) \cdot \mathcal{P}_f\ . \tag{B16}$$

The non-leading, i.e. $(1/M)^1$-potentials are

$$\widetilde{V}^{(1)}_{\sigma+T}(\mathbf{q},\mathbf{k}) = -g_{(\pi K^*);\Lambda N}f_{NN\pi}G_{N\Lambda K^*}\frac{1}{2M_N}\left[\left(\boldsymbol{\sigma}_1 \cdot \mathbf{k}\boldsymbol{\sigma}_2 \cdot \mathbf{k}_2 + \boldsymbol{\sigma}_1 \cdot \mathbf{k}_2\boldsymbol{\sigma}_2 \cdot \mathbf{k}\right)\right]\frac{1}{\omega_1\omega_2(\omega_1 + \omega_2)}$$

$$-g_{(\pi K^*);\Lambda N}f_{\Lambda\Sigma\pi}G_{N\Sigma K^*}\frac{1}{M_\Lambda + M_\Sigma}\left(\boldsymbol{\sigma}_1 \cdot \mathbf{k}\boldsymbol{\sigma}_2 \cdot \mathbf{k}_2 + \boldsymbol{\sigma}_1 \cdot \mathbf{k}_2\boldsymbol{\sigma}_2 \cdot \mathbf{k}\right)\frac{1}{\omega_1\omega_2(\omega_1 + \omega_2)}. \tag{B17}$$

The configuration space potentials are:

$$V^{(1)}_{\sigma+T}(r) = +2g_{(\pi K^*);\Lambda N}f_{NN\pi}G_{N\Lambda K^*}\frac{m_\pi}{2M_N}\left(G^{(1)}_{B,\sigma}(r)\boldsymbol{\sigma}_1 \cdot \boldsymbol{\sigma}_2 + G^{(1)}_{B,T}(r)\ S_{12}\right) \cdot \mathcal{P}_f$$

$$+2g_{(\pi K^*);\Lambda N}f_{\Lambda\Sigma\pi}G_{N\Sigma K^*}\frac{m_\pi}{M_\Lambda + M_\Sigma}\left(G^{(1)}_{B,\sigma}(r)\boldsymbol{\sigma}_1 \cdot \boldsymbol{\sigma}_2 + G^{(1)}_{B,T}(r)\ S_{12}\right) \cdot \mathcal{P}_f. \tag{B18}$$

Above, $\mathcal{P}_f$ is the flavor-exchange operator, discussed in [12, 25]. In addition, we have to multiply these potentials with the isoscalar factors appearing in the Hamiltonian (4.26). For example for $K - \rho$ and $K - \phi$ pairs this factor is $+\sqrt{3}/4$ respectively $-1/4$, etc.

APPENDIX C: EXCHANGE POTENTIALS

In this section we follow our multi-channel description formalism in the treatment of the exchange potentials [7].

In the case of the anti-symmetric spin-orbit the exchange potential requires some attention, because its special features. The potentials in configuration space are described in Pauli-spinor space as follows

$$V = V_C + V_\sigma\boldsymbol{\sigma}_1 \cdot \boldsymbol{\sigma}_2 + V_T\ S_{12} + V_{SLS}\ \mathbf{L} \cdot \mathbf{S}_+ + V_{ALS}\ \mathbf{L} \cdot \mathbf{S}_- + V_Q\ Q_{12}\ . \tag{C1}$$

Here, the definition of the matrix elements of the spin operators are defined as follows

$$\left(\chi^\dagger_{m'}(\Lambda)\chi^\dagger_{n'}(N)|\boldsymbol{\sigma}_1 \cdot \boldsymbol{\sigma}_2|\chi^\dagger_m(\Lambda)\chi^\dagger_n(N)\right) \equiv \left(\chi^\dagger_{m'}(\Lambda)|\boldsymbol{\sigma}_1|\chi^\dagger_m(\Lambda)\right) \cdot \left(\chi^\dagger_{n'}(N)|\boldsymbol{\sigma}_1|\chi^\dagger_n(N)\right)\ , \tag{C2}$$

and similarly for the SU(2) and SU(3) operator matrix elements. In Fig. 8 the labels (m, n, m', n') refer to the spin, and the labels $(\alpha, \beta, \alpha', \beta')$ refer to unitary spin, like SU(2) or SU(3). The momenta on line 1 are $\mathbf{p}$ and $\mathbf{p}'$ for respectively the initial and the final state. Likewise, the momenta on line 2 are $-\mathbf{p}$ and $-\mathbf{p}'$ for respectively the initial and the final state.

In graph Fig. 8 we encounter the matrix elements

$$(\boldsymbol{\sigma}_1)_{m',m} = \left(\chi^\dagger_{m'}(N)|\boldsymbol{\sigma}_1|\chi^\dagger_m(\Lambda)\right),$$
$$(\boldsymbol{\sigma}_2)_{n',n} = \left(\chi^\dagger_{n'}(\Lambda)|\boldsymbol{\sigma}_2|\chi^\dagger_n(N)\right) \tag{C3}$$

1. Spin-Exchange Potentials

In order to project the exchange potentials on the forms in (C1) we have to rewrite these matrix elements
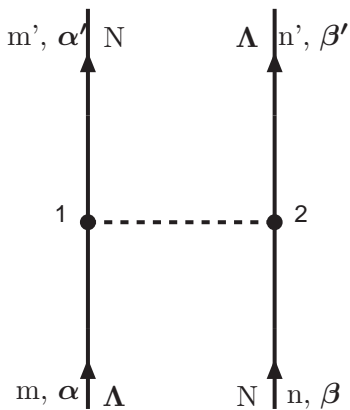
FIG. 8: Particle- and spin-exchange for ΛN.

in terms of those occurring in (C2). This can be done using the spin-exchange operator P_σ:

$$P_\sigma = \frac{1}{2}\left(1 + \boldsymbol{\sigma}_1 \cdot \boldsymbol{\sigma}_2\right) \ . \tag{C4}$$

Properties of this operator are

$$P_\sigma^\dagger = P_\sigma \ , \quad P_\sigma^2 = 1, \tag{C5a}$$
$$P_\sigma \ \chi_{1,m}\chi_{2,n} = \chi_{1,n}\chi_{2,m}, \tag{C5b}$$
$$P_\sigma \ \sigma_{1,k} \ P_\sigma = \sigma_{2,k}, \tag{C5c}$$
$$P_\sigma \ \sigma_{2,k} \ P_\sigma = \sigma_{1,k}. \tag{C5d}$$

Similar properties hold for the flavor-exchange operator P_f, but now for the SU(2) isospin operators τ_k, or the SU(3) octet operators λ_k.

In the following we make only explicit the spin labels, but similar operations apply to the SU(2) or SU(3) labels.

Using this spin-exchange operator, we find that

$$\left(\chi^\dagger_{1,m'}(N)\chi^\dagger_{2,n'}(\Lambda)|\boldsymbol{\sigma}_1 \otimes 1_2 - 1_1 \otimes \boldsymbol{\sigma}_2|\chi^\dagger_{1,m}(\Lambda)\chi^\dagger_{2,n}(N)\right) =$$
$$\left(\chi^\dagger_{2,n'}(N)\chi^\dagger_{1,m'}(\Lambda)|P_\sigma^\dagger\left(\boldsymbol{\sigma}_1 \otimes 1_2 - 1_1 \otimes \boldsymbol{\sigma}_2\right) P_\sigma \ P_\sigma|\chi^\dagger_{1,m}(\Lambda)\chi^\dagger_{2,n}(N)\right) =$$
$$-\left(\chi^\dagger_{1,m'}(\Lambda)\chi^\dagger_{1,n'}(N)|\left(\boldsymbol{\sigma}_1 \otimes 1_2 - 1_1 \otimes \boldsymbol{\sigma}_2\right) \ P_\sigma|\chi^\dagger_{1,m}(\Lambda)\chi^\dagger_{2,n}(N)\right) \ . \tag{C6}$$

Above, we added the subscripts 1 and 2 to indicate explicitly the baryon line that is involved.

2. Spin- and Strangeness-Exchange Potentials

In addition to the spin-exchange, we also have the flavor-exchange operator P_f active here. So, in total we have to apply $-P_\sigma \ P_f = P_x$, i.e. the space-exchange operator. This latter relation follows from the anti-symmetry of the two-baryon states, which implies that only states with $P_f P_\sigma P_x = -1$ are physical. All this implies

1. For the ALS-potential derived in K-exchange etc. one has in (C1), considering both spin- and flavor-exchange, the operator

$$\text{ALS} \ \Rightarrow \frac{1}{2}\left(\boldsymbol{\sigma}_1 - \boldsymbol{\sigma}_2\right) \cdot \mathbf{L} \ P_x \tag{C7}$$

2. For the SLS-potential derived in K-exchange etc. one has in (C1), considering both spin- and flavor-exchange, the operator $P_f P_\sigma$, but since

$$\boldsymbol{\sigma}_1 \cdot \boldsymbol{\sigma}_2 \ \sigma_{1,k} = \sigma_{2,k} + i\epsilon_{klm} \ \sigma_{1,l}\sigma_{2,m} \ ,$$
$$\boldsymbol{\sigma}_1 \cdot \boldsymbol{\sigma}_2 \ \sigma_{2,k} = \sigma_{1,k} + i\epsilon_{klm} \ \sigma_{2,l}\sigma_{1,m} \ ,$$

one derives easily that

$$P_\sigma \left(\boldsymbol{\sigma}_1 + \boldsymbol{\sigma}_2\right) \cdot \mathbf{L} = \left(\boldsymbol{\sigma}_1 + \boldsymbol{\sigma}_2\right) \cdot \mathbf{L} \ , \tag{C8}$$

and therefore, similarly to (C6) we have, with the inclusion of the flavor labels,

$$
\begin{aligned}
&\left(\chi^\dagger_{1,m'\alpha'}(N)\chi^\dagger_{2,n'\beta'}(\Lambda)|\boldsymbol{\sigma}_1 \otimes 1_2 + 1_1 \otimes \boldsymbol{\sigma}_2|\chi^\dagger_{1,m\alpha}(\Lambda)\chi^\dagger_{2,n\beta}(N)\right) = \\
&\left(\chi^\dagger_{2,n'\beta'}(N)\chi^\dagger_{1,m'\alpha'}(\Lambda)|P^\dagger_f P^\dagger_\sigma \left(\boldsymbol{\sigma}_1 \otimes 1_2 + 1_1 \otimes \boldsymbol{\sigma}_2\right)|\chi^\dagger_{1,m\alpha}(\Lambda)\chi^\dagger_{2,n\beta}(N)\right) = \\
&\left(\chi^\dagger_{1,m'\alpha'}(\Lambda)\chi^\dagger_{1,n'\beta'}(N)|\left(\boldsymbol{\sigma}_1 \otimes 1_2 + 1_1 \otimes \boldsymbol{\sigma}_2\right) P_f|\chi^\dagger_{1,m\alpha}(\Lambda)\chi^\dagger_{2,n\beta}(N)\right) \ .
\end{aligned}
\tag{C9}
$$

So, for the SLS-potential derived in K-exchange etc. one has in (C1), considering both spin- and flavor-exchange, the operator

$$
\text{SLS} \ \Rightarrow \frac{1}{2}\left(\boldsymbol{\sigma}_1 + \boldsymbol{\sigma}_2\right) \cdot \mathbf{L} \ P_f
\tag{C10}
$$

This treatment for the SLS-potential also applies to the central-, spin-spin-, tensor-, and quadratic-spin-orbit potentials as well, of course.

We conclude this section by noticing that we have found, using our multi-channel set-up the same prescriptions for the treatment of the flavor-exchange potentials as in [25]. For the treatment of the ALS-potential for $S = \pm 1$-exchange, our prescription here is more clear. For example in the case of the coupled $^1P_1 - ^3P_1$ system our prescription is unambiguous, and given by the P_x-operator, which is the same for both partial-waves coupled in this case.
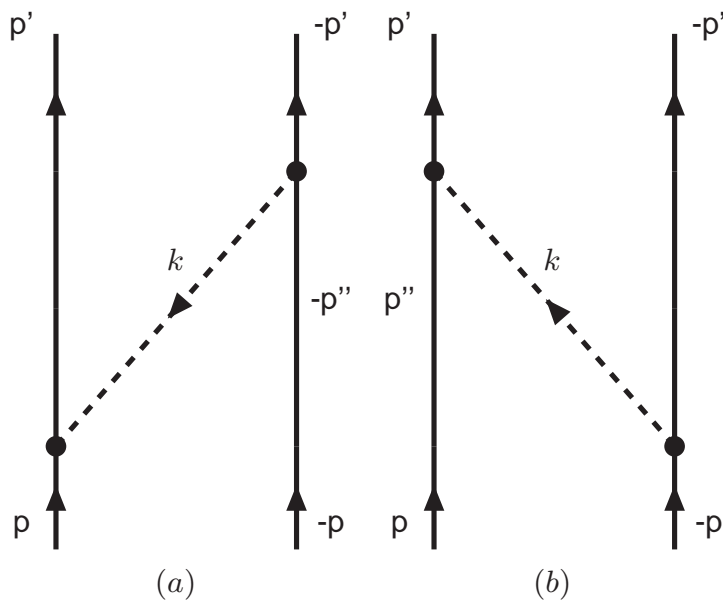

FIG. 9: K- and K*-exchange time-ordered graphs (a) and (b).

APPENDIX D: DERIVATION BDI ALS-POTENTIALS FOR STRANGE-MESON-EXCHANGES

The contributions to the P_8-spinor invariant, see [27],

$$
P_8 = 2\left(\boldsymbol{\sigma}_1 \cdot \mathbf{q}\boldsymbol{\sigma}_2 \cdot \mathbf{k} - \boldsymbol{\sigma}_1 \cdot \mathbf{k}\boldsymbol{\sigma}_2 \cdot \mathbf{q}\right) \ ,
\tag{D1}
$$

for (K, K^*)-exchange were given by Brown, Downs, and Iddings (BDI) [16]. Here we derive these for (K, K^*), and in particular for the pseudoscalar K within the ps-pv theory.

1. K-exchange ALS-potential (PS-PV Theory)

We derive the K-exchange potential using the PV-theory, and show that we get the BDI-answer for the anti-symmetric spin-orbit potential (ALS). For graph (a) we get from the vertices the matrix element

$$
(a) \; : \quad -\frac{f_P^2}{m_\pi^2}\left[\boldsymbol{\sigma}_1\cdot\mathbf{k}+\frac{2\omega}{M_\Lambda+M_N}\boldsymbol{\sigma}_1\cdot\mathbf{q}\right]\left[-\boldsymbol{\sigma}_2\cdot\mathbf{k}+\frac{2\omega}{M_\Lambda+M_N}\boldsymbol{\sigma}_2\cdot\mathbf{q}\right]\cdot\frac{1}{2\omega}\frac{-1}{\omega-a}
$$

$$
= -\frac{f_P^2}{m_\pi^2}\left[\boldsymbol{\sigma}_1\cdot\mathbf{k}\boldsymbol{\sigma}_2\cdot\mathbf{k}-\frac{2\omega}{M_\Lambda+M_N}\left(\boldsymbol{\sigma}_1\cdot\mathbf{k}\boldsymbol{\sigma}_2\cdot\mathbf{q}-\boldsymbol{\sigma}_1\cdot\mathbf{q}\boldsymbol{\sigma}_2\cdot\mathbf{k}\right)\right]\cdot\frac{1}{2\omega(\omega-a)}\;, \tag{D2a}
$$

$$
(b) \; : \quad -\frac{f_P^2}{m_\pi^2}\left[\boldsymbol{\sigma}_1\cdot\mathbf{k}-\frac{2\omega}{M_\Lambda+M_N}\boldsymbol{\sigma}_1\cdot\mathbf{q}\right]\left[-\boldsymbol{\sigma}_2\cdot\mathbf{k}-\frac{2\omega}{M_\Lambda+M_N}\boldsymbol{\sigma}_2\cdot\mathbf{q}\right]\cdot\frac{1}{2\omega}\frac{-1}{\omega+a}
$$

$$
= -\frac{f_P^2}{m_\pi^2}\left[\boldsymbol{\sigma}_1\cdot\mathbf{k}\boldsymbol{\sigma}_2\cdot\mathbf{k}+\frac{2\omega}{M_\Lambda+M_N}\left(\boldsymbol{\sigma}_1\cdot\mathbf{k}\boldsymbol{\sigma}_2\cdot\mathbf{q}-\boldsymbol{\sigma}_1\cdot\mathbf{q}\boldsymbol{\sigma}_2\cdot\mathbf{k}\right)\right]\cdot\frac{1}{2\omega(\omega+a)}\;, \tag{D2b}
$$

where $a=M_\Lambda-M_N$. Summing these contributions gives [1]

$$
\widetilde{V}_K(\mathbf{q},\mathbf{k})=-\frac{f_P^2}{m_\pi^2}\left[\frac{1}{2\omega}\left\{\frac{1}{\omega-a}+\frac{1}{\omega+a}\right\}\boldsymbol{\sigma}_1\cdot\mathbf{k}\boldsymbol{\sigma}_2\cdot\mathbf{k}\right.
$$

$$
\left.+\frac{1}{M_\Lambda+M_N}\left\{\frac{1}{\omega-a}-\frac{1}{\omega+a}\right\}\left(\boldsymbol{\sigma}_1\cdot\mathbf{k}\boldsymbol{\sigma}_2\cdot\mathbf{q}-\boldsymbol{\sigma}_1\cdot\mathbf{q}\boldsymbol{\sigma}_2\cdot\mathbf{k}\right)\right]\mathcal{P}_f
$$

$$
= -\frac{f_P^2}{m_\pi^2}\left[\boldsymbol{\sigma}_1\cdot\mathbf{k}\boldsymbol{\sigma}_2\cdot\mathbf{k}-2\frac{M_\Lambda-M_N}{M_\Lambda+M_N}\left(\boldsymbol{\sigma}_1\cdot\mathbf{k}\boldsymbol{\sigma}_2\cdot\mathbf{q}-\boldsymbol{\sigma}_1\cdot\mathbf{q}\boldsymbol{\sigma}_2\cdot\mathbf{k}\right)\right]\mathcal{P}_f\cdot\frac{1}{\omega^2-a^2} \tag{D3}
$$

We notice that this result corresponds with the answer in the PS-PS theory. All this in the approximation $(M_\Lambda+M_N)^{-1}=(1/M_\Lambda+1/M_N)/4$. Now, using the definitions in [12, 27] we have

$$
P_8 = 2\left(\boldsymbol{\sigma}_1\cdot\mathbf{q}\boldsymbol{\sigma}_2\cdot\mathbf{k}-\boldsymbol{\sigma}_1\cdot\mathbf{k}\boldsymbol{\sigma}_2\cdot\mathbf{q}\right)\;,
$$

$$
P_6 = (i/2)\left(\boldsymbol{\sigma}_1-\boldsymbol{\sigma}_2\right)\cdot\mathbf{n}\;,\quad \mathbf{n}=\mathbf{p}\times\mathbf{p}'=\mathbf{q}\times\mathbf{k}\;,
$$

with the relation [16] $P_8=-\left(1+\boldsymbol{\sigma}_1\cdot\boldsymbol{\sigma}_2\right)P_6=2\mathcal{P}_x\mathcal{P}_f\,P_6$. This leads to the following expression

$$
\widetilde{V}_K(\mathbf{q},\mathbf{k}) = -\frac{f_P^2}{m_\pi^2}\left[\boldsymbol{\sigma}_1\cdot\mathbf{k}\boldsymbol{\sigma}_2\cdot\mathbf{k}+2\frac{M_\Lambda-M_N}{M_\Lambda+M_N}\cdot(i/2)\left(\boldsymbol{\sigma}_1-\boldsymbol{\sigma}_2\right)\cdot\mathbf{n}\,\mathcal{P}_x\mathcal{P}_f\right]\mathcal{P}_f\cdot\frac{1}{\omega^2-a^2} \tag{D4}
$$

2. K*-exchange ALS-potential

Upon inspection, we find that the only contribution to the P_8-invariant is given by

$$
\widetilde{V}_{K^*}(\mathbf{q},\mathbf{k}) \approx \frac{1}{4}\frac{G_{13}G_{24}}{\omega^2-a^2}\boldsymbol{\sigma}_1\cdot\left(\frac{\mathbf{p}}{M_N}-\frac{\mathbf{p}'}{M_\Lambda}\right)\boldsymbol{\sigma}_2\cdot\left(\frac{\mathbf{p}}{M_\Lambda}-\frac{\mathbf{p}'}{M_N}\right)\mathcal{P}_f
$$

$$
= \frac{1}{4}\frac{G_{13}G_{24}}{\omega^2-a^2}\left[\boldsymbol{\sigma}_1\cdot\left\{\left(\frac{1}{M_N}-\frac{1}{M_\Lambda}\right)\mathbf{q}-\frac{1}{2}\left(\frac{1}{M_N}+\frac{1}{M_\Lambda}\right)\mathbf{k}\right\}\cdot\right.
$$

$$
\left.\boldsymbol{\sigma}_2\cdot\left\{\left(\frac{1}{M_\Lambda}-\frac{1}{M_M}\right)\mathbf{q}-\frac{1}{2}\left(\frac{1}{M_\Lambda}+\frac{1}{M_N}\right)\mathbf{k}\right\}\right]\mathcal{P}_f
$$

$$
= \frac{1}{4}\frac{G_{13}G_{24}}{\omega^2-a^2}\left[\frac{1}{4}\left(\frac{1}{M_N}+\frac{1}{M_\Lambda}\right)^2\boldsymbol{\sigma}_1\cdot\mathbf{k}\boldsymbol{\sigma}_2\cdot\mathbf{k}-\left(\frac{1}{M_N}-\frac{1}{M_\Lambda}\right)^2\boldsymbol{\sigma}_1\cdot\mathbf{q}\boldsymbol{\sigma}_2\cdot\mathbf{q}\right.
$$

$$
\left.-\frac{1}{2}\left(\frac{1}{M_N^2}-\frac{1}{M_\Lambda^2}\right)\left(\boldsymbol{\sigma}_1\cdot\mathbf{q}\boldsymbol{\sigma}_2\cdot\mathbf{k}-\boldsymbol{\sigma}_1\cdot\mathbf{k}\boldsymbol{\sigma}_2\cdot\mathbf{q}\right)\right]\mathcal{P}_f, \tag{D5}
$$

---

[1] The $\mathcal{P}$-operators occur in the transition to configuration space. In this appendix, in contrast to elsewhere in this paper, we include the $\mathcal{P}$-operators in the momentum-space formulas only as a reminder.

which gives the anti-symmetric spin-orbit potential

$$\widetilde{V}_{K^*}(\mathbf{q}, \mathbf{k}) \;=\; \frac{1}{4} \frac{G_{13} G_{24}}{\omega^2 - a^2} \left(\frac{1}{M_N^2} - \frac{1}{M_\Lambda^2} \right) (i/2) \, (\boldsymbol{\sigma}_1 - \boldsymbol{\sigma}_2) \cdot \mathbf{n} \; \mathcal{P}_x \; . \qquad (D6)$$

Finally, we mention the relation with a sometimes used other form for the antisymmetric spin-orbit. Namely, we have $\boldsymbol{\sigma}_1 \cdot \boldsymbol{\sigma}_2 \, (\boldsymbol{\sigma}_1 \times \boldsymbol{\sigma}_2) = -2i(\boldsymbol{\sigma}_1 - \boldsymbol{\sigma}_2) - \boldsymbol{\sigma}_1 \times \boldsymbol{\sigma}_2$, so that

$$(\boldsymbol{\sigma}_1 - \boldsymbol{\sigma}_2) = iP_\sigma \, (\boldsymbol{\sigma}_1 \times \boldsymbol{\sigma}_2) \; . \qquad (D7)$$

[1] M.M. Nagels, Th.A. Rijken, and Y. Yamamoto, *Extended-soft-core Baryon-Baryon Model ESC08, I. Nucleon-Nucleon Scattering* , arXiv:nucl-th/1408.4825 (2014)

[2] M.M. Nagels, Th.A. Rijken, and Y. Yamamoto, *Extended-soft-core Baryon-Baryon Model ESC08, II. Hyperon-Nucleon Interactions* , arXiv:nucl-th/1501.06636 (2015)

[3] M.M. Nagels, Th.A. Rijken, and Y. Yamamoto, *Extended-soft-core Baryon-Baryon Model ESC08, III. S=-2 Hyperon-hyperon/nucleon Interactions*, arXiv:nucl-th/1504.02634 (2015)

[4] Th.A. Rijken, M.M. Nagels, and Y. Yamamoto, Progr. Theor. Phys. **185**, 14 (2010); Y. Yamamoto, T. Motoba, and Th.A. Rijken, ibid 72; E. Hiyama, M. Kamimura, Y. Yamamoto, T. Motoba, and Th.A. Rijken, ibid 106.

[5] Th.A. Rijken, Phys. Rev. **C73**, 044007 (2006).

[6] Th.A. Rijken and Y. Yamamoto, Phys. Rev. **C73**, 044008 (2006).

[7] Th.A. Rijken and Y. Yamamoto, *Extended-soft-core baryon-baryon model III, hyperon-hyperon/nucleon interactions*, arXiv:nucl-th/060807 (2006)

[8] L. Micu, Nucl. Phys. **B10** (1969) 521; R. Carlitz and M. Kislinger, Phys. Rev. D **2** (1970) 336.

[9] A. Le Yaouanc, L. Oliver, O. Péne, and J.-C. Raynal, Phys. Rev. D **8** (1973) 2223; Phys. Rev. D **11** (1975) 1272.

[10] N. Isgur and J. Paton, Phys. Rev. **D31**, 2910 (1985); R. Kokoski and N. Isgur, Phys. Rev. **D35**, 907 (1987).

[11] M.M. Nagels, T.A. Rijken, and J.J. de Swart, Phys. Rev. D **17** (1978) 768.

[12] P.M.M. Maessen, Th.A. Rijken, and J.J. de Swart, Phys. Rev. C **40** (1989) 2226.

[13] Th.A. Rijken, V.G.J. Stoks, and Y. Yamamoto, Phys. Rev. C **59**, 21, (1999).

[14] E. Hiyama, M. Kamimura, T. Motoba, T. Yamada, and Y. Yamamoto, Phys. Rev. Lett. 85 (2000) 270.

[15] O. Hashimoto and H. Tamura, Progr. Part. Phys. **57** (2006) 564.

[16] J.T. Brown, B.W. Downs, and C.K. Iddings, Ann. Phys. (N.Y.) **60**, 148 (1970).

[17] For the OBE-potentials we have included the Brown-Downs-Iddings anti-symmetric spin-orbit potentials from pseudo-scalar, vector-, and scalar- meson exchange [16]. Also we derived new anti-symmetric spin-orbit contributions from MPE. Since we do not fit P-waves for YN, these play no role in the construction of the ERSC07-

model. Therefore, these potentials will be published elsewhere.

[18] In principle, the off-mass-shell J=0 contribution from the tensor-meson nonet A_2, K_2 etc. is included with the diffractive soft-core potentials, see e.g. [11, 12]. Although the couplings are zero in ESC08 models, we include these potentials in the text for completeness.

[19] For a review see: C. Ewerz, *The Odderon in Quantum Chromodynamics*, hep-ph/0306137.

[20] M. Oka, K. Shimizu, and K. Yazaki, Progr. Theor. Phys., Suppl. **137**, p. 1 (2000).

[21] Y. Fujiwara, Y. Suzuki, and C. Nakamoto, Progr. in Part. and Nuclear Physics, **58** (2007) 439.

[22] R. Tamagaki and H. Tanaka, Progr. Theor. Physics, **34**, 191 (1965); R. Tamagaki, Suppl. Progr. Theor. Phys., Extra Number, p.242, 1968; R. Tamagaki, Progr. Theor. Phys. **39**, 91 (1968).

[23] J. Dabrowski, Phys. Rev. C 60 (1999) 025205.

[24] H. Noumi et al., Phys. Rev. Lett. 89 (2002) 072301.

[25] M.M. Nagels, T.A. Rijken, and J.J. deSwart, Phys. Rev. D 15 (1977) 2547.

[26] The fortran code ESC08C.YN16 is available on the website NN-Online: URL *http://NN-Online.org*.

[27] J.J. de Swart, M.M. Nagels, T.A. Rijken, and P.A. Verhoeven, Springer Tracts in Modern Physics, **60**, 138 (1971).

[28] M.M. Nagels, T.A. Rijken, and J.J. de Swart, Ann. Phys. (N.Y.) **79**, 338 (1973).

[29] R.H. Dalitz and F. von Hippel, Phys. Lett. **10**, 153 (1964).

[30] C. Itzykson and J-B. Zuber, *Quantum Field Theory*, section 2-3-2, McGraw-Hill Inc. 1980.

[31] Th.A. Rijken, Ann. Phys. (N.Y.), **208**, 253 (1991).

[32] Th.A. Rijken and V.G.J. Stoks, Phys. Rev. C 54 (1996) 2869; ibid. C 54 (1996) 2869.

[33] E. Hiyama, T. Motoba, Y. Yamamoto, and Th.A. Rijken, in preparation.

[34] V.G.J. Stoks, R.A.M. Klomp, M.C.M. Rentmeester, and J.J. de Swart, Phys. Rev. C 48 (1993) 792.

[35] R.A.M. Klomp, private communication (unpublished).

[36] J.K. Ahn et al., Nucl. Phys. A 761 (2005) 41.

[37] J.A. Kadyk, G. Alexander, J.H. Chan, P. Gaposchkin and G.H. Trilling, Nucl. Phys. B27 (1971) 13.

[38] Y. Kondo et al., Nucl. Phys. A 676 (2000) 371.

[39] T. Takahashi et al., Phys. Rev. Lett. 87 (2001) 212502.

[40] E. Hiyama, M. Kamimura, T. Motoba, T. Yamada, and Y. Yamamoto, Phys. Rev. C66 (2002) 024007.

[41] P. Khaustov et al., Phys. Rev. C 61 (2000) 054603.

[42] V.G.J. Stoks, R. Timmermans, and J.J. de Swart, Phys. Rev. C 47 (1993) 512.

[43] V.G.J. Stoks, R.A.M. Klomp, C.P.F. Terheggen, and J.J. de Swart, Phys. Rev. C 49 (1994) 2950.

[44] R.A. Bryan and A. Gersten, Phys. Rev. D **6** (1972) 341.

[45] V.G.J. Stoks and Th.A. Rijken, Nucl. Phys. **A 613** (1997) 311.

[46] G. Alexander, U. Karshon, A. Shapira, G. Yekutieli, R. Engelmann, H. Filthuth, and W. Lughofer, Phys. Rev. **173**, 1452 (1968).

[47] B. Sechi-Zorn, B. Kehoe, J. Twitty, and R.A. Burnstein, Phys. Rev. **175**, 1735 (1968).

[48] F. Eisele, H. Filthuth, W. Fölisch, V. Hepp, E. Leitner, and G. Zech, Phys. Lett. **37B**, 204 (1971).

[49] F.E. Close, and R.G. Roberts, Phys. Lett. **B 316**, 165 (1993).

[50] R. Engelmann, H. Filthuth, V. Hepp, and E. Kluge, Phys. Lett. **21**, 587 (1966).

[51] V. Hepp and M. Schleich, Z. Phys. **214**, 71 (1968).

[52] D. Stephen, Ph.D. thesis, University of Massachusetts, 1970. Z. Phys. **214**, 71 (1968).

[53] T. Inoue et al, Nucl. Phys. **A 881** (2012) 28.

[54] Y. Yamamoto and H.Bandō, Prog. Theor. Phys. Suppl. **No.81** (1985), 9.

[55] Y. Yamamoto, T.Motoba, H.Himeno, K.Ikeda and S.Nagata, Prog. Theor. Phys. Suppl. **No.117** (1994), 361.

[56] Y. Yamamoto, T.Motoba, Th.A. Rijken, Prog. Theor. Phys. Suppl. **No.185** (2010), 72.

[57] Y. Yamamoto, T.Furumoto, N.Yasutake and Th.A. Rijken, Phys. Rev. **C 88** (2013), 022801(R).

[58] Y. Yamamoto, T.Furumoto, N.Yasutake and Th.A. Rijken, Phys. Rev. **C 90** (2014), 045805.

[59] R.R. Scheerbaum, Nucl. Phys. **A257** (1976), 77.

[60] O. Hashimoto and H. Tamura Prog. Part. Nucl. Phys. **57** (2006), 564.

[61] T. Harada and Y. Hirabayashi, Nucl. Phys. A759, 143 (2005).

[62] M. Kohno, Y. Fujiwara, Y. Watanabe, K. Ogata and M. Kawai Phys. Rev. **C74** (2006), 064613.

[63] T. Fukuda *et al.*, Phys. Rev.**C58** (1998), 1306. P. Khaustov *et al.*, Phys. Rev. **C61** (2000), 054603.

[64] T. Gogami *et al.*, Phys. Rev. **C93** (1995), 034314.

[65] A. Gal, Prog. Theor. Phys. Suppl. **No.186** (2010), 270.

[66] M.M. nagels, T.A. Rijken, and J.J. deSwart, Phys. Rev. **D20** (1979), 1633.

[67] G.A. Miller, Phys. Rev. **C** (1989) 1563.

[68] Th.A. Rijken and Y. Yamamoto, Proceedings of *The IX International Conference on Hypernuclear and Strange Particle Physics*, edited by J. Pochodzalla and Th. Walcher, October 10-14, 2006, p. 279. ISBN-10 3-540-76365-1 Springer Berlin Heidelberg New York.